Crustal Seismic Velocity Structure of the Intermontane and Coast Belts,
Southwestern Canadian Cordillera

by

Nancy Ann McLean
B. Sc., University of Victoria, 1990

A Thesis Submitted in Partial Fulfillment of the
Requirements for the Degree of
MASTER OF SCIENCE
in the Department of Earth and Ocean Sciences

We accept this thesis as conforming
to the required standard

[redacted]

Dr. G. D. Spence, Supervisor (School of Earth and Ocean Sciences)

[redacted]

Dr. C. R. Barnes, Departmental Member (School of Earth and Ocean Sciences)

[redacted]

Dr. G. C. Rogers, Outside Member (Geological Survey of Canada)

[redacted]

Dr. T. Hamilton, External Examiner (Geological Survey of Canada)

Supervisor: Dr. George D. Spence

ABSTRACT

One phase of LITHOPROBE's seismic program for the Southern Cordillera included a seismic refraction experiment (SCoRE '89) focussing on the Coast and Intermontane Belts of the Southern Canadian Cordillera. Primary objectives of the refraction program include; i) determining 2-D velocity structure and interrelationships of the component terranes, ii) defining the depth and configuration of the Mohorovic discontinuity, and iii) determining the extent of vertical displacement of major faults within the region. In particular, it was hoped that any differences in structure across the boundaries of the Coast Belt, either in the west beneath Georgia Strait or in the east beneath the Fraser fault system, could be resolved.

In this study, seismic refraction data were recorded from 10 shot points along a 450 km profile, cross-strike the Fraser fault system, across the Intermontane, Coast and Insular Belts. From these data, a two-dimensional P-wave velocity structural model of the crust and upper mantle was interpreted using a combination of traveltime inversion and amplitude forward modelling. The structural model features a varying-thickness near-surface layer with large vertical and lateral velocity variations. This uppermost stratum overlies a crustal velocity structure which is divided into three crustal layers separated by wide-angle reflections. The velocity of the upper crustal structure changes abruptly at the Harrison fault. West of the fault, the average upper crustal velocity was 6.4 km/s, while east of the fault the average upper crustal velocity was 6.1 km/s. The mid-crust and lower crust have average velocities of 6.5 km/s and 6.6 - 6.8 km/s, respectively. A transition to lower velocities in the east is maintained in these crustal units, although it is less abrupt. The depth to the Mohorovic discontinuity was typically 34 km with variations up to 1.5 km. The interpreted depth to the Moho along SCoRE '89 Line 2 contrasts with interpretations of SCoRE surveys to the south. Analyses of these data indicate an abrupt thickening from 34 km to 37 km below the Central Coast Belt and a further decrease to 30 km beneath the Insular Belt. This variability is probably an indication of the true 3-D structure beneath the Cordillera. Upper mantle velocities were typically 7.9 km/s. An upper mantle reflector was interpreted at ~ 46 km depth below which lies the top of the asthenosphere.

In general, the crustal and upper mantle structure across the refraction line is well-resolved with the exception of the deep structure in the Western Coast Belt and Insular Belt. The lower structure of the subduction complex interpreted from previous surveys could not be correlated with the rest of the region. This is largely due to an unusual disruption of lower crust and upper mantle energy propagating into the region. A striking feature of the velocity structural model is an abrupt transition to lower crustal velocities east of the Harrison fault. Interpretations of LITHOPROBE reflection data and other refraction surveys in the region display a similar characteristic. The location of this transition is interpreted as representing the suture zone between the Insular and Intermontane superterranes. It is inferred that the Harrison fault penetrates the upper crustal layer, perhaps to 10 km depth. Analysis of the Line 2 data indicate a structural discontinuity in the reflecting horizons of the lower crust beneath the surface location of the Fraser fault. This implies deep crustal penetration of the Fraser fault, consistent with magnetotelluric data and analysis of reflection profile 88-18.

Examiners:

[redacted]

Dr. G. D. Spence, Supervisor (School of Earth and Ocean Sciences)

[redacted]

Dr. C. R. Barnes, Departmental Member (School of Earth and Ocean Sciences)

[redacted]

Dr. G. C. Rogers, Outside Member (Geological Survey of Canada)

[redacted]

Dr. T. Hamilton, External Examiner (Geological Survey of Canada)

Table of Contents

List of Tables

List of Figures

Acknowledgements

I would like to thank my supervisor, Dr. George Spence, for providing many hours of support. I would also like to thank the other members of my committee, Dr. Chris Barnes and Dr. Garry Rogers, for critically reviewing this manuscript and Dr. Tark Hamilton for taking the time to be my external examiner.

Many thanks to my parents, Ruth and Chas McLean, for their patient support and encouragement. To Garnet Lick, I would like to say, "The end is near!" Thank-you for understanding and standing by me these past years. To all those members of the University of Victoria whose assistance or facilities I required, you have my gratitude.

SCoRE '89 was carried out by about ~ 35 field participants under the leadership of Dr. R. M. Ellis. I would like to thank all of them for their efforts in the field. Dr. Colin Zelt provided the traveltime inversion and synthetic seismogram codes used in this study. Financial support for my student stipend was received from NSERC Research grants to Dr. George Spence and Teaching Assistant support from the University of Victoria.

I: INTRODUCTION

1.1 Experimental Objectives

The Canadian Cordillera is an area of complicated geology and tectonics. Many geophysical studies hoping to resolve the structure of the area have been carried out over the past three decades. It is only recently that a regional tectonic interpretation has been completed, but many problems still remain unanswered.

The LITHOPROBE Southern Cordillera Research Program was a five year experiment designed to address some of these unresolved problems. As one phase of the Transect, a refraction experiment was conducted in 1989 (SCoRE '89) centered over the Fraser Fault system. The research in this thesis is a subset of the data collected during this experiment and consists of a refraction profile running northeast-southwest cross-strike the Fraser-Straight Creek Fault from the Intermontane Belt across the Coast Belt and into the eastern edge of the Insular Belt (Line 2, Figure 1). Specific objectives of this investigation are:

(i) To determine the 2-D crustal and upper mantle velocity structure within the western Cordillera, and the interrelationships between this and its component terranes as mapped at the surface and inferred at depth.

(ii) To define the depth and configuration of the Mohorovic discontinuity (Moho) throughout the region.

(iii) To determine the extent of vertical displacement of the Fraser-Straight Creek Fault, specifically to what depth this and other major faults in the region cut through the crust and/or Moho.

(iv) To determine the deep structure of the Coast Belt and its relationship with the ongoing subduction of the Juan de Fuca plate.

After addressing these issues the ultimate goal of the LITHOPROBE Southern Cordillera Project is; (i) to construct a regional structural model incorporating past and present refraction and reflection models from the convergent western margin (Juan de Fuca subduction zone) to the interior of the continent (Omineca Belt to Alberta Plains) and, (ii) to

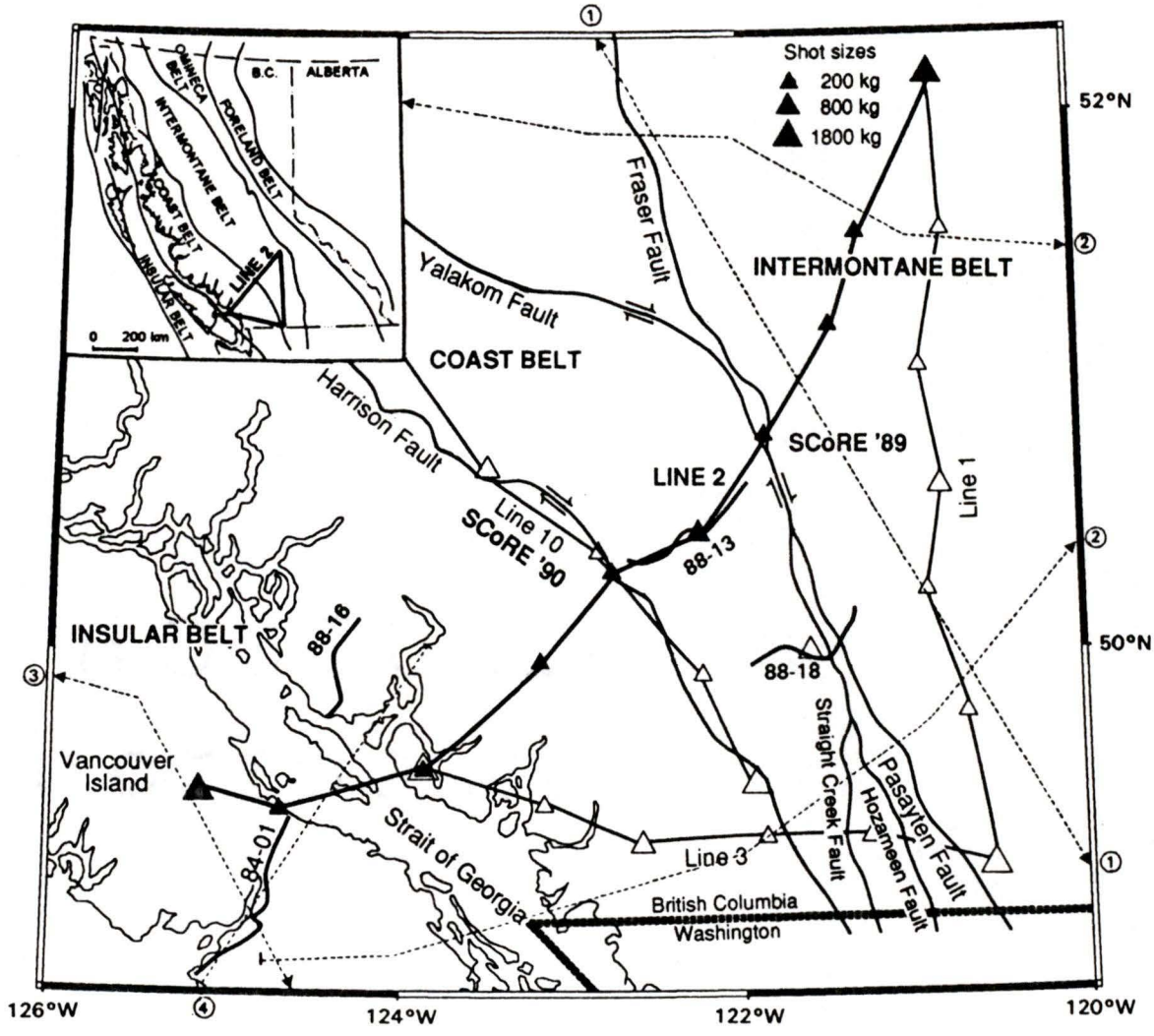

FIGURE 1: Location map showing the triangular array of shot points (triangles) and recording lines (Lines 1, 2, and 3) of SCoRE '89. Previous refraction surveys are represented by numbered dotted lines, these include; (1) White et al. (1968), (2) Berry and Forsyth (1975), (3) McMechan and Spence (1983), and (4) Spence et al. (1985). Also shown are the locations of the LITHOPROBE reflection profiles; (i) 84-01 of Green et al. (1986), (ii) 88-13 of Varsek et al. (1993), (iii) 88-16 of Varsek et al. (1993), (iv) 88-18 of Perz (1992) and Varsek et al. (1993), and the LITHOPROBE refraction Line 10 of SCoRE '90. The inset displays the approximate boundaries of the morphogeological belts of the Canadian Cordillera, adapted from Zelt et al. (1992).

discuss the implications of the structural model in relation to the development of the Southern Canadian Cordillera.

1.2 Tectonic Setting

The Canadian Cordillera can be divided into five morphogeological belts each with its own distinct tectonic history and lithological structure. From east to west they are the Rocky Mountain Foreland Belt, the Omineca Crystalline Belt, the Intermontane Belt, the Coast Plutonic Complex or Coast Belt, and the Insular Belt (Gabrielse and Yorath, 1989). Of particular interest in this study is the westernmost Intermontane Belt, the southern Coast Belt and the easternmost Insular Belt (Figure 1).

Each belt is composed of distinct crustal units defined as terranes (Gabrielse and Yorath, 1989). A terrane is bounded on each side by faults and possesses a unique tectono-stratigraphic record. The Intermontane Belt is composed of the island arc-type Stikinia and Quesnellia terranes and the oceanic Cache Creek and Slide Mountain terranes. The predominant terranes of the Coast Belt include the island arc Cadwallader and Harrison terranes and the oceanic Bridge River, Methow and Shuksan terranes. The Alexander arc terrane and the Wrangellia oceanic-arc terrane comprise the Insular Belt. A complete breakdown of the morphogeological belts is found in Gabrielse and Yorath (1989).

The present terrane framework of the Cordillera is regarded as the result of the accretion of two large allochthonous masses, the Intermontane superterrane and the Insular superterrane, onto the western edge of ancient North America (Monger et al., 1982). The Intermontane composite terrane was first to collide with ancestral North America during the Middle Jurassic followed by the accretion of the Insular composite terrane prior to Mid-Cretaceous (Journeay, 1990). The accretion of these two superterranes to ancient North America were succeeded by a series of smaller scale tectonic processes resulting in the creation of the Coast Belt.

The two possible hypotheses for the creation of the Coast Belt are given by Monger et al. (1982) and van der Heyden (1992). A widely-accepted theory is that the Coast Belt is a collisional suture that formed in Mid-Cretaceous as the result of the collision between the Insular superterrane and the Mid-Jurassic North American margin, which contained the previously accreted Intermontane superterrane. The collision followed the closure of an intervening subduction-related oceanic basin and the development of a metamorphic and structural welt (Monger et al., 1982). As an alternative explanation, van der Heyden (1992) suggested an Andean arc model in which the Coast Belt is primarily a succession of magmatic arcs formed in response to ongoing subduction of the Pacific Ocean lithosphere. These magmatic arcs were superimposed onto North America as the result of the accretion of a large, composite superterrane consisting of Wrangellia, Alexandria, and Stikinia.

Accompanying the accretion of the Intermontane and Insular superterranes, large sedimentary and volcanic sequences formed in response to or as a consequence of subsequent tectonic processes. Smaller terrane fragments were also accreted onto the margin. As a result, the Canadian Cordillera expanded North America approximately 500 km westward. Succeeding terrane accretion, transcurrent movement of the terranes relative to one another and relative to North America was accommodated by the development of large, right-lateral, strike-slip faults (Irving and Wynne, 1990). The Fraser-Straight Creek Fault and the Harrison Fault are examples of such faults. Detailed descriptions of the tectonic processes involved in the evolution of the Canadian Cordillera are found in Coney et al. (1980), Monger et al. (1982), Monger (1993), Monger and Journeay (1994), Gabrielse and Yorath (1989) and van der Heyden (1992).

1.3 Geological Framework of Study Area

Tectonostratigraphic terranes and geological outcrop/structural belts, the positions of major faults and morphogeological boundaries throughout the study area are indicated in Figure 2. The Intermontane Belt is generally topographically low in elevation and relief with widespread Tertiary volcanic and sedimentary rocks. It is underlain by Stikinia, Cache Creek,

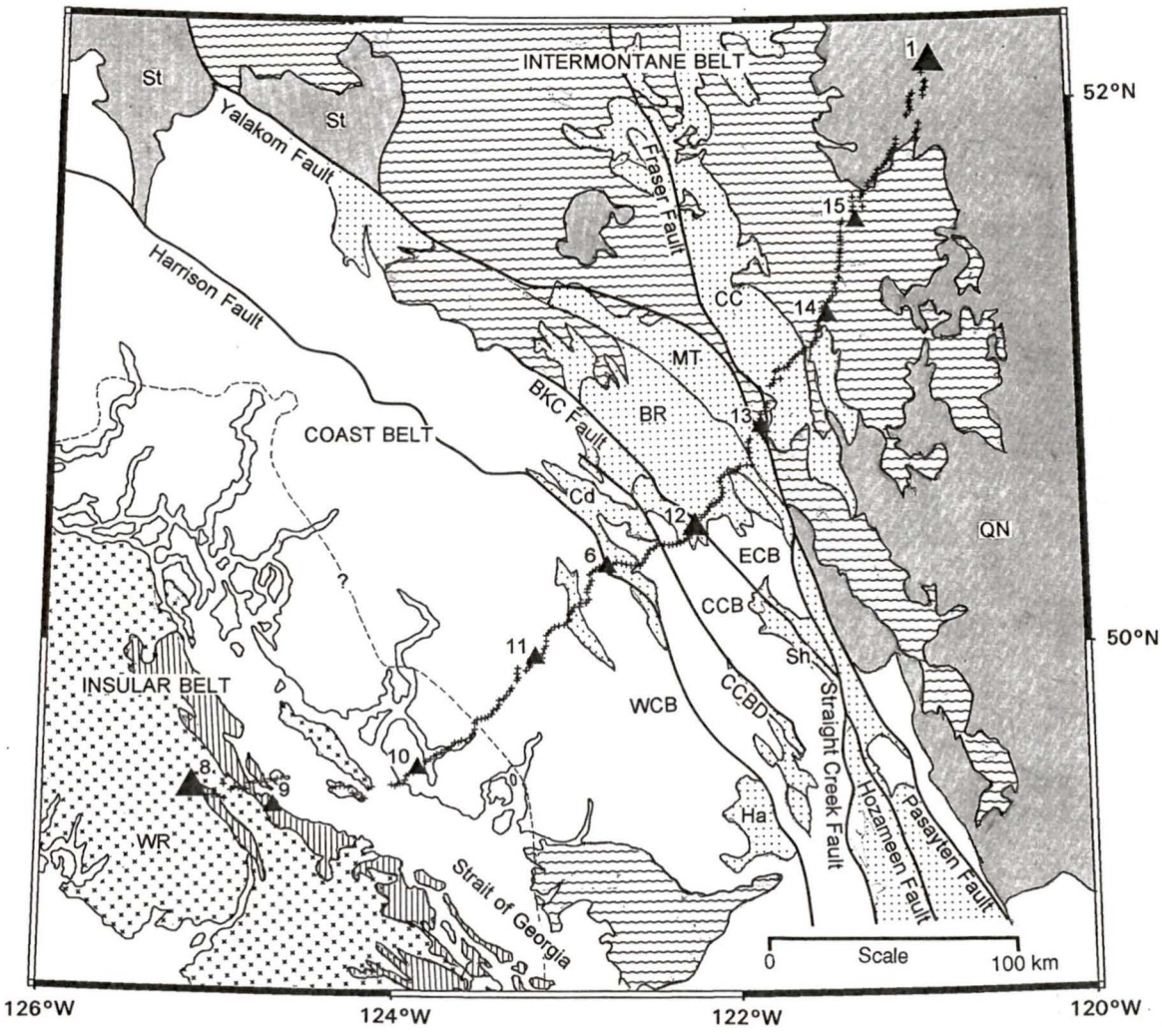

LEGEND:

Upper Triassic to Lower Jurassic volcanics including Quesnellia (QN) and Stikinia (St) terranes.

Permian to Cretaceous volcanics including Bridge River (BR), Methow (MT), Cadwallader (Cd), Cache Creek (CC), Shuksan (Sh) and Harrison (Ha) terranes.

Tertiary sediments and volcanics.

Devonian to Middle Jurassic plutonic/ultramafic rocks.

Cretaceous sediments (Nanaimo group).

Devonian to Permian arc-volcanics (Wrangellia, WR).

FIGURE 2: Location map showing shot points (triangles) and receiver locations (crosses) for SCoRE '89 Line 2. Major features are: CCB, Central Coast Belt; CCBD, Central Coast Belt Detachment; ECB, East Coast Belt; WCB, West Coast Belt; BKC Fault, Bralorne-Kwoiek Creek Fault. The dotted line indicates the speculated subsurface extent of Wrangellia into the Western Coast Belt. Adapted from Wheeler et al. (1991).

Quesnellia and Kootney terranes and overlapped by Tertiary volcano-sedimentary basins. Geological structures vary throughout the region with broad folds associated with thick volcanics and thrust faults observed in sedimentary sequences (Gabrielse and Yorath, 1989). The western boundary of the Intermontane Belt with the Coast Belt coincides with the Fraser Fault system in the south and the Yalakom Fault to the north.

The Coast Belt is a region of rugged, high relief composed mainly of plutonic and greenschist to metamorphic rocks (Roddick et al., 1983). It is bounded to the east by the Intermontane Belt and to the west by the Insular Belt. Similar to the Omineca Belt, the Coast Belt can be classified as a symmetrical orogen with Mid - Late Cretaceous folds and thrusts which verge outward from a central core zone (Monger and Price, 1979; Journeay, 1990). Plutons in the west are Mid-Cretaceous and older while plutons in the east are mainly Late Cretaceous and Tertiary (van der Heyden, 1992). Recently, a division of the Coast Belt into three distinct units (West, East and Central) has been interpreted by Journeay and Friedman (1993). The boundary between the Western and Central Coast Belts is defined by Journeay and Friedman (1993) as the Central Coast Belt Detachment (CCBD), a steeply dipping reverse fault. The boundary between the Eastern and Central Coast Belts is the Bralorne-Kwoiek Creek Fault.

The Insular Belt is rugged, but topographically lower than the Coast Belt, and consists of Upper Palaeozoic island arc volcanics and Triassic pillow basalts and flows (Karmutsen Group) deposited in a marginal basin setting and Middle Jurassic Bonanza arc volcanics (Isachsen, 1984). Northwesterly strike-slip faults and westerly thrust faults are the primary structures in the area (Gabrielse and Yorath, 1989).

1.4 Seismic Studies in the Southern Cordillera

1.4.1 Past Refraction Surveys

Prior to the LITHOPROBE program the seismic structure of the Coast and Intermontane

Belts was based on surveys completed in the 1960's and 70's. Many of these refraction surveys included very large receiver spacings (10 - 20 km) which were rather crude compared to modern standards where receiver spacing is 1.0 - 1.5 km. The interpretations are still very important to present day analysis as they provided estimates of average crustal velocities, depth to the Mohorovic discontinuity and upper mantle velocities throughout the region.

White et al. (1968) completed a refraction survey running northwest-southeast along-strike the Fraser Fault system within the Intermontane Belt crossing the Cache Creek and Quesnellia terranes (Figure 1). They identified two crustal layers, a near-surface layer of velocity ~ 5.1 km/s and a crustal layer with an average velocity of 6.1 km/s. The crust-mantle boundary was determined to be at an average depth of 30 km, below which upper mantle velocities were 8.0 km/s or less.

Berry and Forsyth (1975) analyzed refraction data from a number of surveys in the Cordillera. Two of these lines are shown in Figure 1. The northern survey cut across the Cache Creek and Stikinia terranes intersecting the northwest end of the SCoRE '89 study area in the Intermontane Belt. Interpretation of these data revealed an average upper crustal velocity of 6.5 km/s and a Moho depth of 35 km, yielding a slightly thicker crust than that determined by White et al. (1968). Upper mantle velocities were modeled at 8.0 km/s.

The southern survey of Berry and Forsyth (1975) ran approximately parallel to Line 2 crossing the Insular, Coast and Intermontane Belts but offset to the south by about 100 km. This survey was one of the first to examine the Insular-Coast Belt boundary. The analysis of these data uncovered a number of important features. Significantly, there was a discontinuity in mantle arrivals between the Coast and Insular Belts. There appeared to be a "scattering zone" in the Western Coast Belt which noticeably reduced the amplitude of the crustal arrivals. Average crustal velocities were 6.4 km/s in the Intermontane and Coast Belts, increasing slightly to the west of the "scattering zone". The average depth to the Moho was 34 km in the Intermontane Belt, thinning to ~ 23 km at the "scattering zone" in the Western

Coast Belt. The interpreted depth to the Moho rapidly increased to 45 km under Vancouver Island but was not well-constrained by the data. Upper mantle velocities appeared to be slower for the southern profile and were modelled at 7.8 km/s across the entire profile. To account for the apparent discontinuity in mantle arrivals between the Insular and Western Coast Belts, Berry and Forsyth (1975) concluded that a lower crustal discontinuity existed where velocities increased from 6.5 km/s to 7.1 km/s at a depth of ~ 30 km. They were unable to tie in the high velocity lower crustal layer and the deep crust-mantle boundary in the Insular Belt with the rest of the model.

A detailed investigation of the Insular Belt was completed in the early 1980's. McMechan and Spence (1983) analyzed data from a north-south refraction survey and Spence et al. (1985) analyzed data from an onshore-offshore refraction survey which crossed a portion of the Western Coast Belt (Figure 1). Each interpretation was later modified by Drew and Clowes (1990). The interpreted structural model for the north-south survey (McMechan and Spence, 1983) included an upper crustal layer in which the velocity increased linearly from 6.4 km/s to 6.75 km/s at 15.5 km depth, below which velocities increased to ~ 7.0 km/s. Near central Vancouver Island, the 15.5 km discontinuity deepened to 23 km over a range of ~ 50 km. Of the three models developed that could fit the data, the preferred model contained a low velocity zone between 20 km and 37 km depth where velocities decreased to 6.2 km/s and below which upper mantle velocities were 7.5 km/s. This model was consistent with the data except for central Vancouver Island where there appeared to be a high velocity (7.7 km/s) anomaly in the lower crust between 20 km and 25 km depth.

The east-west refraction survey (Figure 1) recorded data from shot points located in the western Coast Mountains and from shot points located off the west coast of Vancouver Island. Spence et al. (1985) determined that the velocity structure across this region was analogous to that observed on the north-south survey, but were able to further constrain the upper mantle by incorporating information from associated seismic data sets. The model presented included a similar localized region of high-velocity material at 20 km depth above

the subducting Juan de Fuca plate. Spence et al. (1985) suggested this material represented a remnant of subducted lithosphere which was stranded as the subduction zone jumped westward to its current position. Inherent in the velocity structure model presented by Spence et al. (1985) was low-velocity but high-density material within of the lower crust to satisfy the gravity interpretation. The Moho was modelled at 37 km depth with upper mantle velocities ranging from 7.95 - 8.2 km/s.

Drew and Clowes (1990) developed a broadly similar model for the region, but included additional layers in the lower crust consistent with prominent reflectors interpreted from the multichannel reflection data that were acquired in the region (Green et al., 1986; Clowes et al., 1987). The high velocity (6.4 - 6.75 km/s) upper crustal structure determined by the two previous studies was not altered. Drew and Clowes (1990) interpreted this material as the upper crust of the Wrangellia terrane. In the lower crust, the high velocity anomaly above the subducting Juan de Fuca plate (McMechan and Spence, 1983; Spence et al., 1985) was represented by a four-layer velocity structure; two low-velocity layers (6.35 km/s) alternated with two high velocity layers (~ 7.2 km/s). The lower crustal layer beneath the Strait of Georgia and the mainland determined by the two previous surveys remained approximately the same (~ 9 km thick, 6.6 - 6.9 km/s). The Moho depth and upper mantle velocity structure were poorly constrained by all data recorded in the region.

1.4.2 LITHOPROBE Phase I and II Reflection Surveys

As part of the LITHOPROBE Phase I program, seismic reflection data were recorded along profile 84-01 (Green et al., 1986; Clowes et al., 1987). This profile ran east-west across Vancouver Island (Figure 1), virtually coincident with the east-west refraction survey of Spence et al. (1985). The data displayed two prominent bands of gently dipping reflectors, the 'C' and 'E' reflectors, which bound a high density and high velocity slab of material previously detected by gravity data (Riddihough, 1979) and seismic refraction data (Spence et at., 1985; Drew and Clowes, 1990). Clowes et al. (1987) defined the upper reflection zone ('C') as the top of the subduction complex which truncates the base of the Wrangellia terrane

and limits it to the upper crust. The lower reflection zone ('E') is nearly coincident with the top of the subducting Juan de Fuca plate and coincides with a highly conductive layer attributed to the presence of fluids (Kurtz et al., 1986). Alternatively, the lower reflective zone may be a result of recent continuous accretion and underplating of material from the subducting oceanic plate (Clowes et al., 1987).

During the LITHOPROBE Phase II program, a number of seismic reflection surveys were completed extending across the width of the southern Canadian Cordillera. Profiles relevant to this study include 88-13, 88-16, and 88-18 (Figure 1). Analysis of these data yield significant results in the Coast Belt and near the Fraser Fault system. Profile 88-13 (Varsek et al., 1993) provided coverage across the Central Coast Belt. The data displayed strong east-dipping reflectors truncated by west-dipping reflectors throughout the crust, a characteristic observed on all profiles in the area. Varsek et al. (1993) interpreted this distinctive structure as representing the interfingering of the Insular and Intermontane superterranes and concluded that the suture zone between the composite terranes was near the Central Coast Belt Detachment, consistent with the geological interpretation (Monger et al., 1990).

In the Western Coast Belt, profile 88-16 (Varsek et al., 1993) imaged a number of reflections in the middle and lower crust and upper mantle. Varsek et al. (1993) provided two scenarios which linked the structures observed beneath Vancouver Island to those observed in the Western Coast Belt. The preferred interpretation for profile 88-16 was that the mid-crustal ramps represented imbricated structures of the Wrangellia terrane while the top of the lower crustal wedge was possibly a continuation of the 'C' reflector observed beneath Vancouver Island (Clowes et al., 1987). The upper mantle reflector, imaged at 13.5 s on profile 88-16, was linked to the 'E' reflector observed beneath Vancouver Island (Clowes et al., 1987). In this interpretation, the Moho beneath the Western Coast Belt was at 12.0 s or 39 km depth.

Profile 88-18 (Varsek et al., 1993; Perz, 1992) provided coverage across the Fraser Fault system. The prominent feature displayed by the data was a difference in structural styles on either side of the fault. West of the fault, the upper crust displayed west-dipping reflectors while the lower crust imaged a strong east-dipping reflector. A reverse pattern was observed east of the fault; east-dipping reflectors in the upper crust and west-dipping reflectors in the lower crust. A surprising anomaly imaged by the data was a sub-horizontal band of reflectors in the middle crust observed west and east of the fault but not in the region of the fault. Varsek et al. (1993) inferred that the band of reflectivity was continuous across the fault region and that the Fraser-Straight Creek Fault flattened into a broad band of reflectors in the middle crust. In contrast, Perz (1992) suggested deep crustal extent, or possibly crustal penetration, for the fault zone. This hypothesis was based on the observed differences in structural style on either side of the fault and the lack of evidence (no recorded image) for mid-crustal continuity of the horizontal band of reflectors across the fault. This is fundamental to the interpretation of the Fraser-Straight Creek Fault and other faults within the region and requires more data to resolve.

1.4.3 LITHOPROBE Phase II Refraction Surveys

Two refraction surveys, SCoRE '89 and SCoRE '90, were completed during Phase II of the LITHOPROBE program. Analyses of Lines 1 and 3 of SCoRE' 89 and Line 10 of SCoRE '90 are highly relevant to the interpretation of the Line 2 data. Line 1 of SCoRE '89 crosses Quesnellia in the Intermontane Belt and is coincident with Line 2 at the easternmost end of the survey (Figure 1). Analysis of these data (Zelt et al., 1992) reveal that the velocities in the upper and middle crust are typically 6.2 - 6.3 km/s with the base of the middle crust at about 24.5 km. In the lower crust, velocities average 6.5 - 6.7 km/s. No significant lateral or vertical velocity contrasts were observed in the upper crust; however, the data indicated a pronounced velocity contrast at the middle-lower crust boundary. Zelt et al. (1992) concluded that the observed crustal velocities typify the rocks of the Quesnellia terrane of the Intermontane Belt. The crust-mantle boundary was modelled at 34 km depth. Upper mantle velocities varied slightly from south to north, 7.9 - 7.7 km/s, respectively.

Similar to Line 2, Line 3 of SCoRE '89 was cross-strike the Fraser Fault system, running from the Intermontane Belt across the Coast Belt into the eastern edge of the Insular Belt on Vancouver Island. Three of the shot points (SP8, SP9 and SP10) were recorded by both Line 2 and Line 3. The velocity structural model presented by Zelt et al. (1993) featured a crustal section divided into three layers with a pronounced increase in velocity values from east to west across the Harrison Fault (refer to Chapter 4). Zelt et al. (1993) interpreted this contrast as the position of the suture of the Insular and Intermontane superterranes, consistent with the reflection data (Varsek et al., 1993). In the Insular Belt, the data indicated a thin crust (30 km) in contrast with previous estimates (37 - 45 km) as outlined above. Moho depths across the Coast and Intermontane Belts were consistent with other surveys in the region, typically 34 km, except below the Central Coast Belt where the Moho was modeled at 37 km depth.

The refraction survey Line 10 of SCoRE' 90 was completed entirely within the Coast Belt, coincident with the Harrison Fault along much of its length. Analysis of these data (O'Leary et al., 1993) indicated upper crustal velocities of 6.2 km/s, middle crustal velocities of 6.4 km/s and lower crustal velocities ranging from 6.5 km/s at the top to 6.7 km/s at the base of the lower crust. The depth to Moho was typically 34 km, below which upper mantle velocities were 8.0 km/s or greater. O'Leary et al. (1993) concluded that the position of Line 10 must be the easternmost extent reached by Wrangellia as the Line 10 crustal velocity values were more representative of the Intermontane Belt (Zelt et al., 1992) than of the Coast Belt (Zelt et al., 1993).

1.5 Other Geophysical Studies

Other geophysical parameters which must be integrated into any analysis of seismic data are results from heat flow, gravity and electromagnetic studies. Geothermal data acquired along the LITHOPROBE Southern Cordillera Transect have recently been compiled with existing data (Lewis et al., 1992). The general pattern indicates that crustal temperatures are

low on the continental shelf and decrease eastward across Vancouver Island to extremely low values at the western edge of the Coast Belt. In the Coast Belt, the heat flow pattern changes abruptly from very low values to extremely high values over a 20 km transition just west of the Garibaldi Volcanic Belt. East of the transition zone heat flow values subside to a moderately high average value which is maintained throughout the Intermontane and Omineca Belts. The heat flow pattern is interpreted to be a result of the 'heat sink' effect of the subducting Juan de Fuca Plate and is consistent with the heat flow patterns at trench and island arc continental margins (Hyndman et al., 1976, Lewis et. al, 1988). The location of the sharp transition to high heat flow values corresponds to an apparent lateral discontinuity in the crust-mantle boundary observed by Berry and Forsyth (1975). High temperatures in the Intermontane Belt indicate a thin crust, consistent with past and present seismic data.

Gravity anomaly data across the study region are characteristic of active subduction zones (Riddihough, 1979). The data reveal a band of negative Bouguer values over the trench, a band of positive values across Vancouver Island and the Strait of Georgia, and a wide region of negative Bouguer values in the Coast and Intermontane Belts. Positive Bouguer values across Vancouver Island conflict with the seismic work prior to the 1980's which indicated a thick crust beneath Vancouver Island. Both Stacey (1973) and Riddihough (1979) concluded that there must exist a wedge of high-density material overlying the downgoing Juan de Fuca plate to account for the gravity high. It was revealed in the seismic work of the 1980's that a wedge of high-velocity and high-density material existed in the lower crust corresponding to a region between two prominent reflectors, the 'C' and 'E' reflectors. Recent gravity modelling by Dehler and Clowes (1992;1995) incorporated this information and concluded that a wedge of material with higher than normal crustal density (3140 kgm^{-3}) was required to satisfy the gravity data. Farther landward, the large gravity low does not result from a thick crust compensating high surface topography, since seismic results indicate a thin crust in the interior. Rather, the density of the upper crust is lower in the Coast Belt, consistent with the presence of lower density plutonic rocks (Dehler and Clowes, 1995). Or, mantle densities must be lower in the Coast and Intermontane Belts to produce the

negative Bouguer anomaly (Stacey, 1973). Low mantle densities are also consistent with high heat flow in the interior (Lewis et al., 1985).

Electromagnetic studies in the southern Cordillera reveal high electrical conductivity in the lower crust and upper mantle (Gough, 1986). Associated with high heat flow, a thin crust, and a low-velocity mantle, this indicates that mantle upwelling over the Juan de Fuca subduction zone may dominate the tectonics of the region. Detailed studies in the region have revealed an abrupt lateral variation in conductivity of the upper and lower crust across the Fraser Fault system (Jones et al., 1992a). Values indicate that the Intermontane Belt is less resistive in the upper crust and more resistive in the lower crust than the Coast Belt. Higher resistivity values observed in the upper crust of the Coast Belt can be attributed to the presence of dry (highly resistive) plutons in the Coast Belt. More conductive values in the lower crust of the Coast Belt may be due to a slight increase in porosity or salinity of pore fluid, or the presence of partial melt (Jones et al., 1992a). The Insular Belt has resistivity values similar to the Coast Belt with no significant changes across the morphogeological boundary. The resitivity variation observed across the Fraser Fault system indicates that the fault may penetrate the whole crust (Jones et al., 1992b), consistent with the analysis of seismic reflection profile 88-18 by Perz (1992).

II: DATA ACQUISITION AND PROCESSING

2.1 Data Acquisition

2.1.1 SCoRE '89 Experiment Geometry

The Southern Cordillera Refraction Experiment (SCoRE '89) was a LITHOPROBE funded survey resulting in more than 14,000 km of mostly-reversed in-line and broadside seismic data. Institutions involved in this survey include the Universities of British Columbia, Alberta, Victoria, Saskatchewan, Manitoba and Western Ontario/Nagoya, the Geological Survey of Canada (GSC) and the United States Geological Survey (USGS).

The experiment employed the Spatial Seismic Refraction Recording (S^2R^2) method (Kanasewich and Chui, 1985) to obtain 2-D and 3-D coverage of the crust and upper mantle. The survey consisted of six recording lines. Three lines formed a triangular array centered over the Fraser Fault system; the western and southern lines were extended from the apex of the triangle onto Vancouver Island (Figure 1). Three smaller profiles, not shown on Figure 1, were deployed within the triangle. Broadside data were obtained by recording shots from each apex of the triangle, the center of each leg, and the center of the array. In-line data provide the basis for developing 2-D structure along each leg whereas broadside data provide the coverage for a 3-D tomographic study of the interior of the array.

Lines 1, 2 and 3 complete the triangle while Lines 4, 5 and 6 were deployed within the array. The specifics of each line are given in Table 1. One leg of the triangle (Line 1, Zelt et al., 1992) ran north-south along strike within the Intermontane Belt. The other legs of the triangle were cross-strike lines running from the Intermontane Belt across the Coast Belt into the eastern edge of the Insular Belt on Vancouver Island. Line 2, which is the focus of this research, is oriented northeast-southwest. Line 3 (Zelt et al., 1993) is oriented east-west. The three shorter profiles provide additional in-line and broadside coverage in the region of the Fraser Fault system (Zelt et al., 1995).

Line Number	Length (km)	Shots recorded	Number of receivers	Ave. receiver spacing (km)
1	330	1-5, 7, 12, 16-19	269	1.2
2	**425**	**1, 3, 4, 6-15, 17, 20-22, 98, 99**	**265**	**1.6**
3	250	1,3,4,6-15,17,20-22	198	1.25
4	80	1,3,4,7,8,12,17,20-22	60	1.35
5	25	1-4,7,12,16-19	20	1.35
6	40	1,3,4,7,8,12,17,20-22	22	2.0

TABLE 1. SCoRE '89 Line Specifications.
Line 2 is designated in bold. In-line data recorded on Line 2 included shot points 1, 6, 8-15, 98 and 99. Broadside data recorded on Line 2 included shot points 3, 4, 7, and 20-22.

Shot Point	Shot Size (kg)	Recorded Traces
8	1800	259
9	200	265
10	200	265
11	200	259
6	200	264
12	800	259
13	200	261
14	200	261
15	200	249
1	1800	264

TABLE 2. Shot Sizes (kg) and the Number of Recorded Traces for Line 2 of SCoRE '89.

Three different shot sizes (Table 2) were used throughout the survey to ensure complete coverage from the upper crust to the upper mantle. Larger shots (1800 kg of explosives) were used at the vertices of the triangle, moderate shots (800 kg) were detonated near the centre of each line and smaller shots (200 kg) were used elsewhere. Line 2 recorded data from ten shot points on 265 portable seismographs. Average shot spacing was ~ 50 km. Seismographs were deployed at intervals varying from 0.2 to 4.5 km except across the Strait of Georgia, here a 20 km interval was required. A full description of the experiment and details of data acquisition is given in Zelt et al. (1990).

2.1.2 Shot and Receiver Site Positioning

Each of the shot points were positioned using Trimble Advanced Navigation Sensor GPS (Global Position System) instruments. Shot point (SP) positions for SP1, SP8, and SP10 to SP13 were obtained with 3-D global satellite fixes (i.e., 4 satellites used in the positioning solution) and are considered accurate to within 10 m. Positions for SP9, SP6, SP14 and SP15 were obtained from 2-D global satellite fixes and are considered accurate to within 50 m. Approximately 83% of the receiver sites for SCoRE '89 were positioned using 2-D or 3-D satellite fixes. The remaining sites were located using 1:50,000 topographic maps either because satellite fixes were unattainable or because sites were easily located with sufficient accuracy on the maps. Receiver positions are everywhere considered accurate to within 50 m or less. Elevations, which range from sea level to 1845 m on Line 2, were obtained by either 3-D satellite fixes or determined from 1:50,000 topographic maps. The accuracy in elevations is variable but they are generally accurate to within 10 m.

2.1.3 Instrumentation

During the SCoRE '89 experiment, instrumentation used to record the data consisted of 154 EDA model PRS1 digital systems, 120 USGS analog cassette recorders, 14 EDA model PRS4 digital systems, and 8 Geotech MCR 600 systems. Each of these seismograph units recorded the vertical component response of Mark Products L-4A 2 Hz or 1 Hz

seismometers. The relative velocity responses of these instruments were given in Zelt et al. (1990). Average receiver spacing varied along each line from 1.2 km to 2.0 km (Table 1). Along Line 2, a total of 265 instruments were deployed (145 PRS1 systems and 120 USGS analog cassette recorders) of which 39 instruments were located on Vancouver Island and smaller islands within the Strait of Georgia. The detonation time of the charges and the recording time of the seismograph units were controlled by a satellite-based timing system (GOES). Shot and receiver clock drifts were minimal, with an associated error in timing of less than 10 ms. Sixty seconds of data were recorded sampled at 120 Hz with traveltimes reduced at a velocity of 8.0 km/s.

2.2 Data Processing

2.2.1 Initial Data Reduction

The final format for the field data set was SEGY-LDS, version 2 (refer to SEGY-LDS Format Reference Document, Spencer et al., 1989). In this format, unfiltered data were sampled at 120 Hz and reduced at 8.0 km/s with no elevation corrections. Before final merging and updating of the data could be completed, some initial processing of the USGS data was necessary to make it compatible with the GSC data. Initial data processing was completed at the University of British Columbia (UBC) and is reported in Zelt et al. (1990). The USGS data were originally sampled at 200 Hz and written in SEGY format 3 (2 byte fixed point). These data were re-sampled at 120 Hz and converted to SEGY format 1 (4 byte floating point), consistent with the GSC data. Trace headers were updated with information such as shot and receiver co-ordinates and the USGS and GSC data sets were merged. The complete SCoRE '89 data set was received from the University of British Columbia at the University of Victoria in May of 1990.

2.2.2 Filtering

Subsequent processing of the Line 2 data set included filtering to improve the signal-to-

noise ratio. A bandpass 5-20 Hz Butterworth filter was applied to the data. Testing revealed that a narrower bandpass range did not significantly improve the signal-to-noise ratio and increased the risk of removing important information. This also proved to be the optimum range to filter the data based on the frequency responses of the GSC and USGS instruments. With a larger bandpass range, the complication of picking traveltimes from both unfiltered and filtered data was minimized. For the most part, traveltime picking was completed on the filtered record sections.

2.2.3 Scaling

Each of the record sections were plotted using two different scaling methods. Trace equalized or common maximum amplitude plots refer to plots in which the maximum amplitude on each trace was set to a fixed level and the rest of the trace was scaled accordingly. Trace equalization improves continuity and makes phase identification easier, especially in regions where the signal-to-noise ratio is low. True amplitude plots refer to plots in which amplitudes were corrected for spherical spreading. Each trace was scaled by a function of distance, d, from the shot point, typically $d^{1.5}$. The only exception for the scaling function was for SP14. The near-offset energy attenuation for this shot point was unusually large in comparison to the other 200 kg shot points, and so amplitudes on this record section were scaled by a function of $d^{1.0}$. True amplitude plots were necessary to obtain information for amplitude modelling of synthetic seismograms. Both displays were used in the analysis of the data to ensure accurate phase identification. No amplitude variations were observed between traces recorded by the GSC or USGS seismographs. All data traces were reduced and plotted using an 8.0 km/s velocity.

2.2.4 Editing

Editing was required for the true amplitude record sections to remove traces with high noise levels as these interfered with the identification of phases and picking of traveltimes. The number of traces deleted for each shot point along Line 2 is given in Table 3. High noise

level traces were removed only when they interfered with good traces. High noise levels were particularly evident on the smaller shot points. Some of these record sections required extensive editing to allow observation of weak crustal arrivals, and so gaps in data coverage were produced. During traveltime picking, continuous reference was made to the trace equalized record sections to ensure that no important information was deleted by the editing process. Approximately 14 % of the traces were removed from the dataset during editing. As an example, the true amplitude record section for shot point 6 is shown in Figure 3. On Figure 3a, noisy regions occur over the distance ranges 40-75 km, 120-140 km, and 155-200 km; on Figure 3b, strong arrivals are clearly seen after the high noise level traces are removed.

Shot Point	Number of Deleted Traces
8	32
9	33
10	61
11	40
6	27
12	12
13	30
14	44
15	48
1	33

TABLE 3. Number of Edited Traces per Record Section.
The number of traces which were deleted due to excessive noise are specified for each shot point.

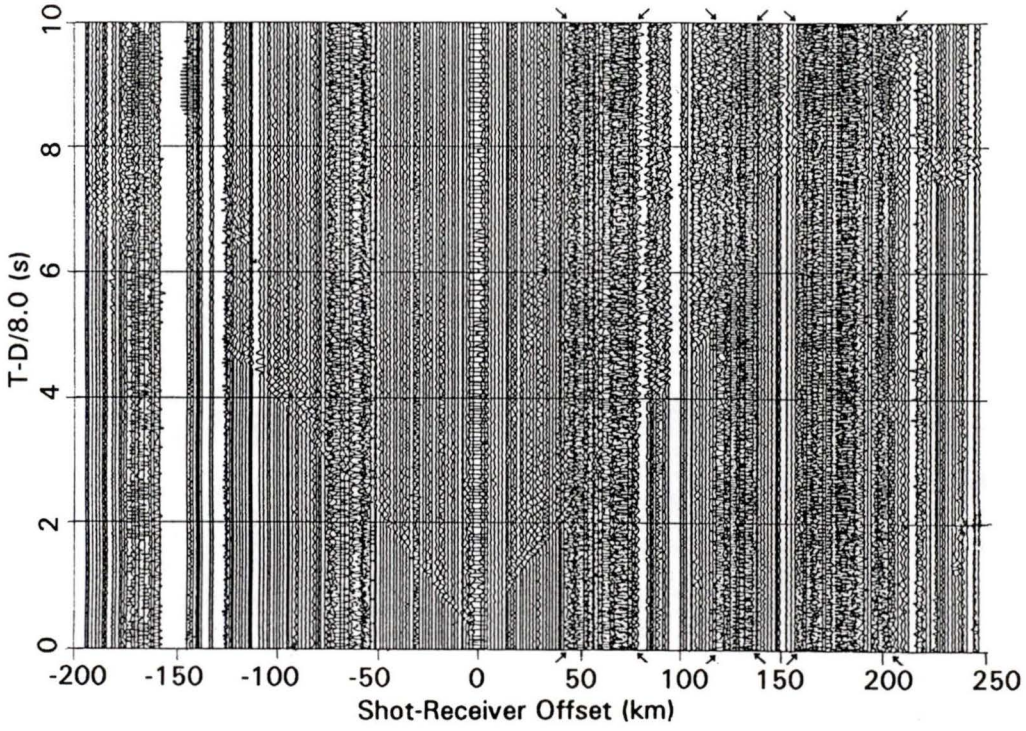

FIGURE 3a. True amplitude record section for shot point 6 (200 kg) before editing. Areas where high noise level traces interfere with phase identification and picking of traveltimes are indicated at 40-75 km, 120-140 km and 155-200 km offsets.

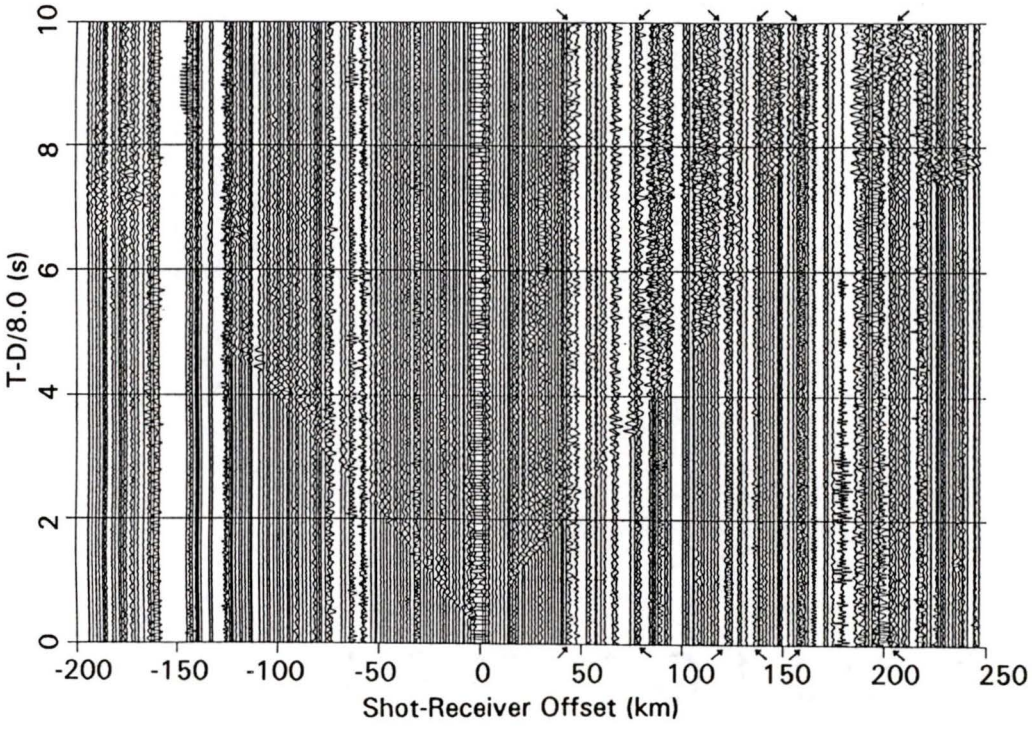

FIGURE 3b. True amplitude record section for shot point 6 after editing. Strong arrivals are clearly visible after high noise level traces are removed.

III: DATA ANALYSIS AND METHOD OF INTERPRETATION

3.1 Data Quality and Characteristics

The ten record sections of SCoRE '89 Line 2 are shown in true amplitude format in Figures 4a - 13a, corresponding to shot points SP8 to SP11, SP6, SP12 to SP15 and SP1, respectively. The traveltime axis corresponds to time reduced at 8.0 km/s. Two distance axes are displayed; the bottom axis refers to shot-receiver offset (distance from the shot point to the receiver) and the top axis indicates the model distance with SP8, located on Vancouver Island, at 0 km. Reference to west (W) or east (E) denotes west or east of the shot point in question. The complete data set consists of 2606 traces of which 360 traces were deleted due to high noise.

Eight distinct phases have been identified on the ten record sections; Ps, Pg, and Pn correspond to refracted energy through the near-surface layer, upper crust, and upper mantle, respectively; R1 and R3 correspond to reflected energy from the base of the upper crustal unit and middle crustal unit, respectively; R2 corresponds to energy from a mid-crustal discontinuity; PmP corresponds to reflected energy from the Mohorovic discontinuity; and PPm corresponds to reflected energy from an upper mantle discontinuity. Not all of the phases are observed on all of the record sections largely due to low signal-to-noise ratios produced by energy attenuation or insufficient shot-receiver offsets. Table 4 displays which phases were observed on each of the record sections. Table 5 indicates the number of traveltime picks for each of the observed phases on each record section.

3.1.1 Data Quality

Data quality varies dramatically with shot size and location. The larger shots (SP8, SP12, and SP1) show clearly distinct phases resulting from refracted and reflected energy throughout the crust. However, SP8 (Figure 4a) does not record phases which can be identified as reflections from the Mohorovic discontinuity or as refracted energy through the

FIGURE 4:

(a) Observed record section for SP8 plotted in true amplitude format. The amplitudes are scaled by a function of distance, d, from the shot point, typically $d^{1.5}$. All data traces were reduced and plotted using an 8.0 km/s velocity. A bandpass filter (5-20 Hz) has been applied to the record section. The bottom axis refers to shot-receiver offset and the top axis indicates model distance. SP8, located in the Insular Belt on Vancouver Island, was at 0 km. The observed phases for the record section have been labelled for this and all other record sections.

(b) Comparison of observed (vertical bars with height equivalent to twice the traveltime pick uncertainty) and calculated (solid lines) traveltimes.

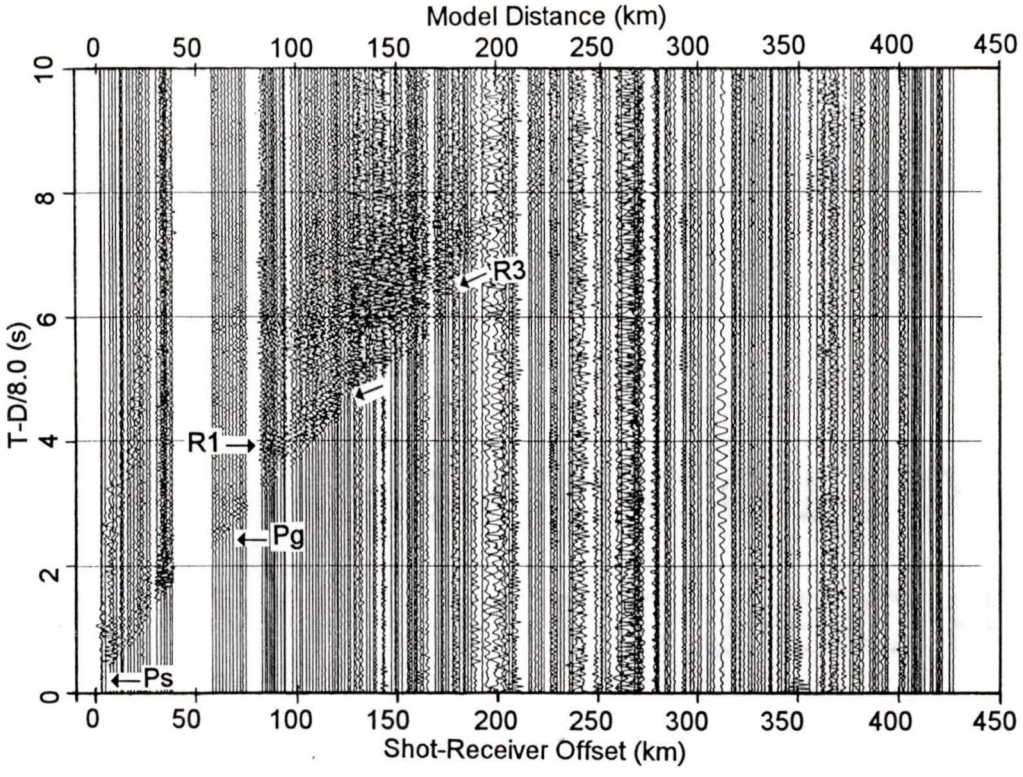
Model Distance (km)
0
50
100
150
200
250
300
350
400
450
T-D/8.0 (s)
0
2
4
6
8
10
R3
R1
Pg
Ps
Shot-Receiver Offset (km)

a)

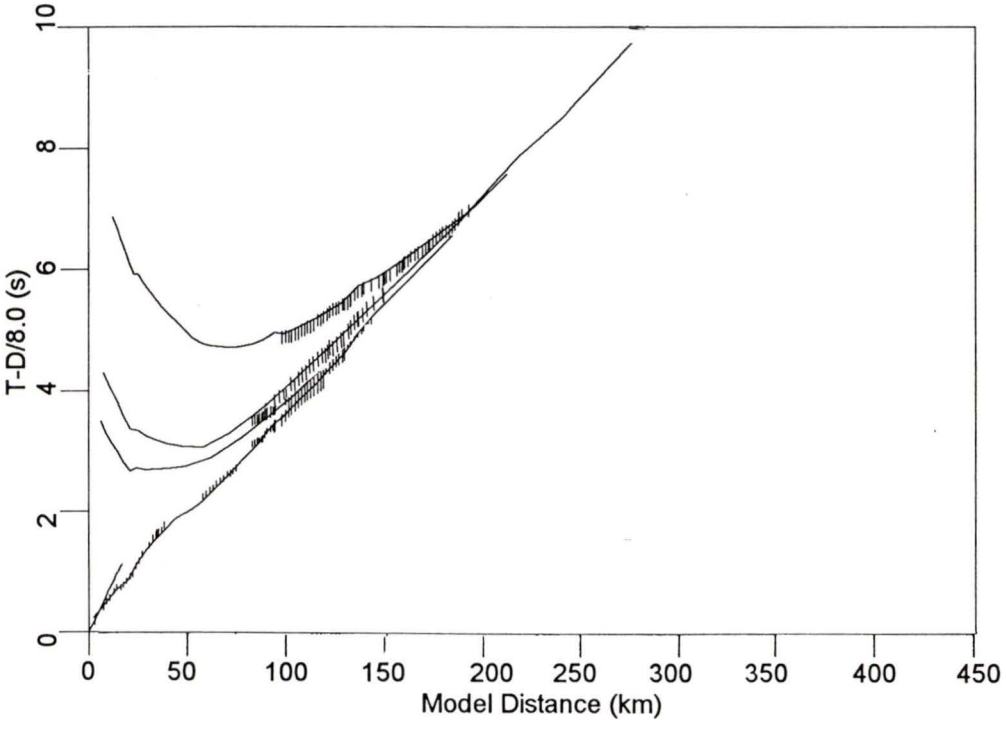
T-D/8.0 (s)
0
2
4
6
8
10
0
50
100
150
200
250
300
350
400
450
Model Distance (km)

b)

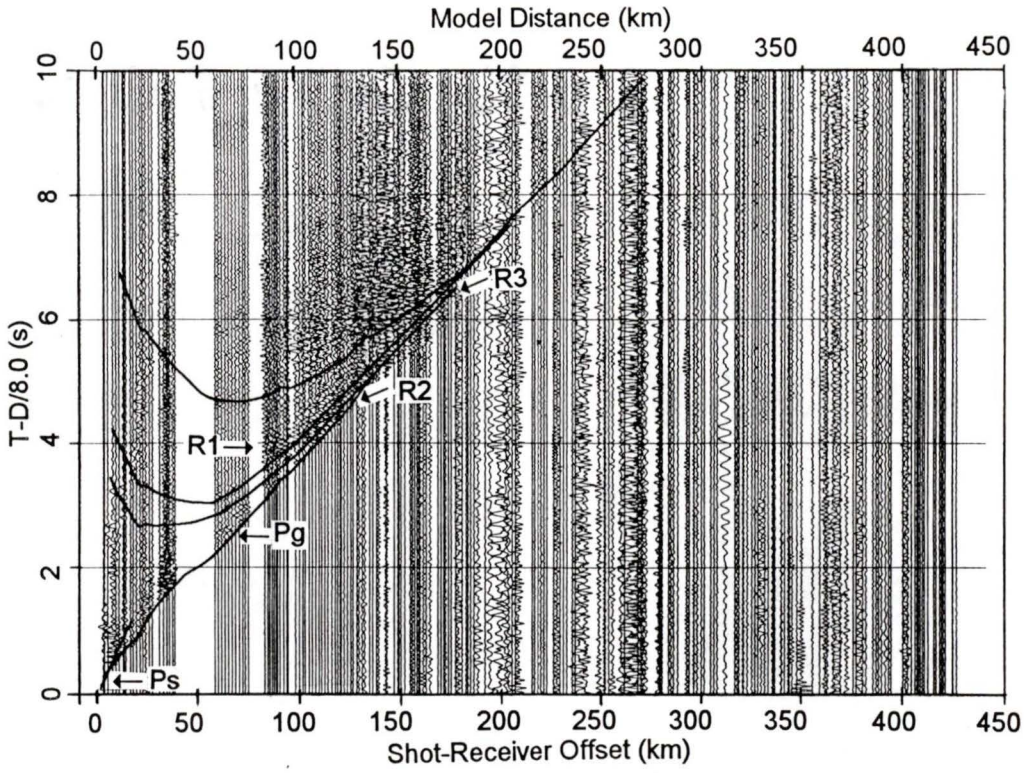

FIGURE 4: (c) Comparison of calculated traveltimes (solid lines) with observed phases. Record section is plotted in true relative amplitude format.

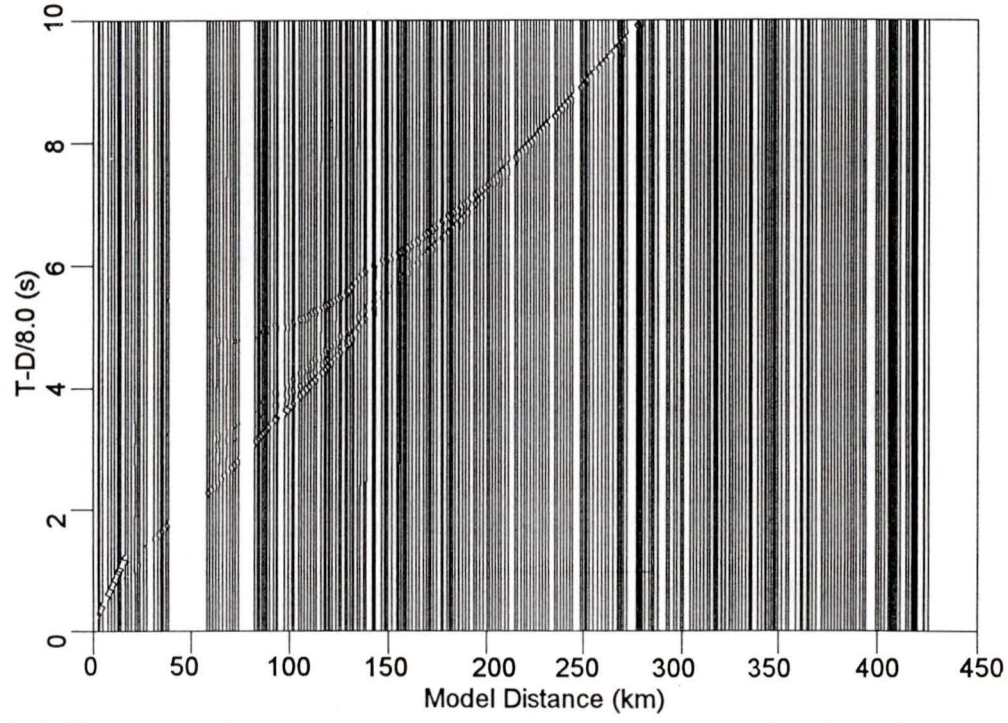

FIGURE 4: (d) Synthetic seismograms for SP8 with amplitude scaling as in (a). The synthetics were generated using a 4 Hz Ricker wavelet.

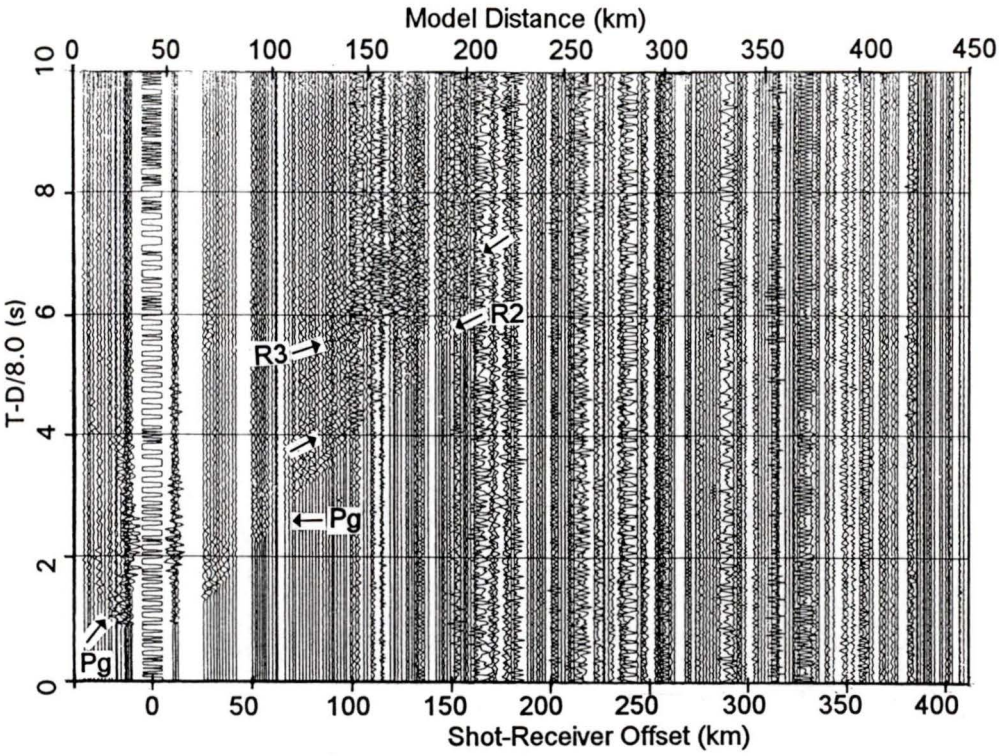

FIGURE 5: (a) Observed record section for SP9 located in the Insular Belt on Vancouver Island (see Figure 4 caption for plotting parameters and general description).

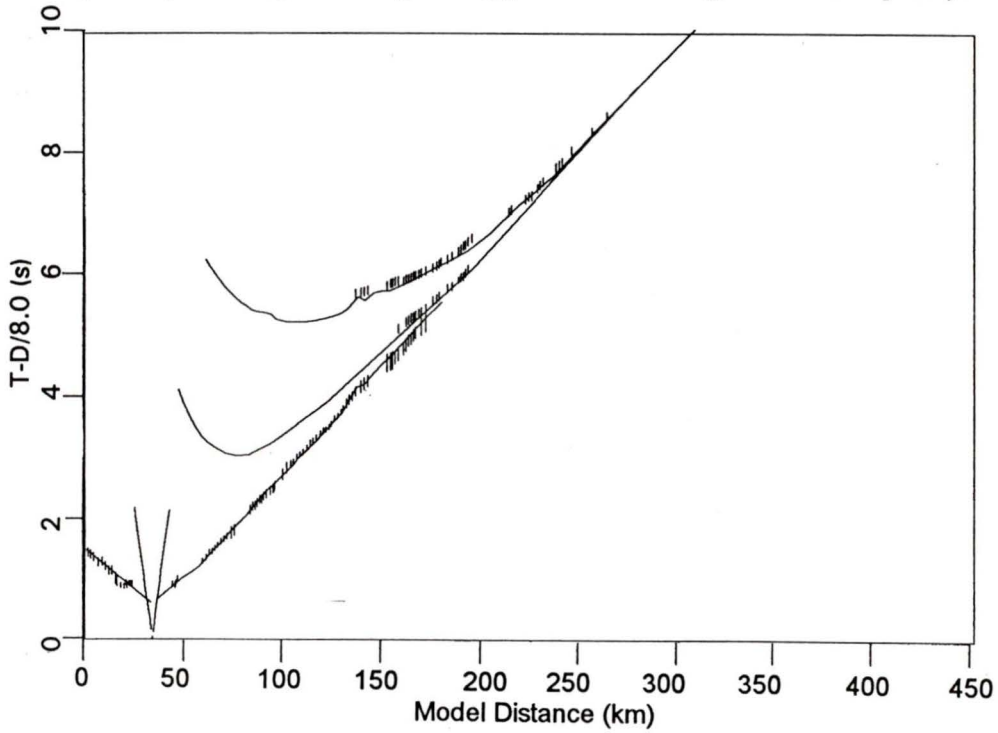

FIGURE 5: (b) Comparison of observed and calculated traveltimes (see Figure 4 caption for plotting style).

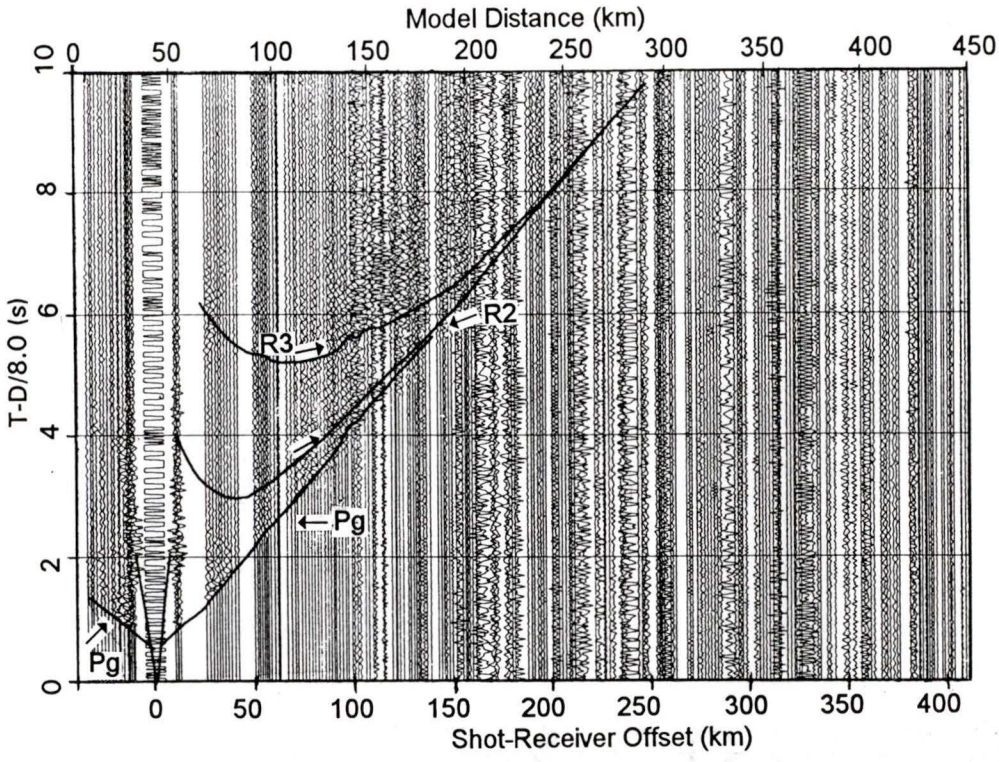

FIGURE 5: (c) Comparison of calculated traveltimes with identified phases (see Figure 4 caption for plotting parameters).

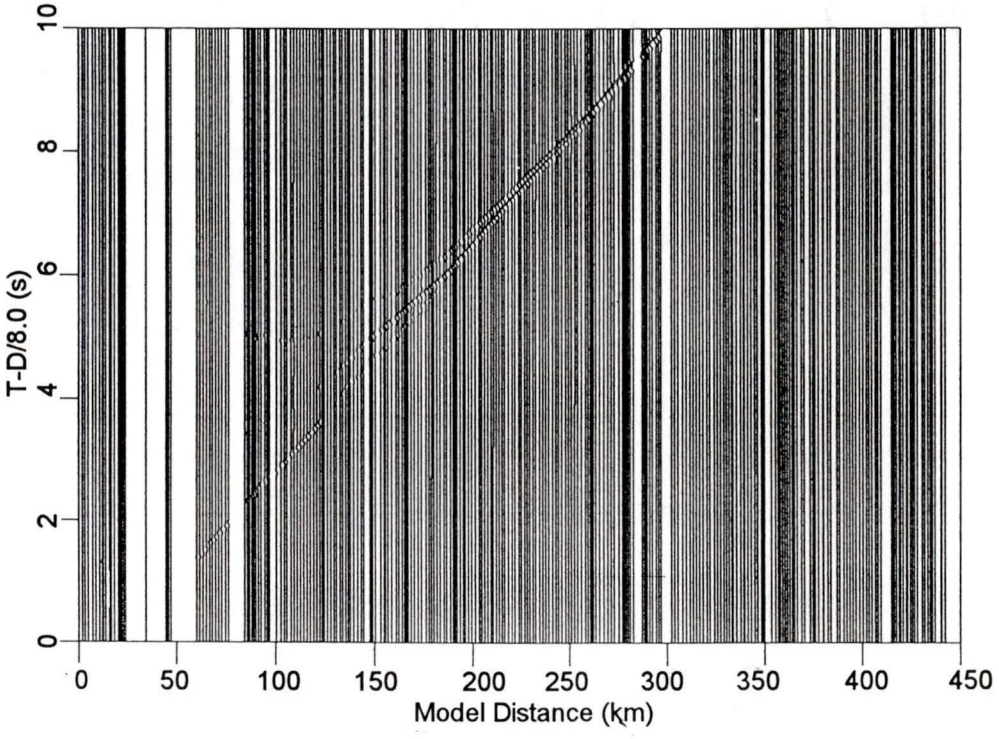

FIGURE 5: (d) Synthetic section for SP9 (see Figure 4 caption for scaling and wavelet).

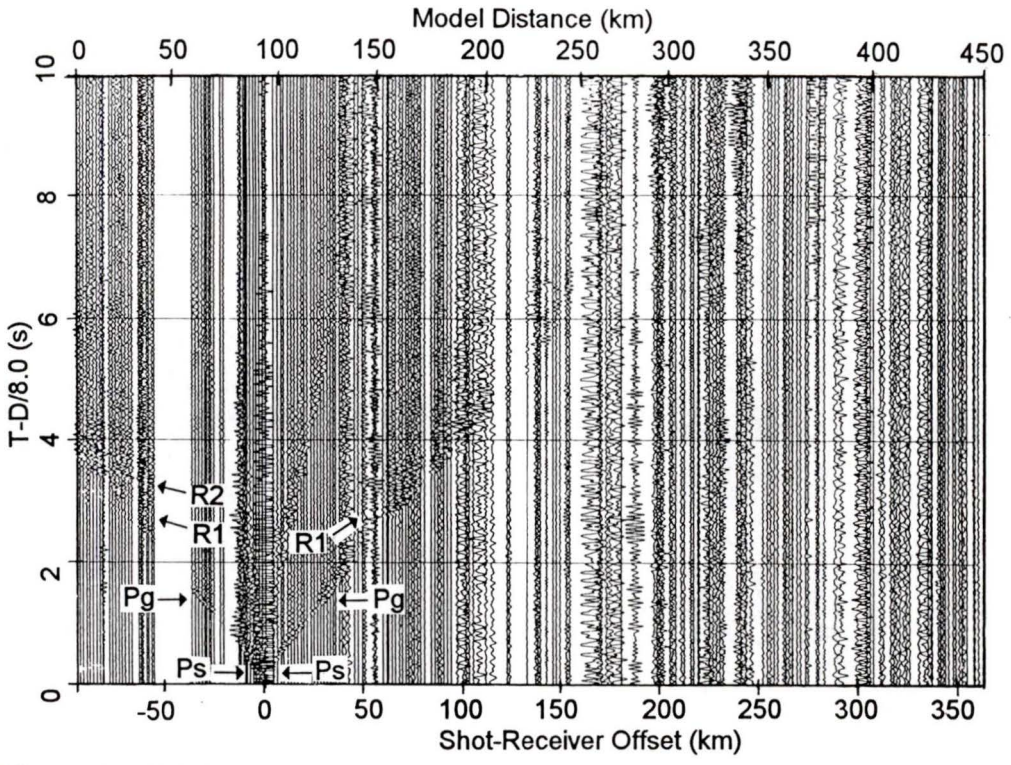

FIGURE 6: (a) Observed record section for SP10 located at the western edge of the Coast Belt near the metropolis of Vancouver (see Figure 4 caption for plotting parameters and general description).

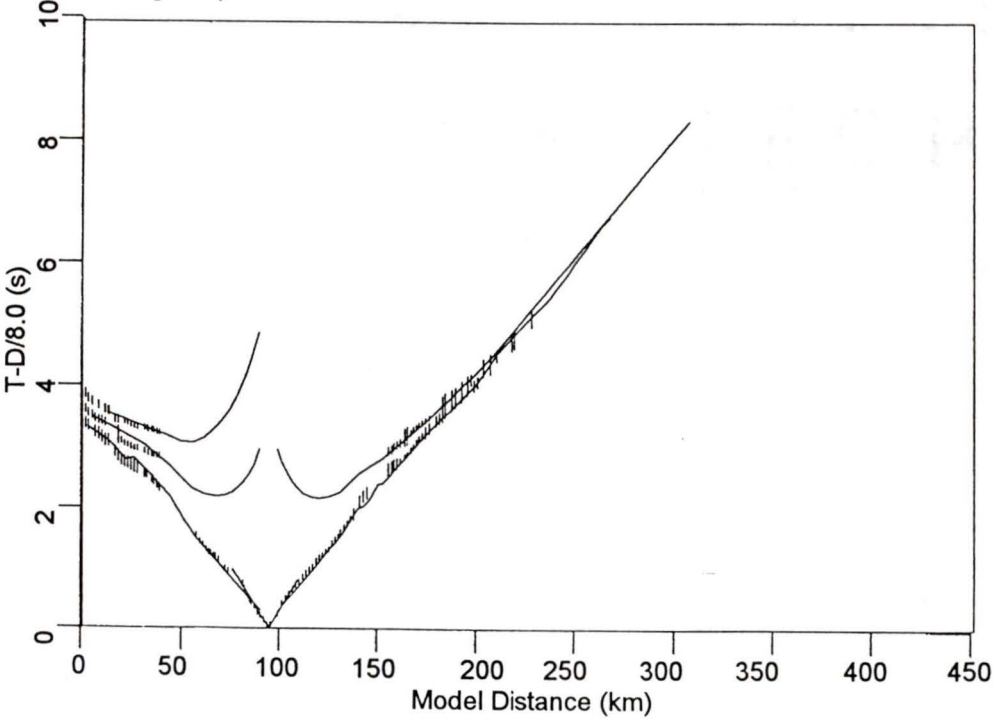

FIGURE 6: (b) Comparison of observed and calculated traveltimes (see Figure 4 caption for plotting style).

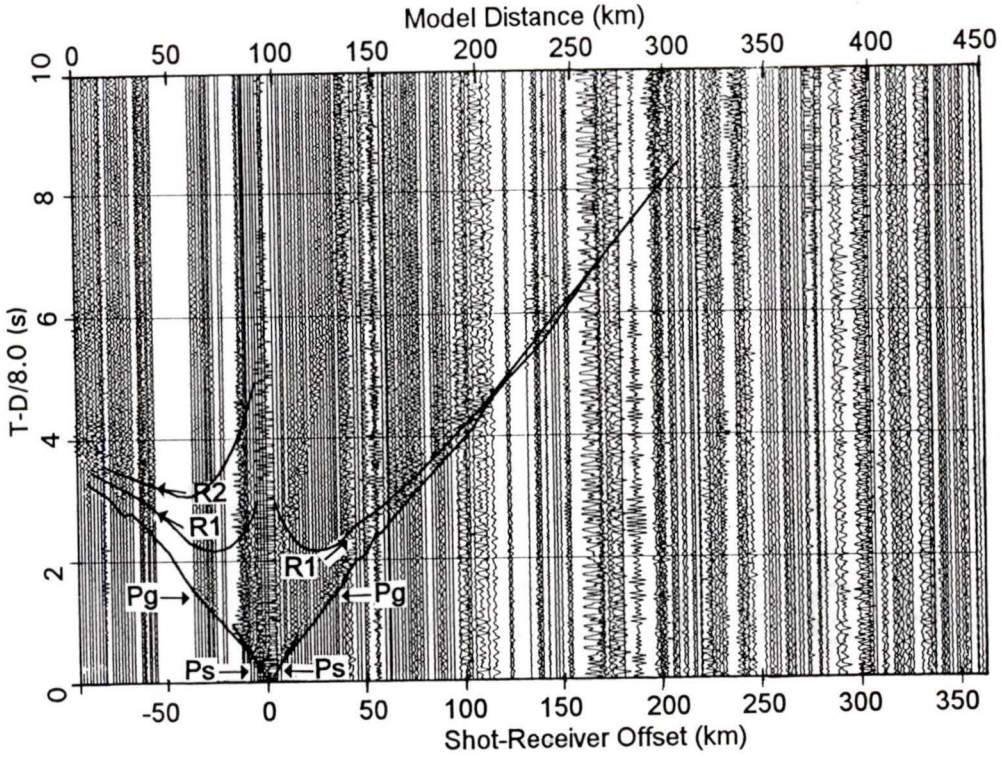

FIGURE 6: (c) Comparison of calculated traveltimes with identified phases (see Figure 4 caption for plotting parameters).

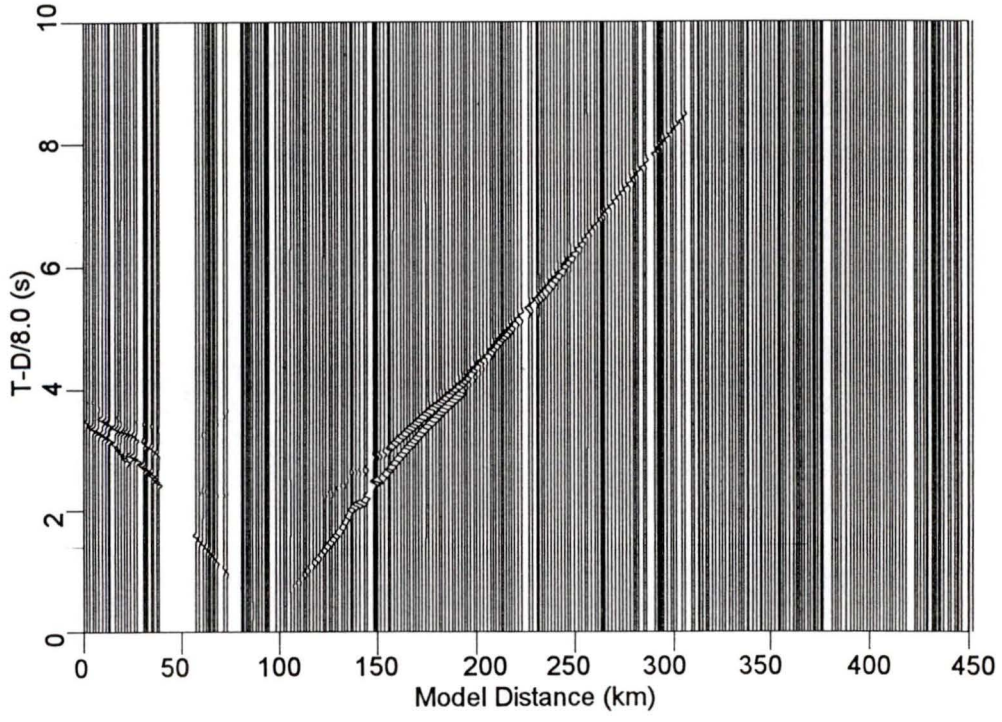

FIGURE 6: (d) Synthetic section for SP10 (see Figure 4 caption for scaling and wavelet).

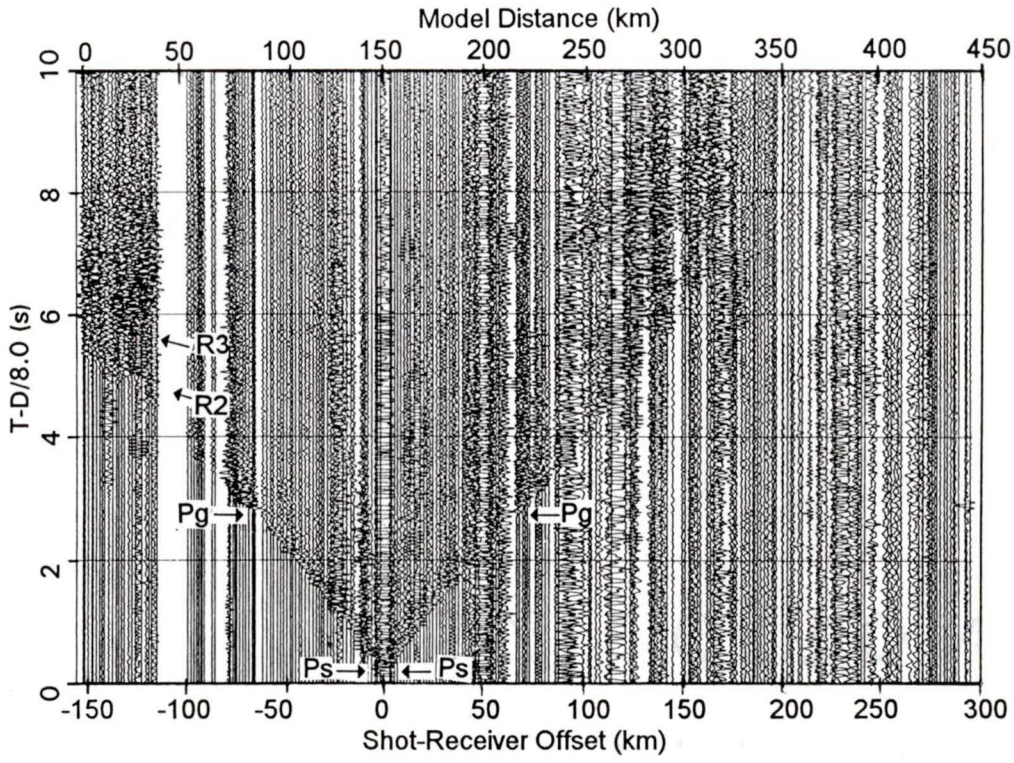

FIGURE 7: (a) Observed record section for SP11 in the Western Coast Belt (see Figure 4 caption for plotting parameters and general description).

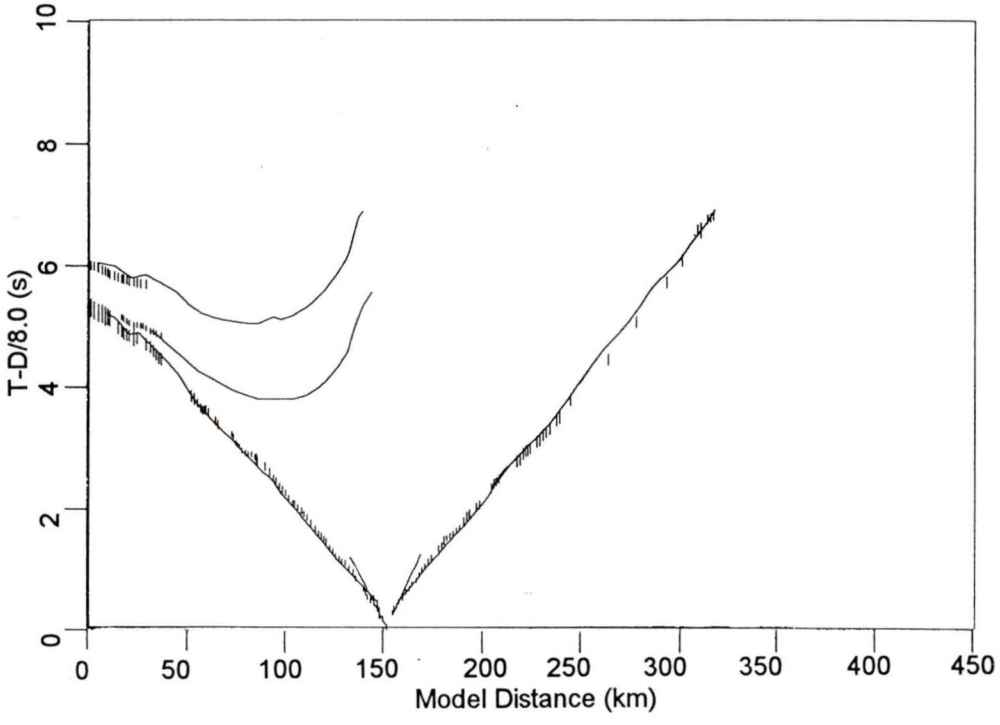

FIGURE 7: (b) Comparison of observed and calculated traveltimes (see Figure 4 caption for plotting style).

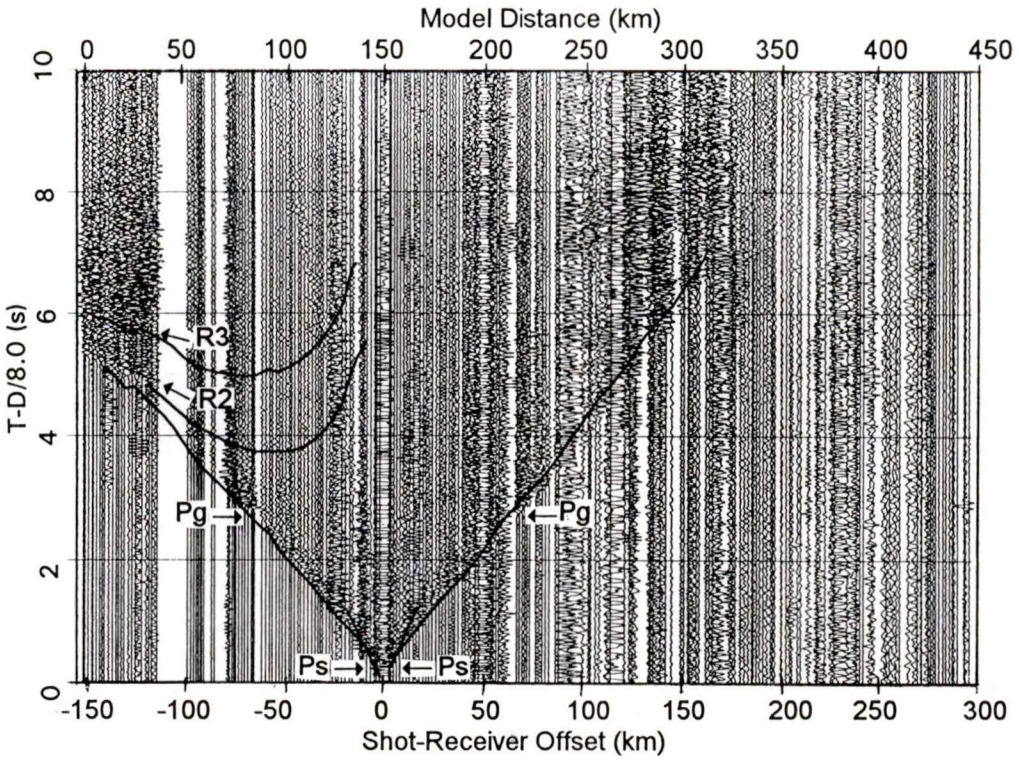

FIGURE 7: (c) Comparison of calculated traveltimes with identified phases (see Figure 4 caption for plotting parameters).

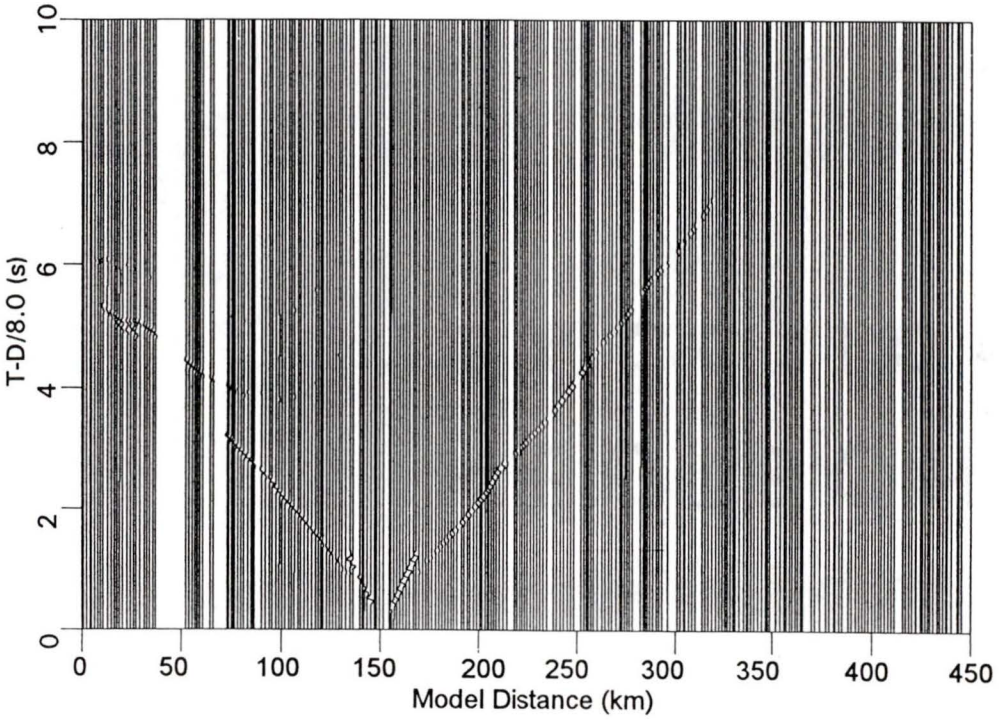

FIGURE 7: (d) Synthetic section for SP11 (see Figure 4 caption for scaling and wavelet).

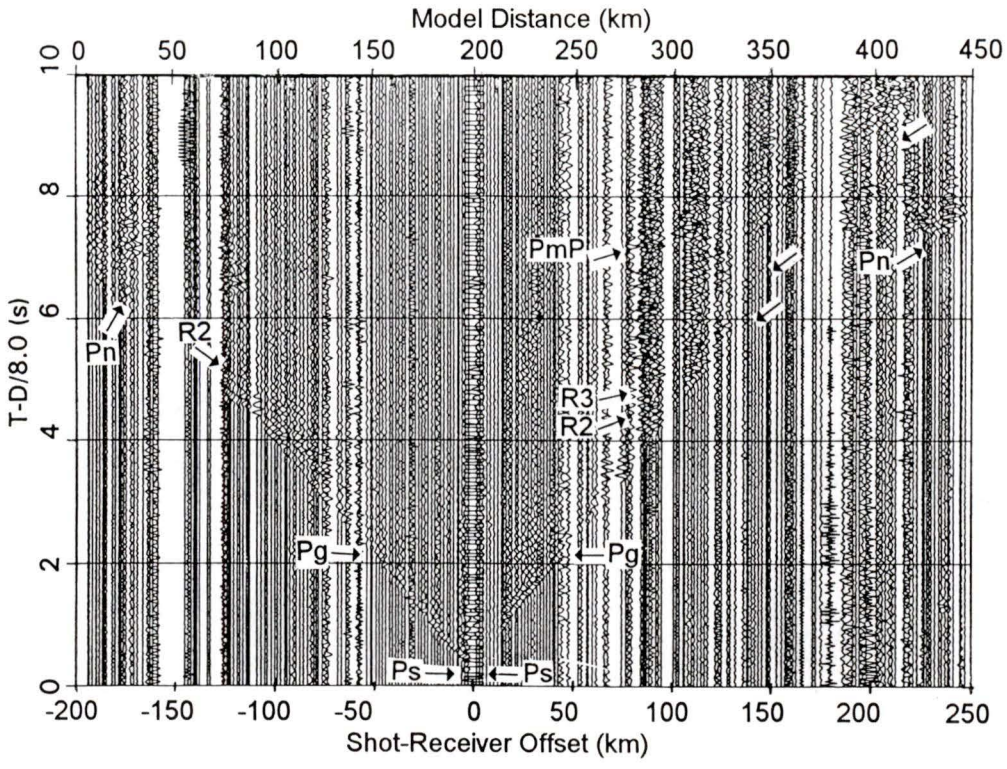

FIGURE 8: (a) Observed record section for SP6 which is located near the Harrison Fault (see Figure 4 caption for plotting parameters and general description).

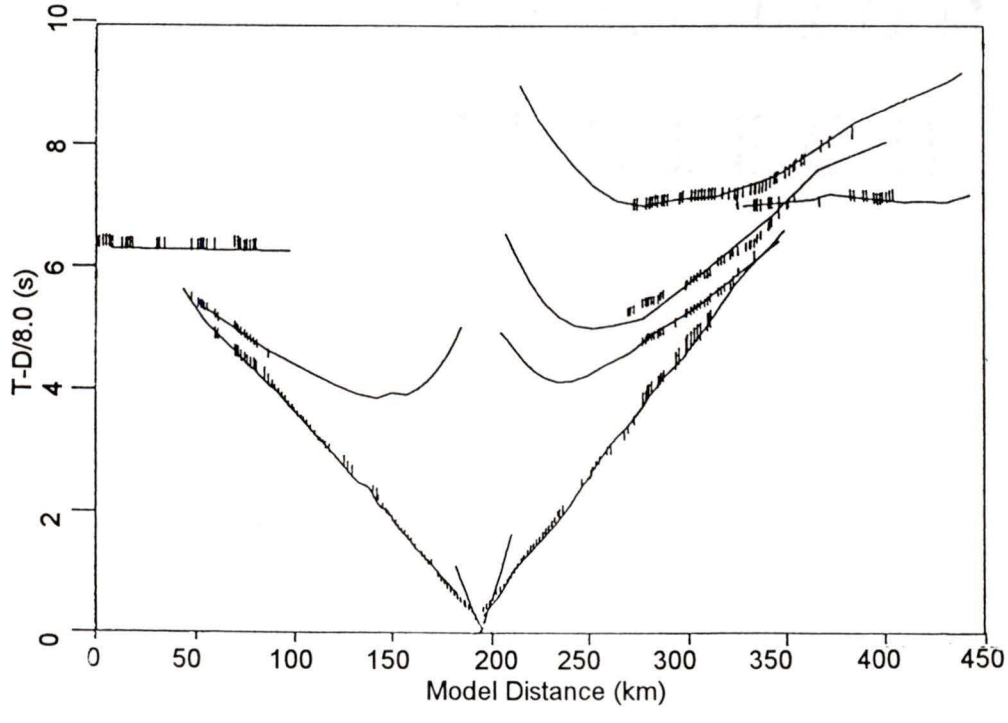

FIGURE 8: (b) Comparison of observed and calculated traveltimes (see Figure 4 caption for plotting style).

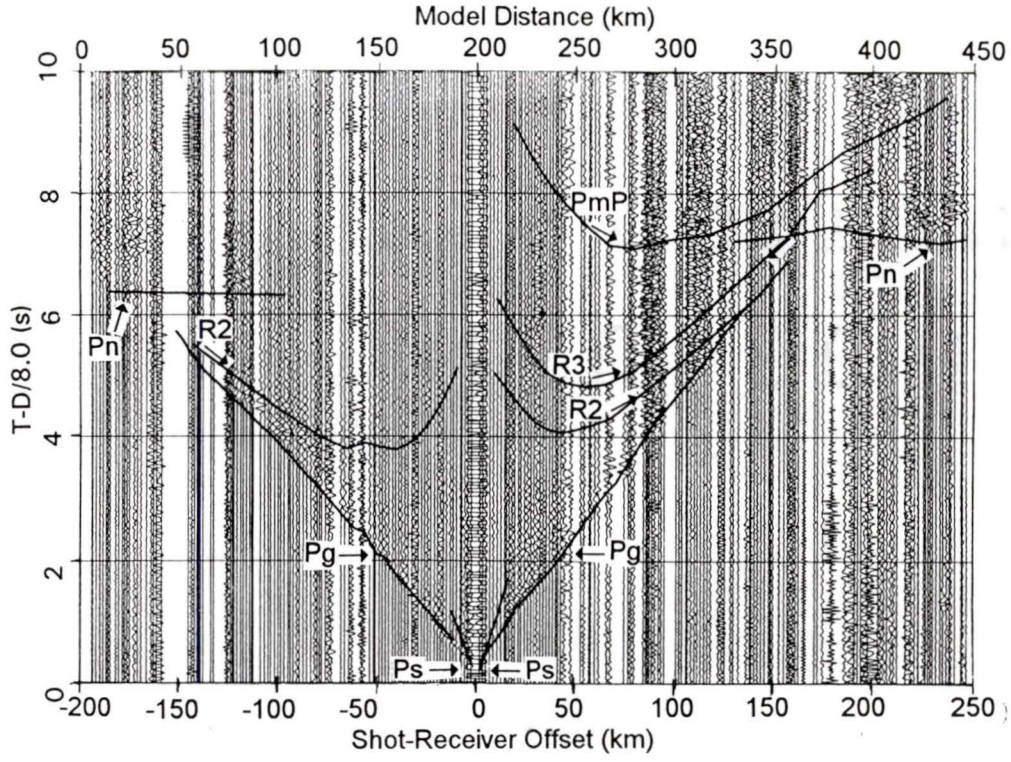

FIGURE 8: (c) Comparison of calculated traveltimes with identified phases (see Figure 4 caption for plotting parameters).

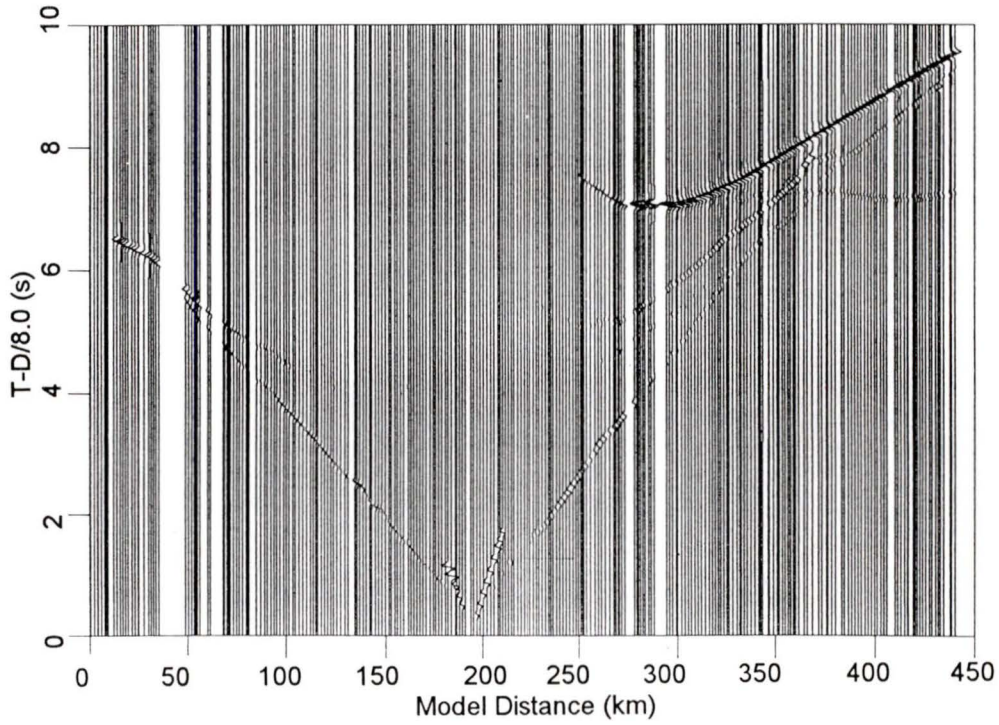

FIGURE 8: (d) Synthetic section for SP6 (see Figure 4 caption for scaling and wavelet).

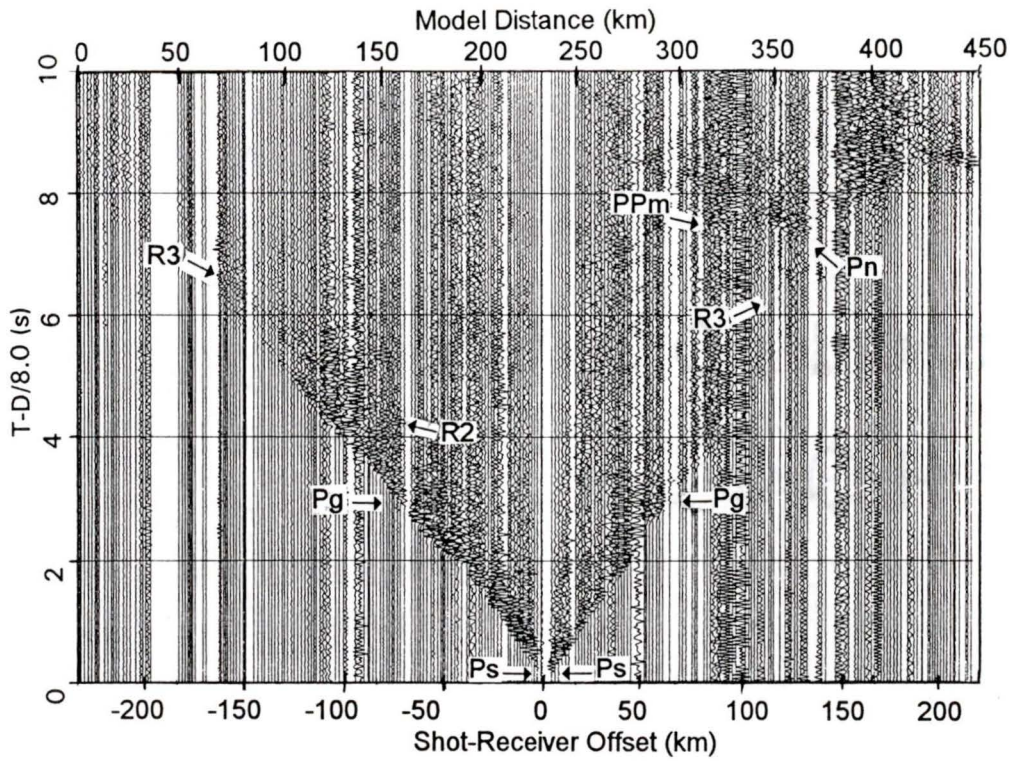

FIGURE 9: (a) Observed record section for SP12 in the Central Coast Belt (see Figure 4 caption for plotting parameters and general description).

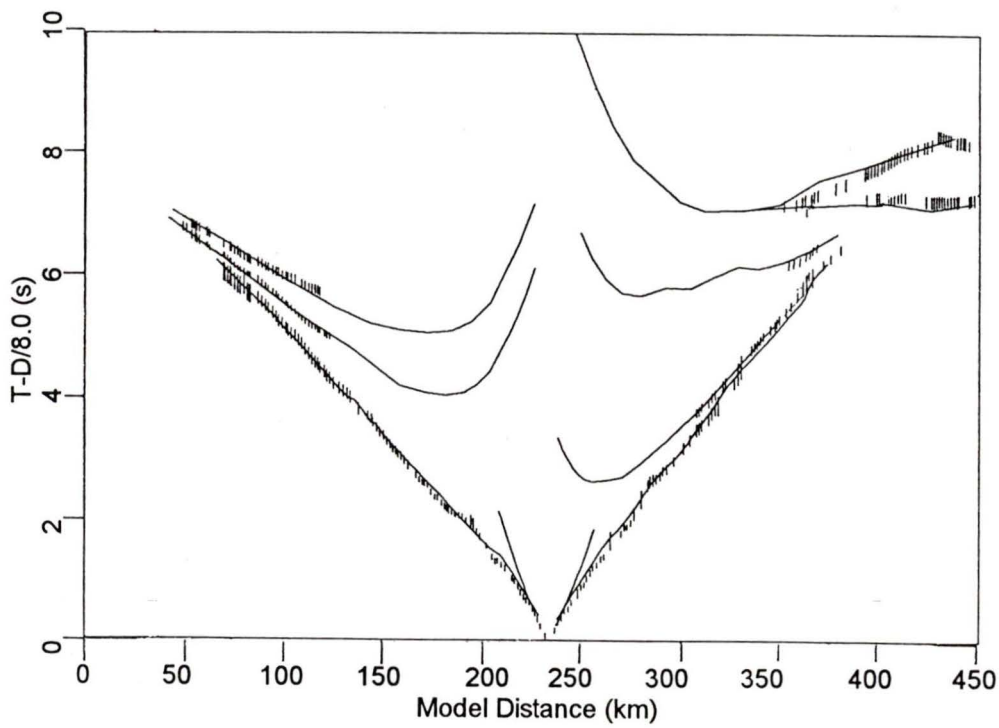

FIGURE 9: (b) Comparison of observed and calculated traveltimes (see Figure 4 caption for plotting style).

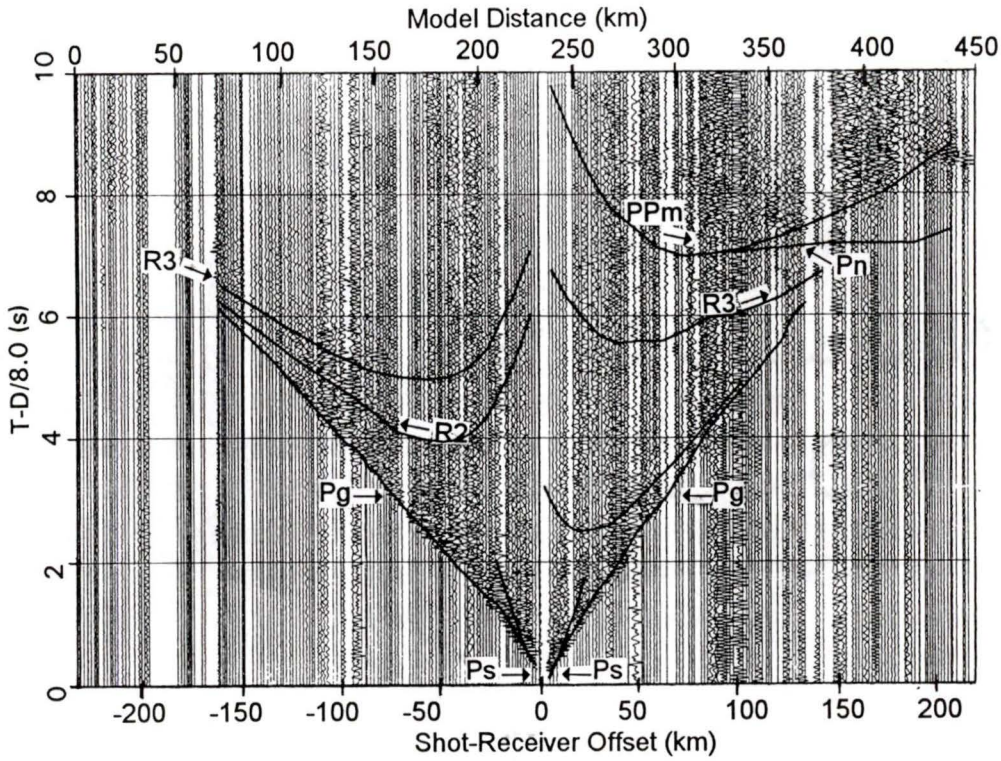

FIGURE 9: (c) Comparison of calculated traveltimes with identified phases (see Figure 4 caption for plotting parameters).

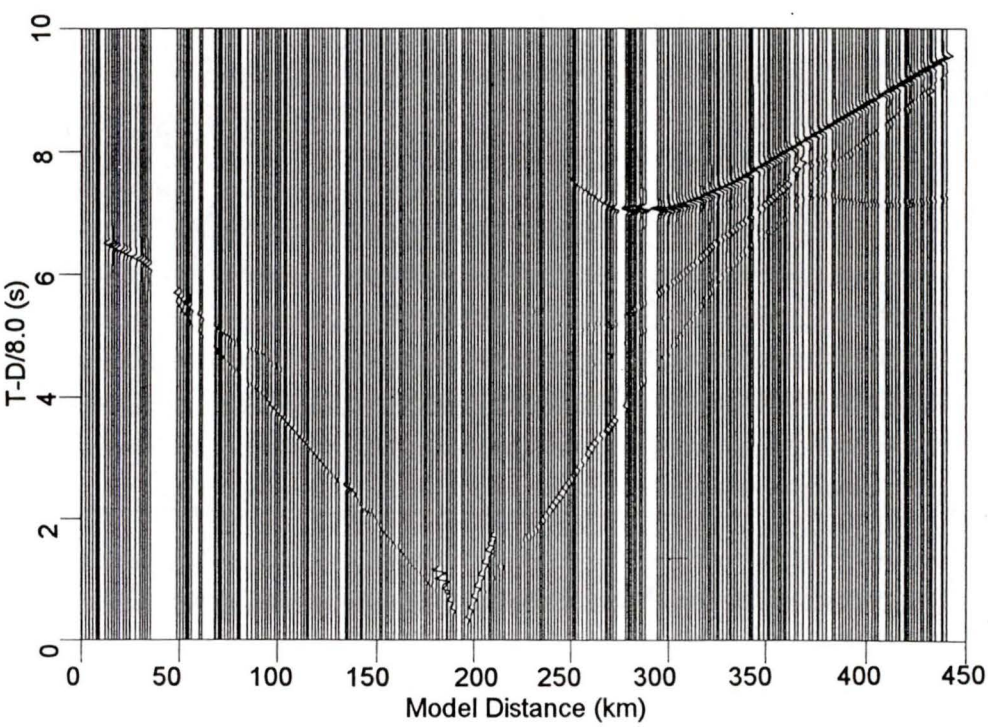

FIGURE 9: (d) Synthetic section for SP12 (see Figure 4 caption for scaling and wavelet).

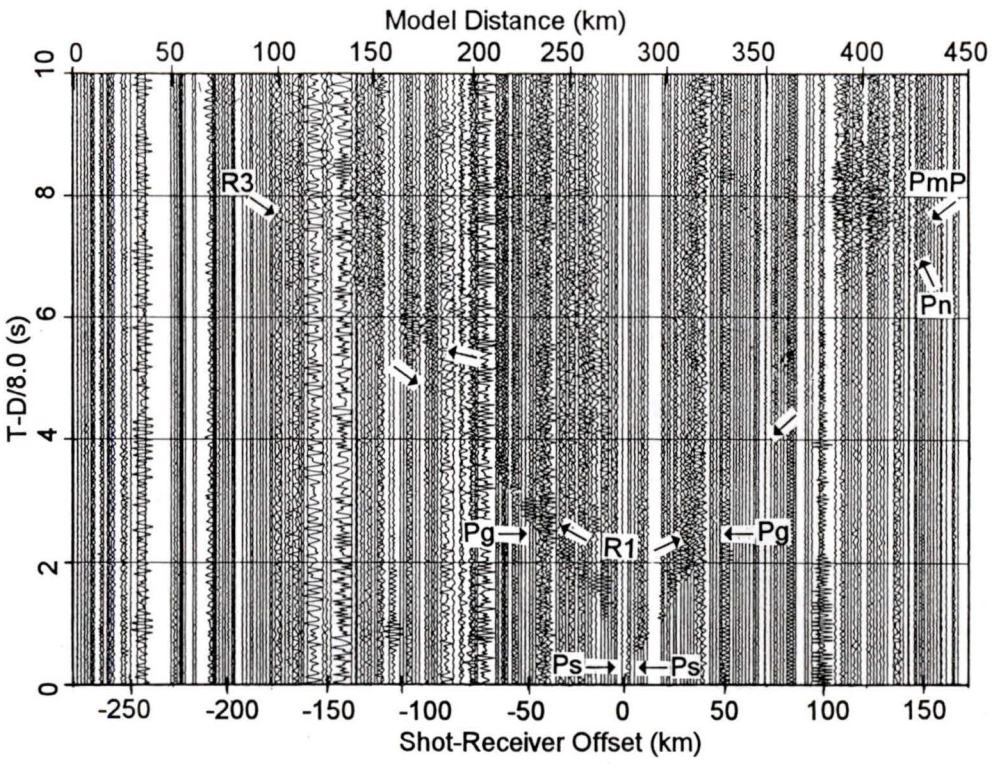

FIGURE 10: (a) Observed record section for SP13 which is located at the Fraser-Straight Creek Fault (see Figure 4 caption for plotting parameters and general description).

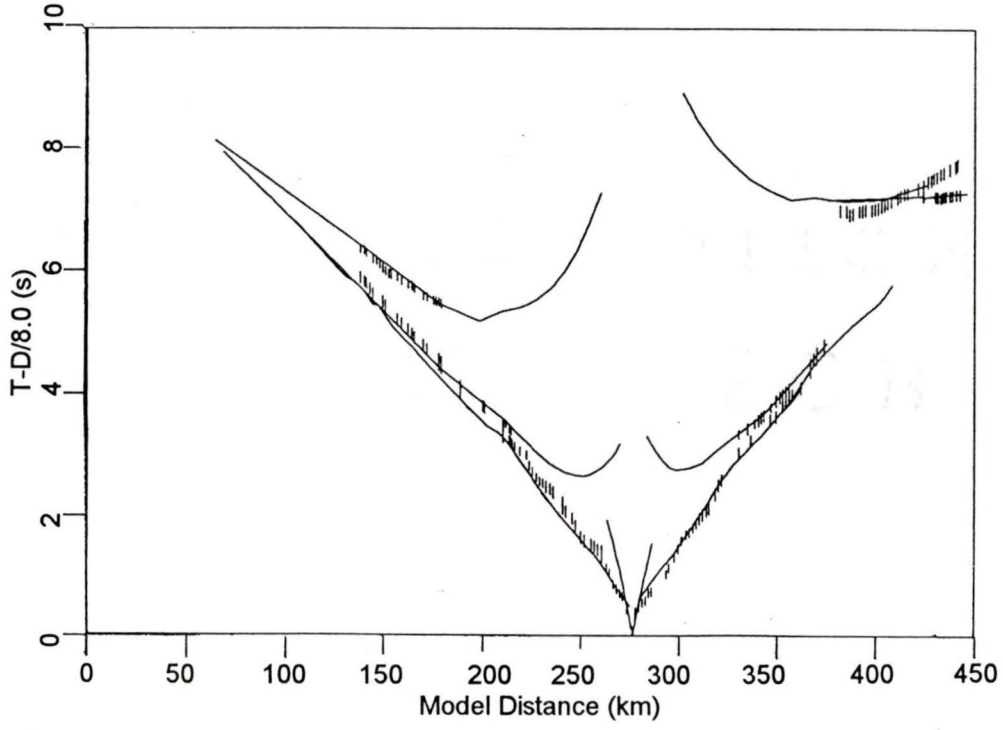

FIGURE 10: (b) Comparison of observed and calculated traveltimes (see Figure 4 caption for plotting style).

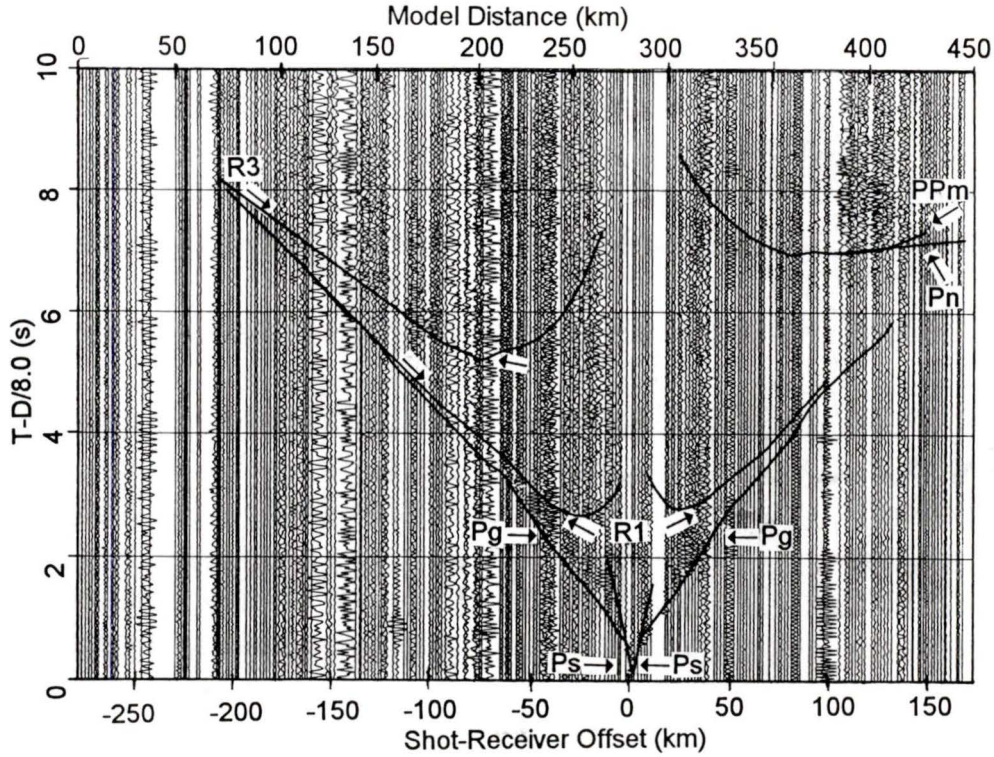

FIGURE 10: (c) Comparison of calculated traveltimes with identified phases (see Figure 4 caption for plotting parameters).

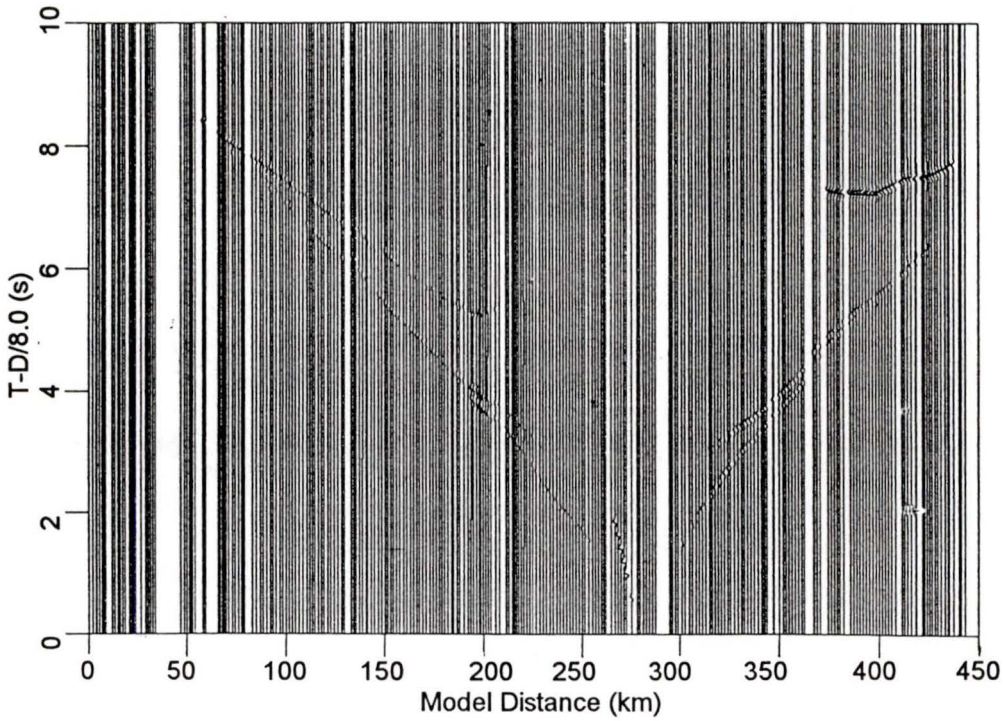

FIGURE 10: (d) Synthetic section for SP13 (see Figure 4 caption for scaling and wavelet).

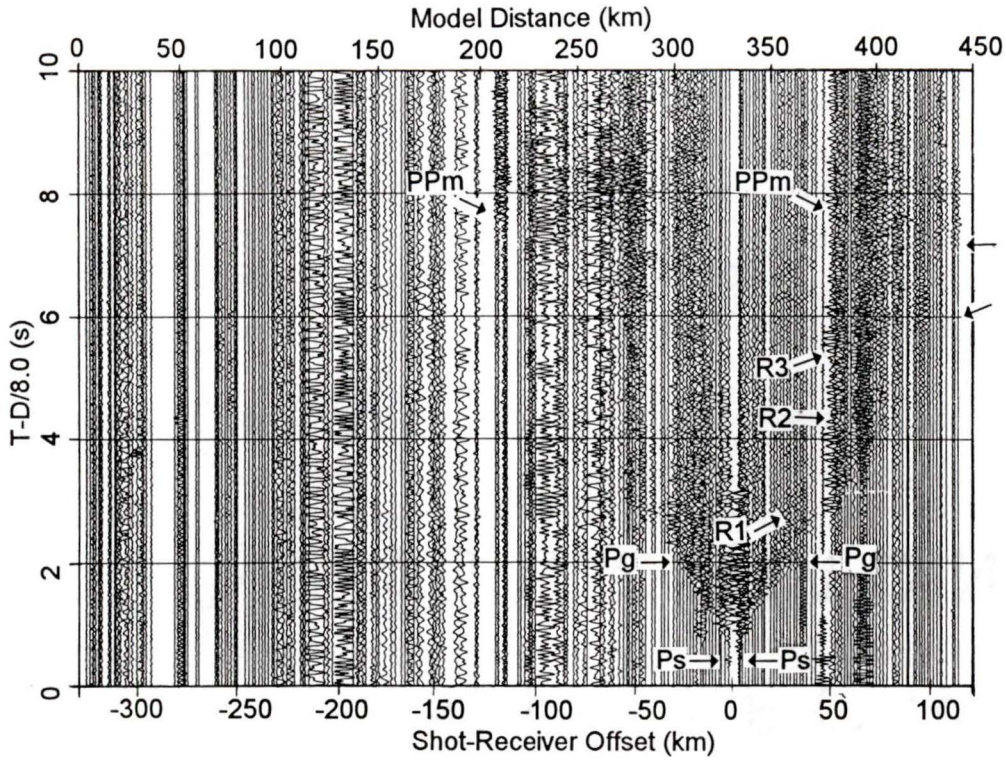

FIGURE 11: (a) Observed record section for SP14 in the western Intermontane Belt (see Figure 4 caption for a general description). SP14 was plotted in true relative amplitude format but using a scaling factor proportional to the 1.0 power.

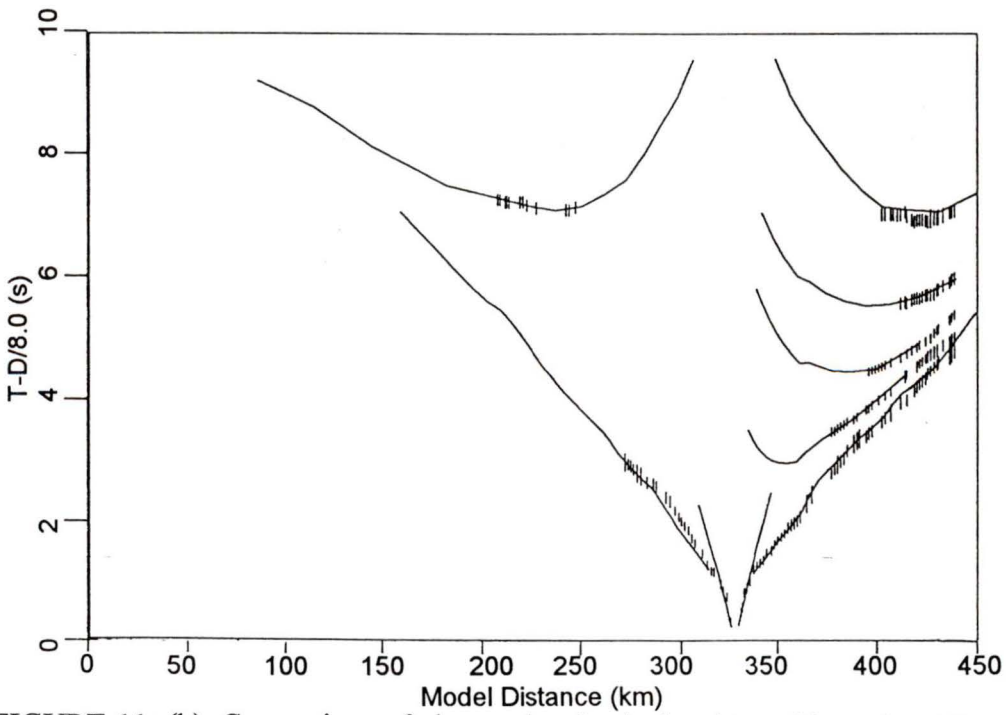

FIGURE 11: (b) Comparison of observed and calculated traveltimes (see Figure 4 caption for plotting style).

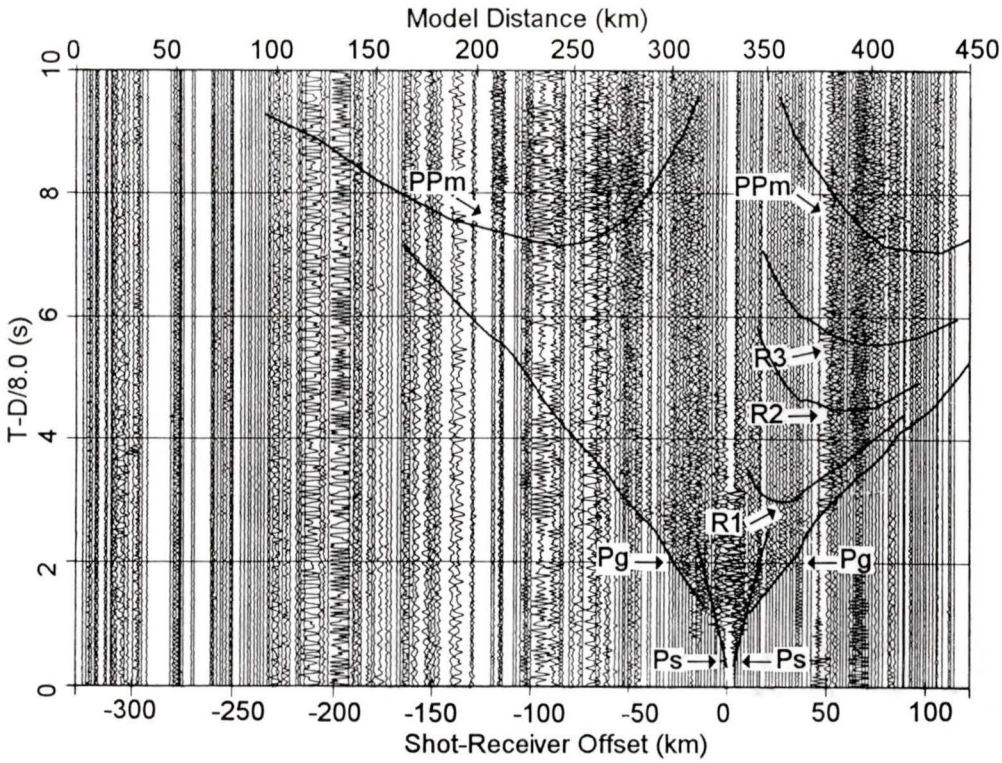

FIGURE 11: (c) Comparison of calculated traveltimes with identified phases (see Figure 4 caption for plotting parameters).

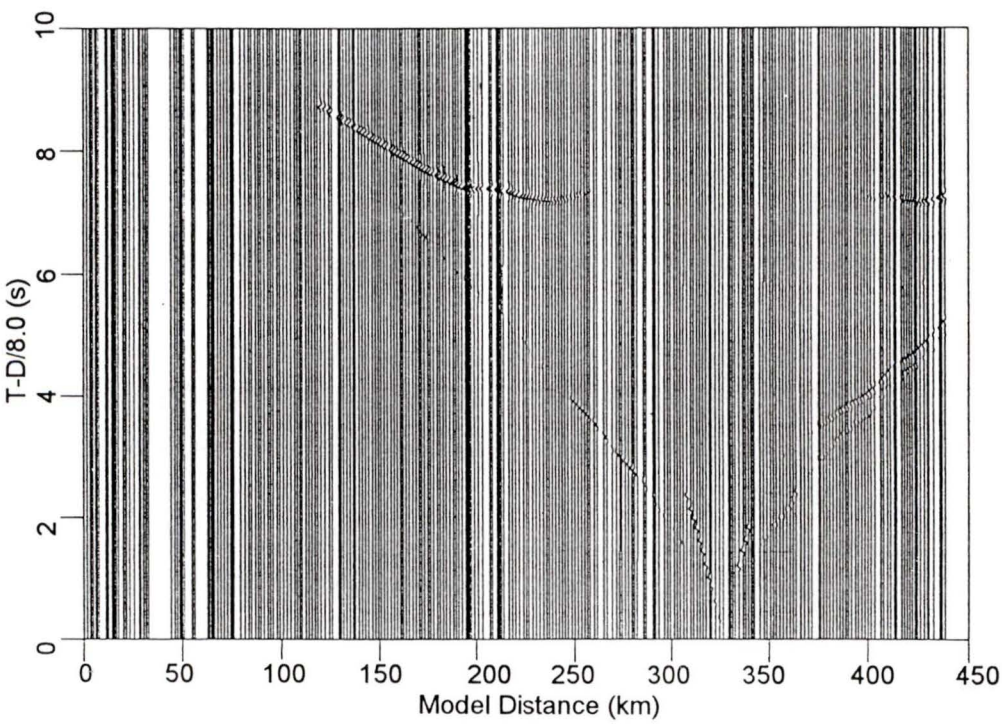

FIGURE 11: (d) Synthetic section for SP14 (see Figure 4 caption for scaling and wavelet).

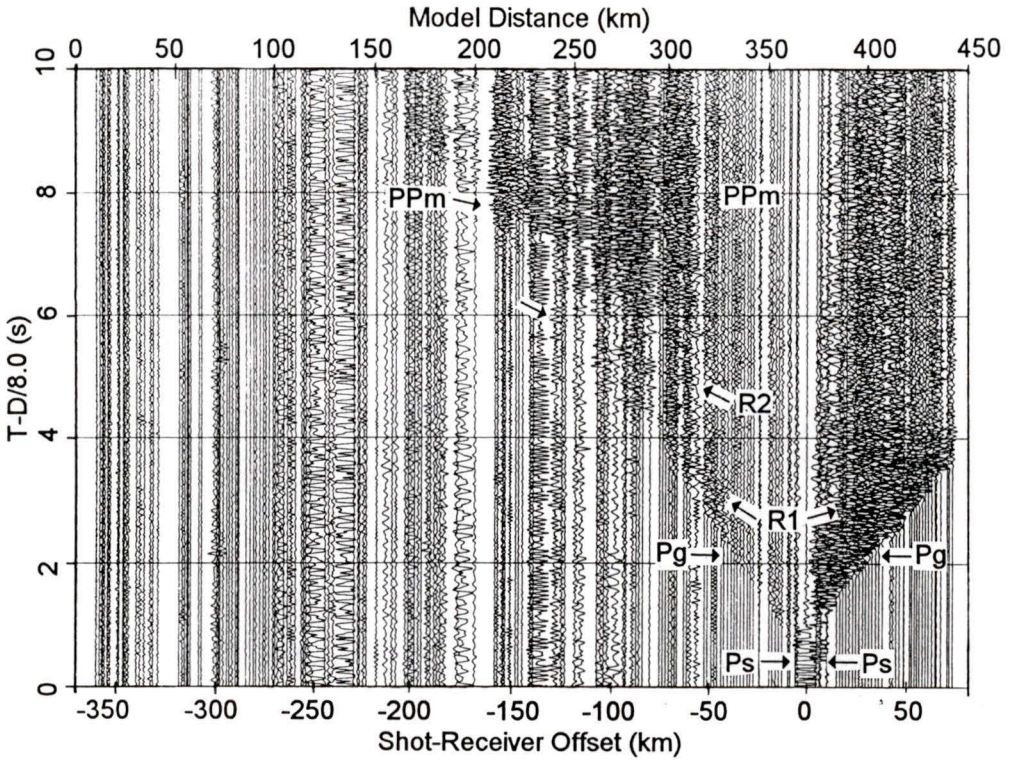

FIGURE 12: (a) Observed record section for SP15 in the western Intermontane Belt (see Figure 4 caption for plotting parameters and general description).

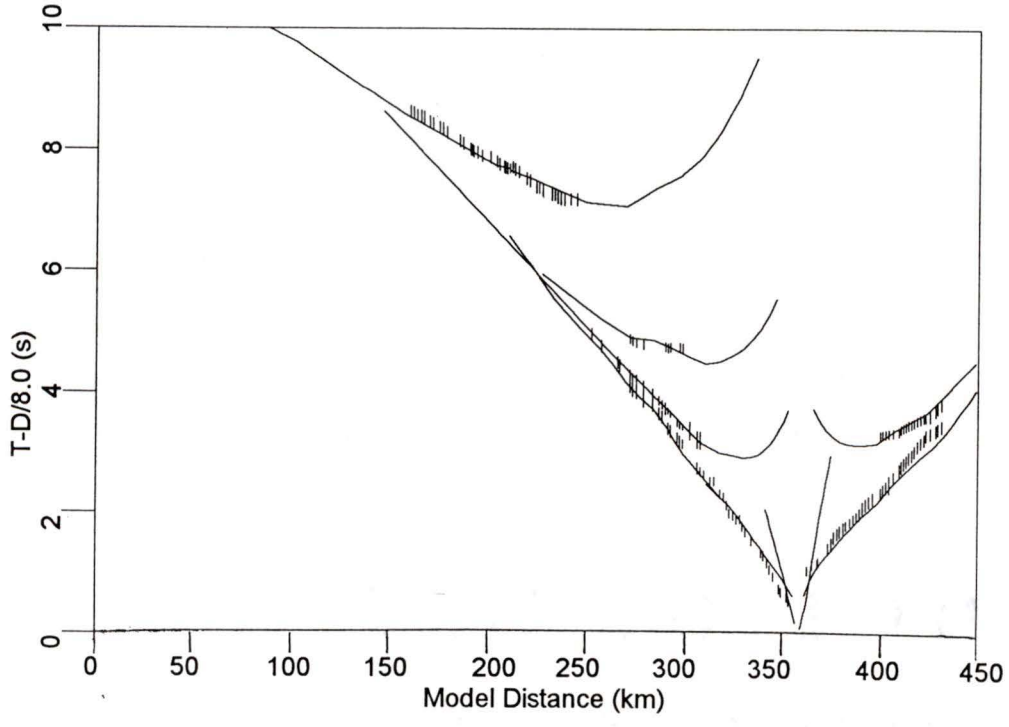

FIGURE 12: (b) Comparison of observed and calculated traveltimes (see Figure 4 caption for plotting style).

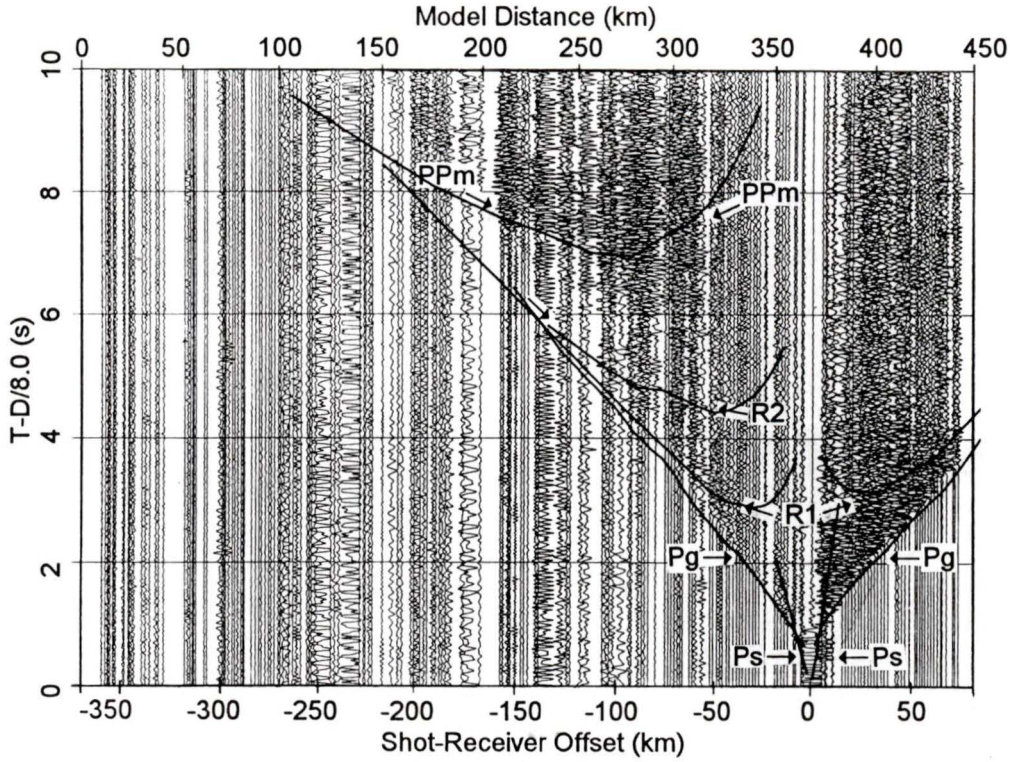

FIGURE 12: (c) Comparison of calculated traveltimes with identified phases (see Figure 4 caption for plotting parameters).

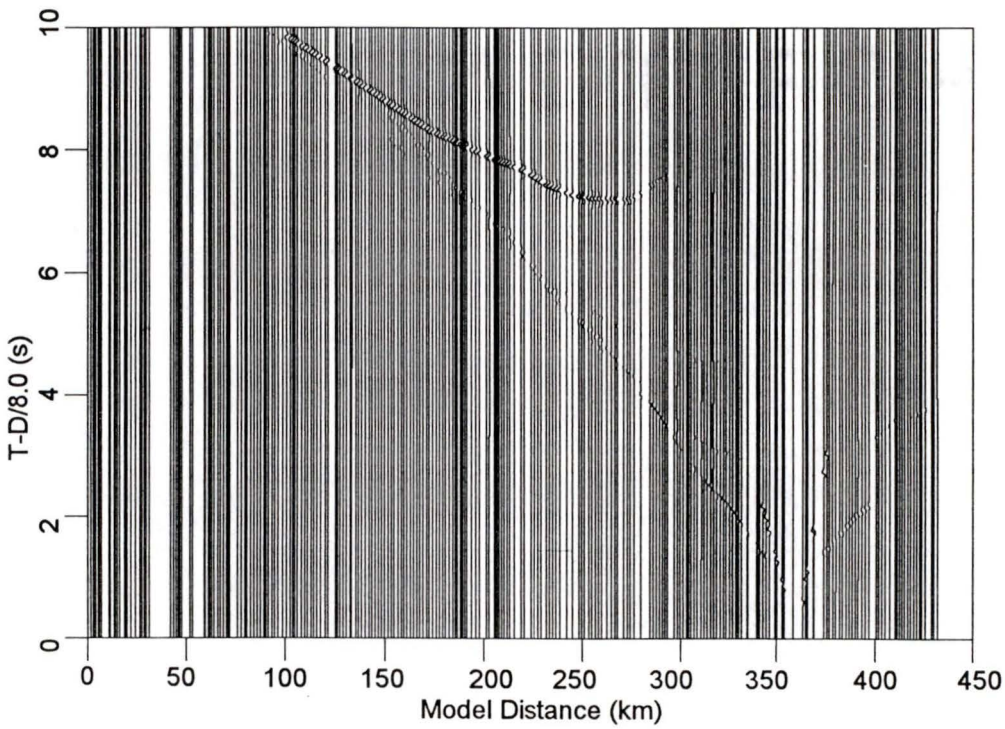

FIGURE 12: (d) Synthetic section for SP15 (see Figure 4 caption for scaling and wavelet).

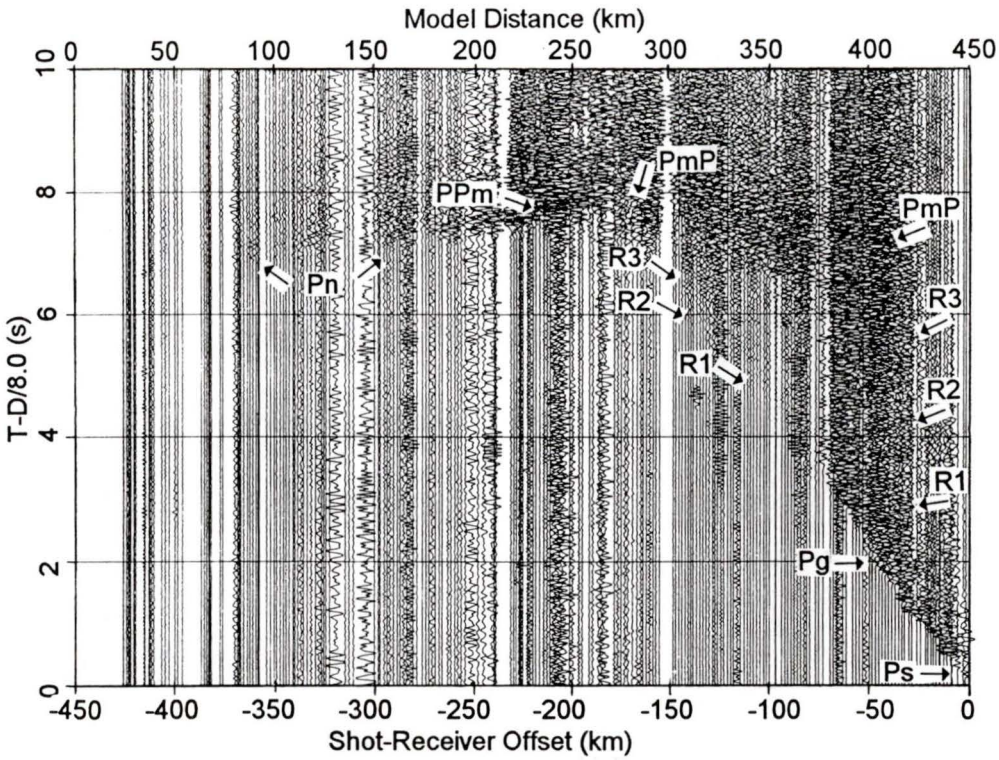

FIGURE 13: (a) Observed record section for SP1 in the western Intermontane Belt (see Figure 4 caption for plotting parameters and general description).

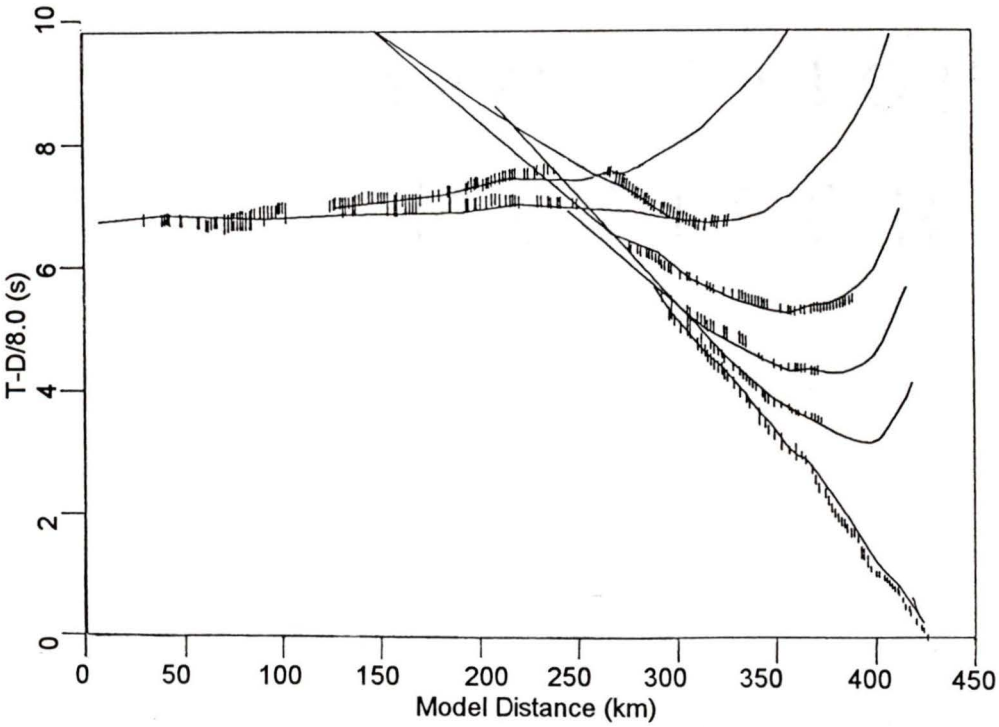

FIGURE 13: (b) Comparison of observed and calculated traveltimes (see Figure 4 caption for plotting style).

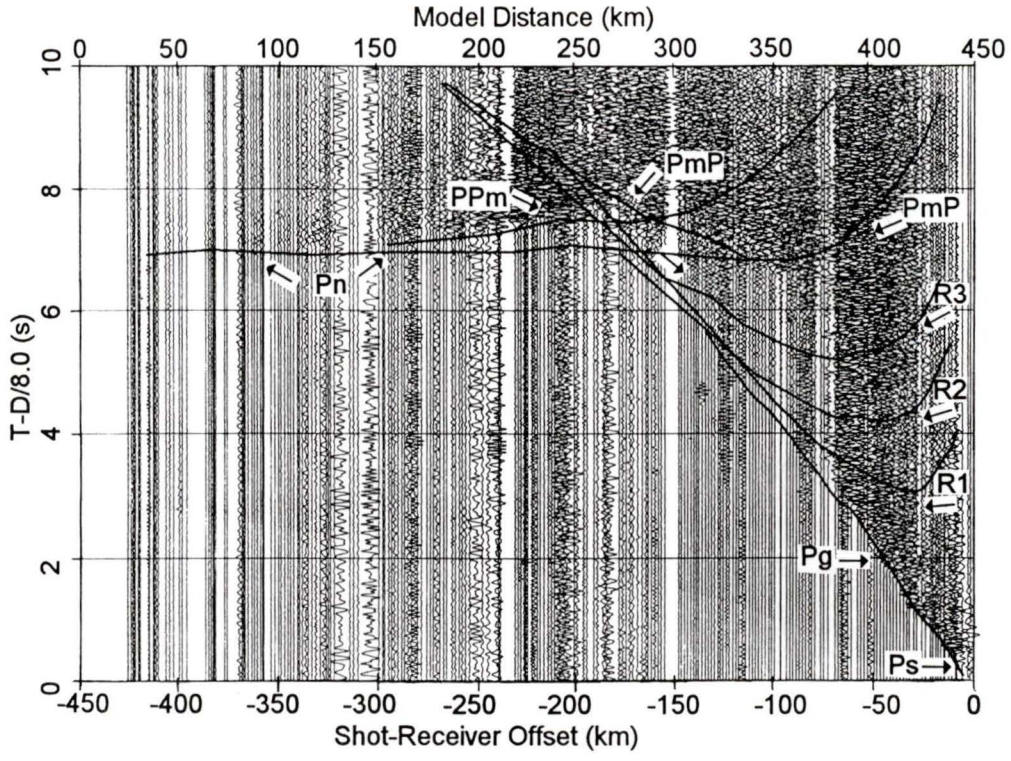

FIGURE 13: (c) Comparison of calculated traveltimes with identified phases (see Figure 4 caption for plotting parameters).

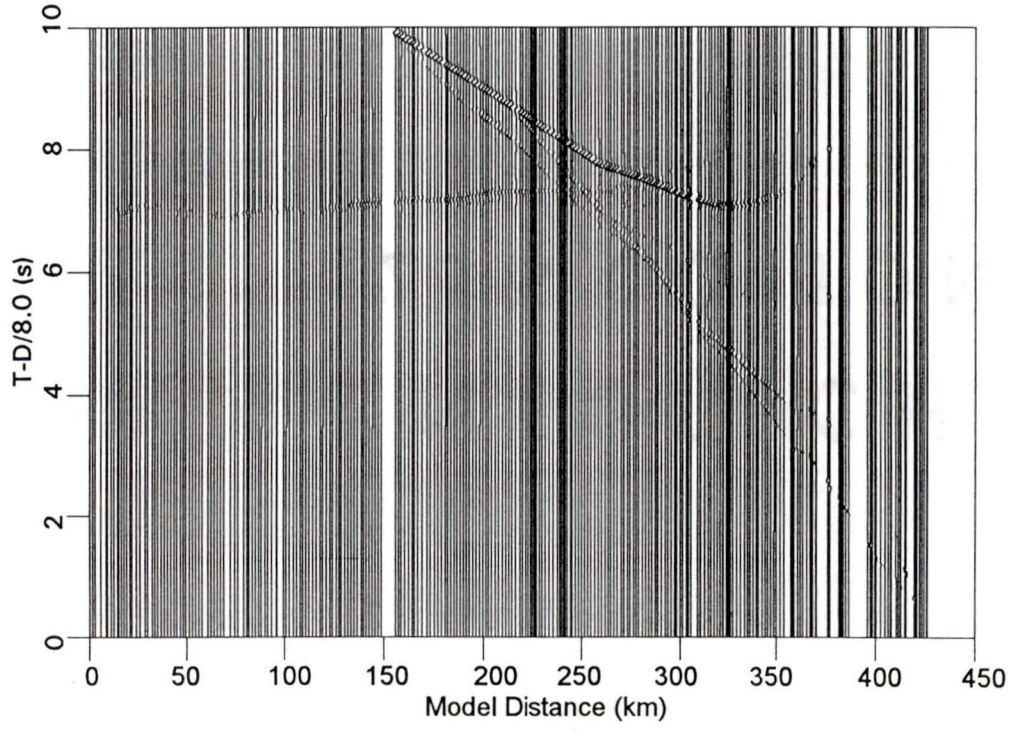

FIGURE 13: (d) Synthetic section for SP1 (see Figure 4 caption for scaling and wavelet).

Shot Point	Phase							
	Ps	Pg	R1	R2	R3	Pn	PmP	PPm
8	E	E	E	E	E			
9		W,E		E	E			
10	W,E	W,E	W,E	W				
11	W,E	W,E		W	W			
6	W,E	W,E		W,E	E	W,E	E	
12	W,E	W,E	E	W	W,E	E	E	
13	W,E	W,E	W,E		W	E	E	
14	W,E	W,E	E	E	E		W,E	
15	W,E	W,E	W,E	W			W	
1	W	W	W	W	W	W	W	W

TABLE 4. Phases Observed on each of the Record Sections.
Indicated are each of the phases which were observed on each of the record sections. Reference to W or E indicates that the phase was observed to the west or east of the shot point or both.

Shot point	Phase								Total
	Ps	Pg	R1	R2	R3	Pn	PmP	PPm	
8	4 (50)	55 (66)	33 (71)	13 (75)	66 (92)				171 (72)
9		86 (73)		19 (75)	44 (75)				149 (74)
10	14 (50)	86 (77)	44 (79)	22 (61)					166 (68)
11	7 (71)	97 (64)		20 (50)	14 (75)				138 (65)
6	4 (50)	118 (73)		46 (75)	40 (78)	69 (101)	35 (100)		312 (80)
12	4 (50)	133 (82)	25 (79)	43 (53)	43 (85)	28 (100)	28 (100)		304 (77)
13	3 (92)	64 (90)	39 (95)		21 (75)	29 (98)	19 (96)		175 (91)
14	8 (75)	70 (101)	28 (84)	20 (75)	30 (75)		29 (87)		185 (83)
15	2 (75)	73 (94)	40 (84)	9 (75)			25 (100)		149 (86)
1	3 (50)	60 (81)	31 (70)	27 (85)	52 (68)	40 (96)	61 (103)	56 (98)	330 (81)
Total	49 (61)	842 (80)	241 (69)	219 (69)	310 (78)	220 (97)	143 (98)	56 (98)	2080 (80)

TABLE 5. Traveltime Picks for each Observed Phase.
The number of traveltime picks of observed phases for each shot point are indicated. Average uncertainties, in ms, are shown in brackets. The right column indicates the total number of traveltime picks per phase and average uncertainty in brackets. The bottom row indicates the total number of traveltime picks for each shot point and the total average uncertainty of all picks per shot point in brackets. The total number of traveltime picks for all ten record sections and all observed phases, and corresponding average uncertainty, is given in the bottom right cell.

upper mantle, in contrast with SP1 (Figure 13a) and SP12 (Figure 9a).

The quality of the data recorded from the smaller shots is variable and most likely a consequence of ground conditions at the locations of the shot points and receivers. Beyond offsets of ~ 100 km, little or no seismic signal is observed on most of the smaller shots. Located within the Insular and Coast Belt, SP9 - SP11 and SP6 (Figures 5a - 8a) show well-defined phases which can be interpreted as arrivals from refracted and reflected energy throughout the crust. Shot point 6 (Figure 8a) is 85 km west of the Fraser Fault system and is the only shot point located in the Insular or Coast Belts to record mantle arrivals west of the fault system. Shot point 11, which is also located in the Coast Belt, indicates a phase which may be associated with reflected arrivals from the Moho, but it is imaging this phase in the Intermontane Belt. Within the Intermontane Belt, SP13 - SP15 (Figures 10a - 12a) generally exhibit poorer data quality, even at near offsets. Each of these shot points record reflections from the Moho, but SP13 (Figure 10a) is the only small shot point in the Intermontane Belt that shows a clearly distinguishable phase which can be associated with refracted arrivals through the upper mantle.

3.1.2 Data Characteristics

Near-offset first arrivals (Ps) were observed on all record sections except SP9 (Figure 6a), which did not record the phase due to the absence of receiver locations across the Strait of Georgia. This phase displayed considerable fluctuation in apparent velocity (inverse of the slope of the traveltime-distance curve) across the line, ranging from 3 km/s to 5 km/s. The offset range over which the branch was observed was highly variable across the line indicating differences in thickness of the near-surface layer. Relatively large amplitudes were observed for this phase by all shot points indicating large velocity gradients in the near-surface layer.

All of the record sections recorded refracted energy through the upper crust (Pg). The apparent velocities of this phase appear to be correlated to the geological belts in which the receivers are located. In the Insular Belt the apparent velocity is ~ 6.45 km/s, slightly

decreasing to 6.25 km/s in the Coast Belt and decreasing further to ~ 6.00 km/s in the Intermontane Belt. The maximum observable offset of this phase ranges from 60 - 200 km. Amplitudes of this phase vary across the line and generally decrease rapidly with increasing offset.

Refracted energy from the upper mantle (Pn) was clearly observed on four of the record sections (SP1, SP6, SP12, and SP13) with an apparent velocity of 7.9 km/s. Shot points 1 (Figure 13a) and 13 (Figure 10a) are located in the Intermontane Belt while shot points 6 (Figure 8a) and 12 (Figure 9a) are located just west of the Fraser Fault system in the Coast Belt. Moderate amplitudes were recorded for the Pn phase. Although SP6 recorded only a small number of arrivals west of the fault system, they are clearly identifiable and the reliability of this phase is not questioned. The maximum observable offset of the Pn phase was 350 km, recorded on SP1 (Figure 13a).

Seven of the record sections (SP8, SP10, SP12 - SP15, and SP1) display a phase which can be identified as a shallow upper crustal reflector (R1) visible at a reduced time of 3.5 s at an offset of ~ 80 km. All of the record sections, with the exception of SP13, display a coherent mid-crustal reflector (R2) visible at about 5.0 s at an offset of 100 km. A lower, strong mid-crustal reflector (R3) was recorded by eight of the shot points (SP8, SP9, SP6, SP11 - SP14, and SP1) visible at 5.0 s at offsets of 80 - 110 km. The reflection from the crust-mantle boundary or Mohorovic discontinuity (PmP phase) was observed on six of the record sections (SP6, SP12 - SP15, and SP1). This phase is typically visible at 7.0 - 7.3 s at an offset of 100 km. The upper mantle reflector, PPm, was clearly exhibited only on SP1 visible at ~ 7.7 s at an offset of 200 km.

3.2 Method of Interpretation

Modelling of the observed refraction data incorporated inversion of traveltimes and forward modelling of amplitude characteristics of the observed phases. Inversion of

traveltimes yields a normalized 2-D velocity structure model which provides constraints for velocities and depths of discontinuities. Forward modelling of amplitude characteristics provides additional velocity information, particularly on velocity gradients and velocity contrasts across interfaces.

Traveltime inversion was carried out using the ray-trace inversion algorithm, RAYINVR, of Zelt and Smith (1992). Amplitude characteristics were modelled using the modified version, TRAMP, of the ray-trace forward modelling algorithm of Zelt and Ellis (1988). These routines were chosen over similar routines for reasons of efficiency, versatility of the velocity parameterization, and data normalization. The efficiency and versatility of both algorithms is fundamentally linked to the model parameterization. Not only do both algorithms incorporate the same parameterization, but they are relatively flexible and easy to use.

3.2.1 Model Parameterization

The 2-D velocity structure is defined by a sequence of horizontal layers, each layer divided into variable-sized trapezoids. A layer boundary can be defined by one or more user-specified boundary nodes which allow the user the option to include detailed topographic relief. A layer boundary is usually used to represent a discontinuity in velocity or it may represent a change in velocity gradient to assist with modelling. The complete horizontal segment is formed by linear interpolation across all nodes defining the boundary.

The division of a layer into trapezoidal blocks is entirely dependent on the number of user-specified upper and lower velocity nodes. Four velocity nodes compose the four corners of a trapezoidal unit, so velocity nodes can only be defined at the upper or lower layer boundaries and not within the layer itself. The number and spacing of velocity nodes are completely arbitrary. The velocity field within each trapezoidal unit, and hence each layer, is a linear interpolation in both the horizontal and vertical directions across the velocity nodes. A discontinuity in velocity can only exist across the horizontal layer boundaries and not across

the vertical sides of the trapezoidal blocks contained within the layer. Both horizontal and vertical velocity gradients may exist within a trapezoid.

Although this type of parameterization is preferable in many aspects, discontinuities in velocity at layer boundaries can produce problems in ray tracing and amplitude calculations. To help alleviate this problem, layer boundaries are uniformly sampled and smoothed by a three-point averaging filter.

3.2.2 Ray Tracing

Both algorithms, RAYINVR and TRAMP, utilize the Runge-Kutta method (Sheriff and Geldart, 1982) to numerically solve the ray-tracing equations according to zero-order asymptotic ray theory (Cěrveny et al., 1977) with the application of Snell's Law at each point of intersection with a layer boundary. Each ray traced through the model is defined by a series of points. The spacing of these points, or ray step length, is adjusted by the algorithms during the inversion process to maintain accuracy. Where ray bending is large, due to high velocity gradients, small ray steps are used and where rays are virtually straight, larger ray steps are used. The total traveltime is obtained by numerically integrating along the ray path using the trapezoidal rule (Zelt and Smith, 1992).

The routines allow three categories of rays to be defined: i) rays which turn or refract within a layer, ii) rays which reflect off the bottom of a layer, and iii) rays which generate head waves along the bottom of the layer. Rays from each of these categories are assigned numerical codes equivalent to those given to the corresponding traveltime pick such that the calculated traveltimes can easily be compared with the observed traveltimes.

The most critical step in modelling the observed data is the proper identification of a phase. Proper identification of a phase, specifically more obscure phases, sometimes involves considerable forward modelling. To aid the initial step of forward modelling, the algorithms incorporate an iterative shooting/bisection technique (Zelt and Ellis, 1988) which rapidly

determines the take-off angles of a ray group.

3.2.3 Traveltime Inversion

The total traveltime along a ray path is a linear combination of path length and slowness (reciprocal of velocity). As a ray is traced through a velocity model, the ray path changes as it encounters variations in velocity structure. When velocity gradients are large, ray bending is large, and when a ray encounters a near-zero velocity gradient, rays are nearly straight. Therefore, traveltime inversion is non-linear application.

To overcome this problem the algorithm, RAYINVR, of Zelt and Smith (1992) linearizes by applying a Taylor series expansion about a starting model and neglecting higher-order terms. Once a suitable starting model has been constructed by forward modelling, any number of parameters may be chosen for inversion. Sensible limits must be maintained to yield stable inversion results. A damped least-squares inversion technique is used to update the model parameters. The inversion is repeated until a suitable match is obtained between observed and calculated traveltimes. For a more detailed mathematical description of the ray-trace inversion algorithm, RAYINVR, refer to Zelt and Smith (1992).

3.2.4 Synthetic Seismograms

The forward modelling algorithm, TRAMP, of Zelt and Ellis (1988), allows for amplitude characteristics of the observed phases to be incorporated into the model. Although this algorithm is not quite as robust as other routines, efficiency is obtained because the model parameterization is equivalent to that used in the traveltime inversion algorithm. The amplitude of the rays travelling through the velocity model are calculated by zero-order asymptotic ray theory (Cěrveny et al., 1977). The routine assumes a uniform point source with all amplitudes proportional to an initial amplitude of unity.

To calculate synthetic seismograms, a value of the physical constant 'Q' must be assumed

to account for anelastic attenuation, the reduction in amplitude or energy caused by the characteristics of the transmitting media. A simple 'Q' structure was inferred and is indicated in Table 6. The values used were adapted from the values of Singh and Herrmann (1983) determined for the Pacific Northwest.

Depth from surface	Q (dimensionless)
1.5 km	100
24.5 km	300
50 km	1000

TABLE 6. The 'Q' Structure.
The 'Q' structure used in the modelling procedure is specified in terms of depth from the surface. Each 'Q' represents the value assigned to a homogeneous Q layer, the top of the layer corresponds to the previously mentioned depth.

3.2.5 Stopping Criteria

An F-test stopping criteria incorporated into the RAYINVR algorithm allows for a more objective and efficient analysis. The statistical F-test gives the probability of significantly different models based on the chi-squared values and the number of observations used in the inversion of the two models. This is a stopping criteria only in the sense that it reveals whether or not applying another inversion will yield more satisfactory results. At this point, the user must decide if perhaps other parameters should be examined to obtain a better fit to the observed data.

The choice to stop adjustment of the velocity model must be based on model parameter resolution, traveltime residual and the ability to trace rays to all observation points (Zelt and Smith, 1992). Since traveltime residuals are usually only reduced at the expense of reducing parameter resolution one must choose the model which gives the best trade-off between the two. The ability to trace rays to all receiver locations through a layered, blocky model

representation is something of a dilemma. Traveltime picks used in the inversion correspond to actual geometrical arrivals, so the model chosen must at least be able to trace rays to the corresponding positions of the traveltime picks (Zelt and Smith, 1992).

3.2.6 Spatial Resolution and Absolute Parameter Uncertainty

Important parameters in damped least squares inversion are overall damping and a priori estimates of the uncertainty of model parameters (Zelt and Smith, 1992). The damping factor controls the trade-off between resolution and uncertainty of model parameters. The optimum values of these parameters are 1 and 0, respectively. The resolution indicates the degree of averaging or linear dependence of the true model as represented by the inverted model (Zelt and Smith, 1992). The ideal value for the damping factor would be 1, in which equal weight is placed on improving resolution and uncertainty of parameters.

Critical factors in determining the resolution and residuals of the seismic data are the shot and receiver spacings and the quality of the data. Ideally the shot-receiver density should be relatively low, separation > 1.5 km, such that fine structure cannot be resolved (Zelt and Smith, 1992). If the shot-receiver density were high, the model may become over parameterized and the inversion unstable. High quality data is also desired, as in any experiment, for more uniform traveltime picking of the selected phase. These types of constraints make inversion algorithm particularly suited for wide-angle refraction experiments (Zelt and Smith, 1992).

Tests for estimating the spatial resolution of a model about a specific node and for estimating the absolute uncertainty of a particular node are described by Zelt and Smith (1992). In general, the procedure is to choose a model parameter, perturb it by a measure of its estimated uncertainty, calculate traveltimes of the perturbed model by forward modelling then invert the perturbed value and the surrounding model parameters. The spatial resolution about the selected parameter is given by the amount that the surrounding values differ from

their non-perturbed values. To determine the absolute uncertainty of a model parameter, the last step of the procedure is continued (inverting for surrounding parameters) while increasing the size of the perturbation until the data cannot be fit based on the value of the statistical F-test. The size of the perturbation gives a measure of the absolute uncertainty. Since completing such tests for all model parameters is unreasonable, Zelt and Smith (1992) suggest testing a number of representative velocity and boundary nodes.

3.3 Modelling the Refraction Data

3.3.1 The Modelling Procedure

The procedure followed to model the data incorporated a "layer-stripping" approach. In this approach, the observed traveltimes associated with a given layer are simultaneously inverted while the parameters of the other model layers are held fixed. Typically the inversion algorithm was used to solve for boundary depths and velocities within a layer. Amplitude forward modelling was then used to check the relative amplitudes of the observed and calculated phases. This provides constraints for velocity boundary contrasts and gradients which may then be included in the next inversion. The process of alternating traveltime inversion and amplitude forward modelling was continued until an acceptable fit of observed and calculated traveltimes and amplitudes was achieved.

In practice, a trade-off between reducing the traveltime residual and improving the computed amplitudes is inevitable. More emphasis was placed upon achieving a satisfactory traveltime fit because of the limitations involved in calculating amplitudes using ray theory (Zelt and Ellis, 1988). Due to large amplitude variations within each phase, which is a common trait of data from refraction surveys on land, the comparison between computed and observed amplitudes was qualitative.

In applying the modelling techniques in this manner, two assumptions were made: (i) the inversion algorithm is capable of resolving trade-offs between velocity and boundary depth,

and (ii) the effects of using a 2-D, or straight line, representation of the actual shot and receiver geometry are negligible. Zelt and Smith (1992) asserted that testing has revealed assumption (i) to be valid. As well, assumption (ii) seems valid in the case of Line 2.

3.3.2 Modelling the Refraction Data

This section describes the application of the modelling procedure to the SCoRE '89 Line 2 data set in order to construct the final velocity structural model (Figure 14). Figures 4b - 13b display the match between the observed and calculated traveltimes while Figures 4c - 13c show how the calculated traveltimes fit the data. The synthetic sections are shown in Figures 4d - 13d. The locations of the boundary and depth nodes used in the inversion procedure are shown in Figure 15, this figure indicates the numbers which were assigned to the boundaries and layers in the text. Figure 16 displays the ray coverage for each phase.

3.3.2a The Upper Crust

The velocity structure of the near-surface layer (Layer 1, Figure 15) was determined by a combination of traveltime inversion and forward ray-tracing. Velocity and depth nodes were placed at the locations of the ten shot points on boundaries 1 and 2, respectively (Figure 15). Starting velocities were between 3.5 km/s and 4.5 km/s. Due to the limited number of Ps arrivals, velocity gradients were not well-constrained and were fixed at about 0.2 km/s/km. The starting thickness of this layer was estimated to be about 1.0 km based on the Ps-Pg cross-over distance. Where there was no clear distinction, layer thickness was assumed less than 500 m. The near-offset arrivals (Ps) were then inverted to determine the velocities in the near-surface layer. The damping factor for inversion, which controls the trade-off between resolution and variance, was set at 1 and the estimated uncertainty of the model velocity nodes was set at 0.1 km/s. The estimated uncertainty of the model depth nodes was set at 0.1 km.

Initial inversion attempts did not prove to be successful due to the limited spatial extent

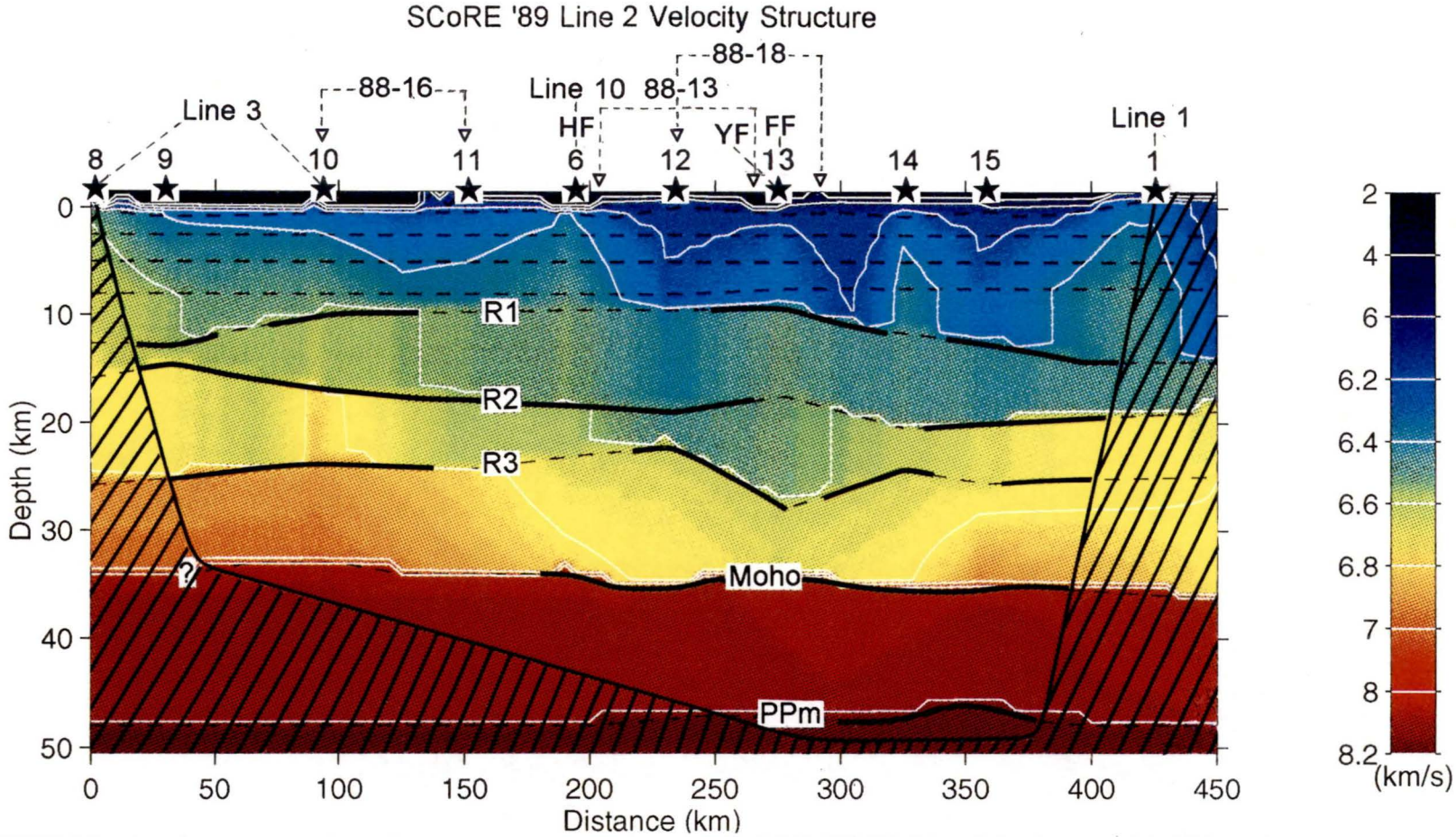

FIGURE 14: A color contour plot of the velocity structure model of SCoRE '89 Line 2 is shown with SP8 and sea level as the origin. The shot point locations are indicated by stars. The white lines display the velocity contours and the thick, solid black lines indicate the regions of the reflectors which are well-constrained by the inversion. The regions of the model which are not constrained by inversion are shaded or indicated by '?'. The Mohorovic discontinuity is designated by 'Moho'. Also indicated are the positions of SCoRE '90 refraction Line 10, SCoRE '89 refraction Lines 1 and 3 and LITHOPROBE reflection profiles 88-13, 88-16 (offset to north by ~ 50 km) and 88-18 (offset to south by ~ 60 km). The Harrison, Yalakom and Fraser-Straight Creek fault are designated HF, YF and FF, respectively.

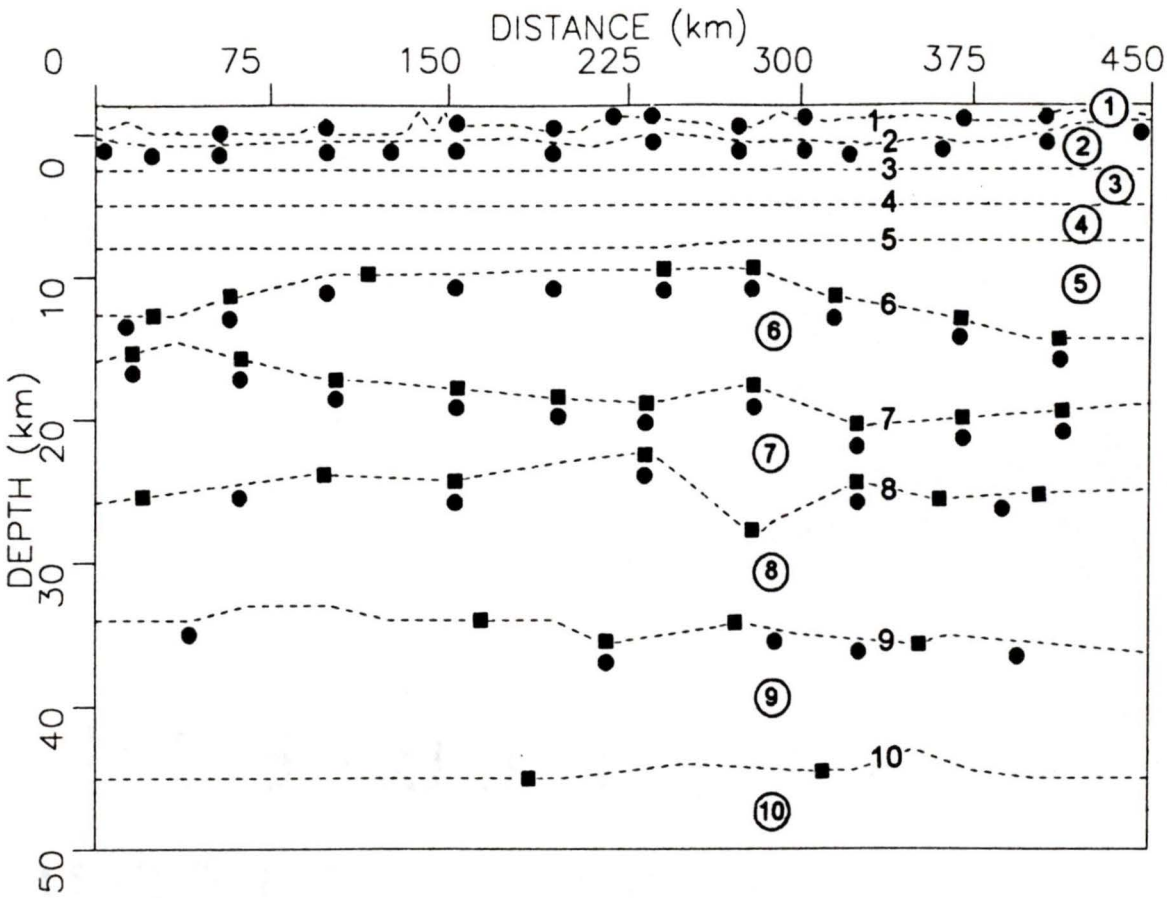

FIGURE 15: Location of depth nodes (squares) and velocity nodes (circles) used in the inversion process. The numbers represent boundary identification numbers used in the text, and circled numbers represent layer identification numbers. Velocity and depth nodes determined through forward modelling are not shown (see text). Boundary 1 represents the surface topography along Line 2. Layer 1 is the near-surface layer. Layers 2-5 comprise the upper crustal unit where boundary 6 represents the base of the upper crust defined by the R1 reflector. Layers 6 and 7 represent the mid-crustal unit. Boundaries 7 and 8 indicate the positions of the mid-crustal reflector (R2) and the base of the mid-crustal unit (R3), respectively. Layer 8 represents the lower crust and boundary 9 indicates the position of the Mohorovic discontinuity. Layers 9 and 10 represent the upper mantle layers separated by the upper mantle reflector (PPm) indicated by boundary 10.

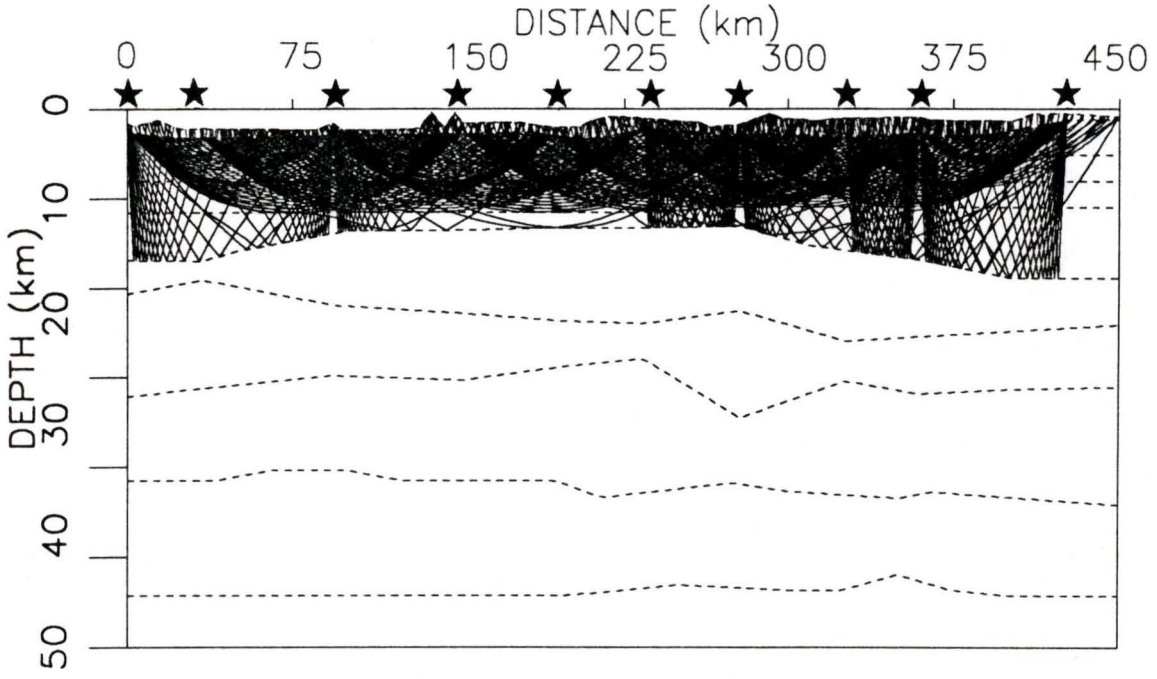

FIGURE 16: (a) Two-point ray tracing diagrams showing the ray coverage in the upper crustal unit by the Pg and R1 phases.

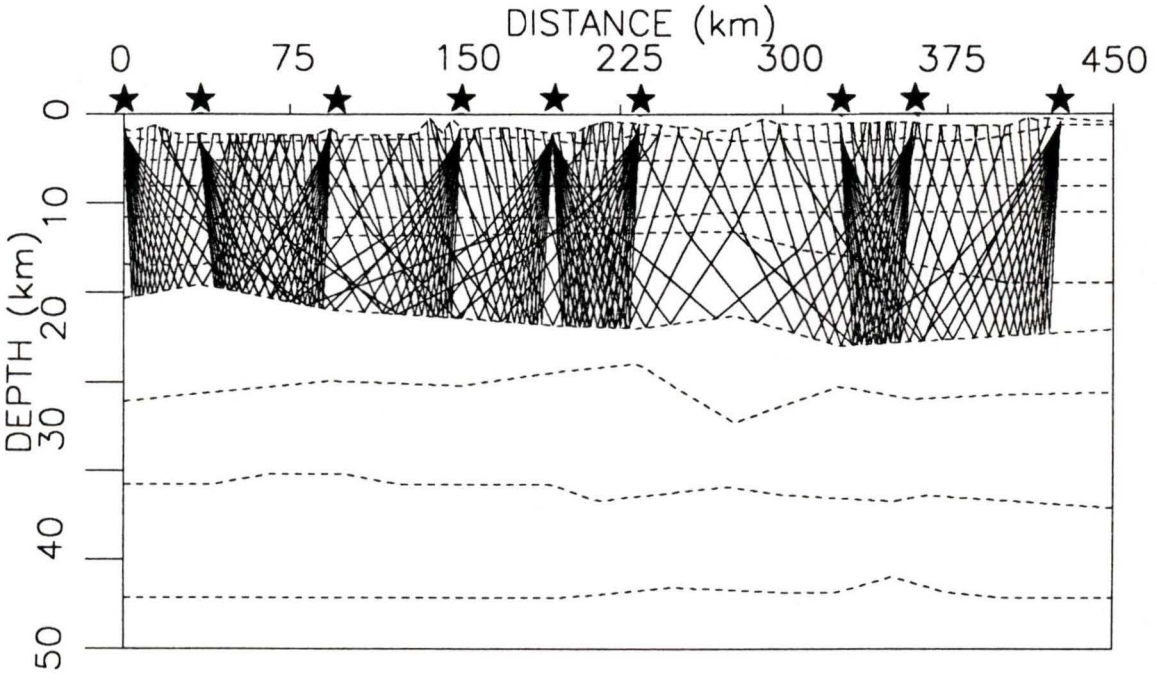

FIGURE 16: (b) Two-point ray tracing diagram showing the ray coverage in the upper mid-crustal unit by the R2 phase.

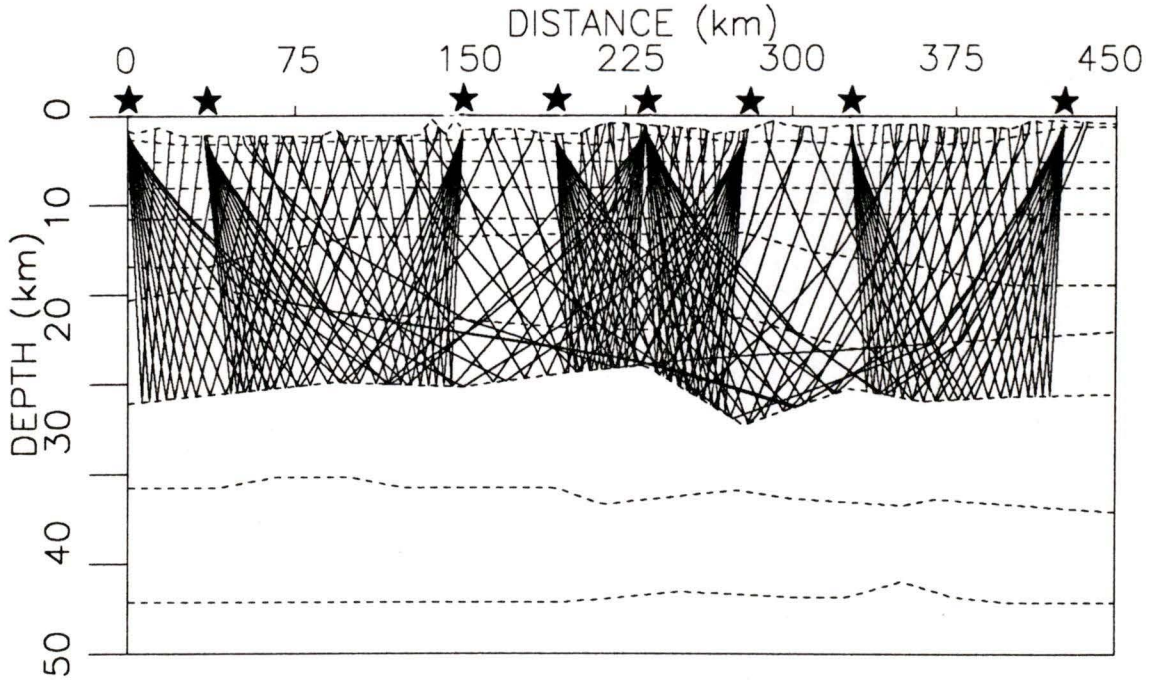

FIGURE 16: (c) Two-point ray tracing diagram showing the ray coverage in the lower mid-crustal unit by the R3 phase.

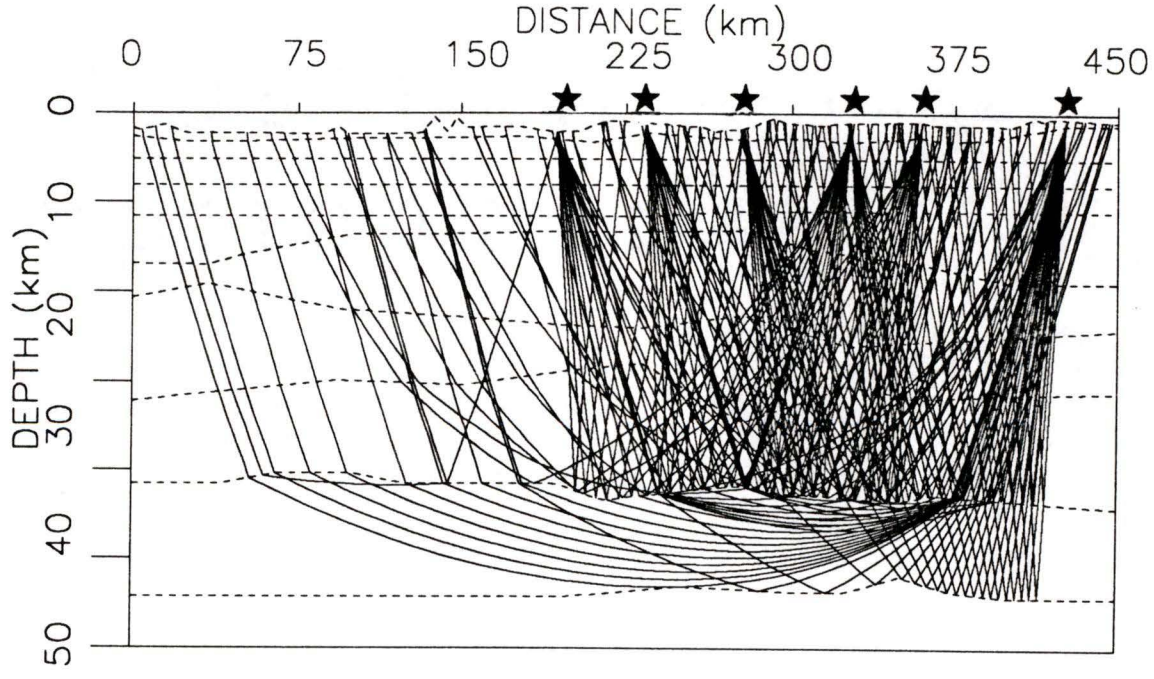

FIGURE 16: (d) Two-point ray tracing diagram showing the ray coverage for the lower crust, the Mohorovic discontinuity and for the upper mantle by the PmP, Pn and PPm phases.

of arrivals. Only seven of the ten velocity nodes were accurately resolved during the inversion; resolution of these values ranged from 0.12 - 0.74. These nodes were then fixed and forward ray tracing was carried out to obtain acceptable values for the other three velocity nodes. Seven velocity nodes were added to layer 1 to model the observed undulations in the Pg phase which correspond to variations in geological structure.

Inverting for the depth of the near-surface layer produced problematic oscillations between maximum and minimum values. Six additional depth nodes were added to Boundary 2 and the depth limit of the near-surface layer was determined by forward ray tracing.

For the upper crustal unit (Layers 2-4, Figure 15), 14 velocity nodes were evenly spaced along Boundary 2 and at the corresponding positions along Boundary 5. Some initial forward modelling was completed to determine the deepest turning point of the Pg arrivals, which depended on the maximum observed offset of the Pg branch. Results indicated that model velocities could be constrained to 8.0 km depth in the west (Insular and Coast Belts), while in the east (Intermontane Belt) upper crustal velocities could only be constrained to about 7.5 km depth. The difference in depth of ray penetration in the west and the east is largely due to higher velocity gradients observed in the Intermontane Belt. The higher velocity gradients increase ray curvature, and so rays do not penetrate to large depths. The boundary (Boundary 5, Figure 16) which appears at about 8.0 km depth does not represent a structural feature, but represents the depth to which velocities in the upper crust are constrained.

During the inversion procedure, it became apparent that allowing the velocity gradients in the upper crust to vary was not feasible. Velocity reversals resulted in large shadow zones in ray coverage in some regions of the model. Increasing the damping factor did not remove the problem. Therefore, gradients were held fixed to small positive values for the remainder of the inversion process.

The velocity structure of the upper 8 km determined by inversion was then used as the

starting model for amplitude forward modelling of the Pg phase. To model the observed decrease in amplitude with distance, two additional boundaries were placed at 2.5 km and 5.0 km depth (Boundaries 3 and 4, Figure 15). These boundaries do not represent a structural discontinuity, but represent gradient changes with depth. Velocity gradients in these layers were adjusted to obtain a satisfactory fit to the amplitude data while maintaining an acceptable traveltime fit to the data.

Once the amplitude information was incorporated into the velocity structure, all Ps and Pg arrivals were re-inverted to constrain the 17 velocity nodes in layer 1. The resolution of the Ps parameters was acceptable, between 0.19 and 0.82 (Table 7). The least resolved values were the 7 nodes which were added to represent geological features. Resolution of these values ranged between 0.19 - 0.49 while the resolution of the velocity nodes at the shot point locations were between 0.55 - 0.82. The resolution of the Pg parameters was good (> 0.72). The total RMS traveltime residual for the 891 Ps and Pg arrivals was 0.088 s (Table 7), which is near the accepted average traveltime uncertainty (Table 5).

To complete the modelling of the upper crust, arrivals from an upper crustal reflector (R1) were inverted using eight depth nodes on a boundary at 12.0 km. Since boundary 5 did not represent a velocity discontinuity and there was no evidence that suggested unusually high or low velocity gradients at this depth, the velocity gradients in layer 5 were held fixed at about 0.02 km/s. The inversion algorithm had difficulties resolving the values of the depth nodes largely due to the lack of data near the center of the model. In the final stages of inversion, the estimated uncertainty of the model depth nodes was increased to 0.2 km and damping was increased to 3.

Inversion of the R1 arrivals produced a reflector at an average depth of 11.5 km. This defined the base of the upper crustal unit. The reflector was well-constrained by the data at the western and eastern ends of the model. In both of these regions, the horizon appeared to deepen. The reflector was not well-constrained at the center of the model; however, it

Phase Inverted	RMS Traveltime Residual	Resolution of Parameters	Number of Velocity Nodes	Normalized χ^2 Misfit	Number of Depth Nodes
Ps	0.088	0.19-0.82	17	4.5	0
Pg, layer 1	0.088	> 0.72	14	1.58	0
Pg, layer 2	0.088		0	1.6	0
Pg, layer 3	0.088		0	1.64	0
R1	0.077	> 0.67	0	1.2	8
R2	0.10	> 0.87v, > 0.7b	10	0.45	10
R3	0.09	> 0.82v, > 0.5b	10	1.3	8
PmP	0.11	> 0.68v,> 0.52b	5	1.2	4
Pn	0.11	> 0.63	5	1.4	0
PPm	0.13	> 0.77	0	0.5	2

TABLE 7. Inversion Results for the Final Velocity Model.
The RMS traveltime residuals, the resolution of the parameters, and the number of boundary and depth nodes used in the inversion procedure are displayed for each phase. The RMS traveltime residual is given in seconds. The letters 'v' and 'b' denote the resolution values of the velocity and depth nodes, respectively. Nodes that were determined by forward modelling are not included. The χ^2 value is the normalized chi-squared misfit to the excepted value of 1.0.

appeared to be flat throughout the Coast Belt and the western edge of the Intermontane Belt. In this region, the reflector was essentially interpolated between the two constrained segments. Resolution of the boundary nodes in the constrained regions of the model was good (> 0.67) and the RMS traveltime residual value for the 241 R1 arrivals was 0.77 s (Table 7).

The upper crustal velocity model was determined from 1132 arrivals of three phases, Ps, Pg and R1. Of the 31 velocity nodes, 24 were accurately resolved (> 0.5) by inversion and

7 of the velocity nodes were determined by forward ray-tracing. Only 8 of the 24 depth nodes were inverted since inversion was unable to constrain the 16 depth nodes of the near-surface layer.

3.3.2b The Middle Crust

The mid-crustal velocity structure was determined by inversion of the R2 arrivals. Ten velocity nodes were evenly spaced at the top of layer 6 (Boundary 6, Figure 15). Initial modelling revealed that the data did not constrain velocity gradients within this layer so the velocity gradient within layer 6 was fixed at zero for the inversion. Ten depth nodes were placed on boundary 7 at regular intervals. During inversion some oscillatory behaviour was observed in the velocity structure at the eastern edge of the model. The "trouble" spots were fixed at reasonable values while resolving the other parameters. Once an acceptable fit was obtained, all parameters were then re-inverted to constrain the structure. Initial inversion iterations produced a R2 reflector at an average depth of 17.7 km, while velocities above the reflector ranged from 6.5 km/s in the west to 6.3 km/s in the east.

The inversion of the R2 arrivals constrained the velocity structure below boundary 6 such that forward amplitude modelling of the R1 reflector could be completed. The observed R1 phases were relatively low in amplitude across the line, therefore no unusually large velocity contrast was necessary across boundary 6. To incorporate the amplitude information from the R1 reflector, minor adjustments were made to the velocity structure in layer 6 until the R1 amplitudes of the synthetic seismograms matched reasonably well with the observed data. Each time a velocity node value was changed in order to model the velocity contrast, forward traveltime modelling was completed to insure that there were no significant changes in the traveltime fit. The arrivals were then re-inverted to constrain the data.

The resulting R2 reflector had an average depth of 17.9 km, while velocities above the reflector ranged from 6.5 km/s in the west to 6.3 km/s in the east. This horizon represented a mid-crustal discontinuity. The resolution of the boundary nodes was good (> 0.7).

Resolution of the velocity nodes was excellent (> 0.87), and the RMS traveltime residual was 0.10 s (Table 7).

The velocity structure for the lower portion of the mid-crustal unit was initiated by inverting for the R3 reflector. Location of velocity and depth nodes was arbitrary as long as the nodes were evenly spaced across the region to constrain the data. Eight depth nodes were placed on boundary 8 (Figure 15) and ten velocity nodes were placed at the top of Layer 7 at roughly the shot point locations. As in modelling the velocity structure of layer 6, the velocity gradient in layer 7 was held fixed at zero.

Inversion of the R3 arrivals produced a reflector at an average depth of 24.2 km with velocities within layer 7 ranging from 6.6 km/s to 6.4 km/s. This model was used as a starting model for amplitude modelling of the R2 reflector. The amplitudes of the synthetic seismograms produced from the R2 reflector were high in comparison to the data. Changes that were made to alleviate the amplitude problem did however deteriorate the traveltime fit in some regions, and so a trade-off between amplitudes and traveltime fit was necessary in order to accurately model the data. Re-inversion of the arrivals produced a R3 reflector with an average depth of 24.7 km. This defined the base of the mid-crustal unit. Resolution of the boundary nodes was acceptable (> 0.5), and resolution of the velocity nodes was good (> 0.82). The RMS traveltime residual for the R3 arrivals was 0.09 s (Table 7).

3.3.2c The Lower Crust and Upper Mantle

To complete the structure of the lower crust and upper mantle, the crust-mantle boundary arrivals (PmP) and upper mantle arrivals (Pn) were inverted simultaneously. Unlike layer 6 and layer 7, the velocity gradients in layer 8 (Figure 15) were fixed at a non-zero value of 0.15 km/s or less. It was also necessary to fix the vertical velocity gradient in the upper mantle (Layer 9, Figure 15) at 0.1 km/s or less. Ten velocity nodes were used to determine the velocity structure of the lower crust (Layer 8) and upper mantle (Layer 9). Four boundary nodes were used to determine the depth to the Moho (Boundary 9).

The initial inversion attempts could only resolve the velocity structure in the east (Intermontane Belt). The average depth to the Moho was 34.5 km. This model was then used as a starting model to incorporate the amplitude information from the R3 phase and the Moho discontinuity (PmP). Velocity adjustments in layer 8 and layer 9 were necessary to model the data. Once an acceptable fit between amplitudes and traveltimes was obtained, the Pn arrivals were inverted to determine the velocity within the upper mantle. The resulting velocity values, in the region constrained by the data, were 7.85 - 7.95 km/s.

Due to the limited number of Pn arrivals and absence of PmP arrivals observed in the west, forward modelling was carried out to determine the velocity structure of the lower crust and upper mantle. Some topography was added to the crust-mantle boundary to better fit the data. The RMS traveltime residual for the PmP and Pn arrivals was 0.11 s. The resolutions of the velocity arrivals determined by inversion were good, > 0.68 and > 0.63, respectively. The resolution of the crust-mantle boundary nodes was acceptable. (.> 0.52, Table 7).

The upper mantle velocity structure was completed by inverting arrivals from a sub-Moho reflector (PPm) visible on the record section of SP1. Two boundary nodes were used in the inversion which resulted in a sub-Moho reflector modelled at 45.8 km depth. The resolution of the boundary nodes was acceptable (> 0.77) and the RMS traveltime residual for these arrivals was 0.13 s (Table 7). Data were modelled using a velocity increase to 8.1 km/s below the sub-Moho reflector; however, it was difficult to determine the polarity of the reflection. The data could be modelled equally well with a velocity decrease below the reflector, for example to values of 7.7 km/s or less.

IV: COMPARISON WITH OTHER GEOPHYSICAL DATA

4.1 Features of the Final Model

The principal features of the final model are shown in Figure 14. The crustal velocity structure has been divided into three layers above which there exists a varying-thickness near-surface layer and below which the upper mantle has been divided into two layers by an upper mantle reflector.

The near-surface layer displays large lateral and vertical velocity gradients which cause fluctuations in the essentially linear Pg phase. Velocities at the surface range from a low of 2.6 km/s to a high of 5.3 km/s. The most significant velocity low (2.6 - 2.8 km/s) is located at SP9 on Vancouver Island and can be linked to the Upper Cretaceous Nanaimo sediments (Figure 2). The thickness of this layer ranges from 0.8 km to 2.0 km.

The upper crustal velocity structure appears to be correlated with the three morphogeological belts, particularly with the Harrison Fault. Velocities tend to be high in the west, with velocities in the Insular Belt being slightly higher than those in the Coast Belt, and lower in the east. At the top of the upper crust, velocities average 6.2 km/s in the west and 5.9 km/s in the east. This trend continues to a depth of 8.0 km, which is the maximum depth of penetration of the Pg phase, with average crustal velocities being 6.4 km/s in the west and 6.1 km/s in the east.

The base of the upper crust is defined by the R1 reflector. The depth to this reflector is well-constrained for two segments of the model, in the Insular and Intermontane Belts (Figure 16a). The segment in the Insular Belt dips westward to a maximum depth of 12.6 km, while the segment in the Intermontane Belt dips eastward to a maximum depth of 13.9 km. Across the center of the model in the Coast Belt, the R1 reflector was flat-lying at average depth of 11.5 km, but was poorly constrained. The largest observed amplitudes for the R1 reflector were in the Intermontane Belt which indicated a larger velocity contrast (up 0.4 km/s) in this

belt than in the Coast and Insular Belts. This is consistent with a lower velocity upper crust in the eastern portion of the model relative to the west.

The mid-crustal velocity structure appears to maintain the above pattern, with higher velocities in the west (6.5 km/s) than in the east (6.3 km/s). The lowest velocities in this crustal unit are localized to a region beneath SP12 which is located at the Bralorne-Kwoiek Creek Fault, a geological boundary separating the Central and Eastern Coast Belts. Within the mid-crustal unit a wide-angle reflector was modeled, the R2 reflector, with an average depth of 18.5 km. This reflector is generated by a moderate velocity contrast between the upper and lower mid-crustal units averaging 0.12 km/s. The R2 reflector is well-constrained for most of the model (Figure 16b). In the Coast and Intermontane Belts, the reflector has several undulations with amplitudes up to 1.5 km. Beneath the Strait of Georgia, this reflector rises to 14.5 km but is not constrained by inversion, as indicated in Figure 14. In this region, the R2 reflector may either; (i) pinch out into the base of the upper crust (R1), or (ii) dip westward beneath Vancouver Island. The latter choice was preferred as Spence et al. (1985) also imaged a westward dipping reflector from the mainland at about this depth.

Below the R2 reflector, the velocity structure in the western and eastern portions of the model tend to become more uniform. The average crustal velocity in the west is 6.57 km/s and in the east 6.50 km/s. The lowest velocities in this crustal unit are found in the region east of the Harrison Fault, where velocities reach a low of 6.3 km/s beneath SP12.

The mid-crustal unit is bounded by the R3 reflector at an average depth of 24.7 km. The average velocity contrast between the upper and lower portions of the crust is only 0.09 km/s. The small velocity contrast is in part due to the reduced amplitudes of the R3 reflector observed in the east, much lower amplitudes than those in the west. The reflected phases in the west (Insular and Western Coast Belt) are generated by a velocity discontinuity of at least 0.12 km/s, while the R3 reflection in the east occurs where the velocity contrast has decreased significantly to 0.07 km/s. Similar to the R2 reflector, the R3 reflector appears to fluctuate

in depth. The most severe fluctuation is imaged in a region directly below the Fraser-Straight Creek Fault where the horizon dips ~ 4 km to 27.9 km depth. On either side of this region, the reflector is characterized as a gently rising horizon in the Coast and Intermontane Belts. The depth to the R3 reflector is offset by ~ 1 km across the fault region, imaged at 23.4 km in the Coast Belt and 24.4 km in the Intermontane Belt.

The lower crustal velocity structure maintains the same pattern as above. Across the model, velocities average 6.6 km/s at the top of the layer to 6.7 km/s at the base. Values are again higher in the west (6.67 - 6.75 km/s) than those in the east (6.59 - 6.68 km/s). The lateral velocity contrasts in this layer are significantly smaller than in the upper crustal units.

The crust is bounded by the Mohorovic discontinuity, the crust-mantle boundary, at an average depth of 34.5 km. The depth of the Moho is well-constrained by the data in the Intermontane Belt and as far west as the Harrison Fault, or eastern edge of the West Coast Belt (Figure 16d). The velocity contrast across this discontinuity is large (> 1.1 km/s), as expected in the transition from the crust to the upper mantle. The upper mantle velocities are uniform across the region with no lateral changes to low velocity regions as observed in the crust; the velocity values below the Moho range from 7.89 km/s to 7.95 km/s. The upper mantle is divided into upper and lower portions by the presence of an upper mantle reflector at ~ 46 km, constrained in a small region of the Intermontane Belt only (Figure 16d). Although a velocity contrast of at least 0.2 km/s was required, mantle velocities below the reflector were poorly constrained by the seismic data and could be either higher (8.1 km/s) or lower (7.7 km/s) than velocities above the reflector.

4.2 Non-uniqueness of the Final Model

A measure of the non-uniqueness of a final model is given by the range of final models that can fit the observed data, i.e., produce an acceptable fit to the traveltime data, appear physically acceptable and be well-resolved. This is in turn dependent upon the choice of node

placement. Zelt and Smith (1992) asserted that to attempt to achieve a χ^2 (the probability of significantly different models) value of 1 would be possible only for a case of optimum conditions, which is not usually the case of any real data set. This implies that non-uniqueness is inherent to any final model. The resultant χ^2 values for the final iterations of inversion for each of the phases are given in Table 7.

Node placement, along with different a priori estimates of parameter uncertainties and different damping parameters, is subjective in nature. To increase the stability of the inversion algorithm, and hence to reduce the non-unique nature of the final model, the number of independent model parameters to obtain essentially the same structure must be maintained at an absolute minimum (Zelt and Smith, 1992). Attempts that were made in restricting the number of inversion parameters include the following: (i) no velocity discontinuities were included for the four upper crustal layers (Layers 2-5, Figure 15), thus reducing the number of independent variables in the upper crust; (ii) the vertical velocity gradients in the mid-crustal unit were held fixed (Layers 6 and 7, Figure 15), and so the lower layer velocities were not determined independently of the upper layer velocities.

Recognizing the above issues, it is emphasised that the final model presented is a model that fits the observed data, is well-resolved and is a physically acceptable model of the real Earth. It is not a unique solution to the inverse problem. Table 8 displays the results for testing the spatial resolution of the model nodes and indicates the estimated absolute uncertainties of the parameters. Generally, the traveltime residuals are reduced at the expense of reducing the parameter resolution. It is also apparent that the resolution decreases and the uncertainties increase with depth.

Nodes	Estimated lateral resolution (km)	Estimated absolute uncertainty
Velocities in the upper crust (Layers 2-4)	10-20	0.1-0.3 km/s
Depth nodes of the R1 reflector in the west (boundary 6)	25	1.0 km
Depth nodes of the R1 reflector in the east (Boundary 6)	40-65	1.5 km
Velocities at the top of the middle crust (Layer 6)	50	0.2 km/s
Depth nodes of the R2 reflector (Boundary 7)	40-65	2-3 km
Velocities in the lower portion of the mid-crustal unit (Layer 7)	40	0.2-0.3 km/s
Depth nodes of the R3 reflector (Boundary 8)	50	2.0 km
Velocities in the lower crust (Layer 8)	30	0.2-0.3 km/s
Depth nodes at the Moho (Boundary 9)	50	1.5-2.0 km
Velocities in the upper mantle (Layer 9)	80	0.1 km/s
Depth nodes of upper mantle reflector (Boundary 10)	50	2.0-2.4 km

TABLE 8. Estimated Lateral Resolution and Absolute Uncertainties of Model Parameters. The estimated lateral resolution of the velocity model about specific nodes and the absolute uncertainty of velocity and depth nodes are indicated. The resolution and uncertainty values were based on tests applied to nodes representing the important features of the velocity model.

4.3 Summary of Results from Seismic Data

Proper analysis of any seismic data would not be complete without comparing the proposed structure with other seismic surveys carried out in the region. Ideally, the intent of comparing structural models is to tie in the proposed model with existing models, which will provide insight into the structure of the Earth's crust and upper mantle. It is inevitable that there will be inconsistencies in velocity structural models. Being able to resolve these inconsistencies, or not, plays a significant role in the interpretation of the data.

Briefly, the important features of previously interpreted seismic surveys in the region of Line 2 (as outlined in Chapter I) indicate: (i) that the crust is typically divided into 2 or 3 crustal layers separated by interfaces across which velocities increase discontinuously; (ii) the crust is generally thin in the Intermontane and Coast Belts; (iii) contradictory values have been interpreted for the thickness of the crust in the Insular Belt; and (iv) contradictory views exist on extent of crustal penetration of the Fraser-Straight Creek Fault.

4.3.1 Comparison with LITHOPROBE Refraction Data

The refraction Lines 1 and 3 of SCoRE '89 are coincident with the east and west ends of Line 2. The data have been interpreted by Zelt et al. (1992) and Zelt et al. (1993), respectively. The refraction Line 10 of SCoRE '90 crosses Line 2 at SP6, which is located near the Harrison Fault. Analysis of these data has been completed by O'Leary et al. (1993). The modelling technique applied to the above data sets was the same as that employed in the analysis of Line 2.

4.3.1a Comparison of Line 2 with Line 1:

Line 1 (Zelt et al., 1992) and Line 2 are coincident at the vertex of a triangle, so it is not reasonable to compare the models at this location since the region is not constrained by ray tracing. The velocity structure of these models was compared ~ 70 km south of the vertex,

where Lines 1 and 2 are offset by ~ 40 km. The average velocity values are very close for the two models (Figure 17a), typically 6.1 km/s and 6.3 km/s in the upper and middle crust, respectively. Line 1 maintains these relatively low upper crustal velocities throughout the extent of the survey, whereas the velocities along Line 2 change abruptly in the west. Velocities in the lower crust average 6.5 km/s and both models indicate an upper mantle velocity of 7.9 km/s.

Within the upper crust, Zelt et al. (1992) imaged a thin low velocity zone where velocities decreased from 6.2 km/s to 6.0 km/s (Figure 17c). This upper crustal discontinuity (R1a) was not observed by the Line 2 data. Zelt et al. (1992) indicated that although the low velocity zone is present in the final model, it was not considered to be a significant feature of the model and could be explained as resulting from fine-scale layering. In light of this conclusion, no emphasis will be placed on attempting to resolve this inconsistency between the models. The depth to the base of the upper crust (R1) is consistent between the two velocity structure models at the point of comparison.

Apparent discrepancies between the two velocity models for the middle and lower crustal units can be attributed to the difference in orientation of the two surveys. The Line 2 data imaged a mid-crustal discontinuity (R2) at ~ 20 km depth beneath SP15. Although the depth to this reflector is near the discontinuity imaged at 22 km (R3) by the Line 1 survey, it cannot be interpreted as the same horizon due to the difference in the nature of the associated phases which define the discontinuities. The R2 reflector defined by the Line 2 data was generated by a relatively small velocity contrast (< 0.7 km/s); the corresponding phase along Line 1 may have been obscured by the larger amplitudes of the R3 phase observed by Line 1 data set. Approximately 50 km farther south along Line 1, the R3 reflector dips to values near 25 km which is consistent with the base of the middle crust (R3) as defined by the Line 2 data set.

Both surveys indicate that the Moho is essentially flat throughout the region. The interpreted depth to this discontinuity is 35 km along Line 2 and 33 km along Line 1.

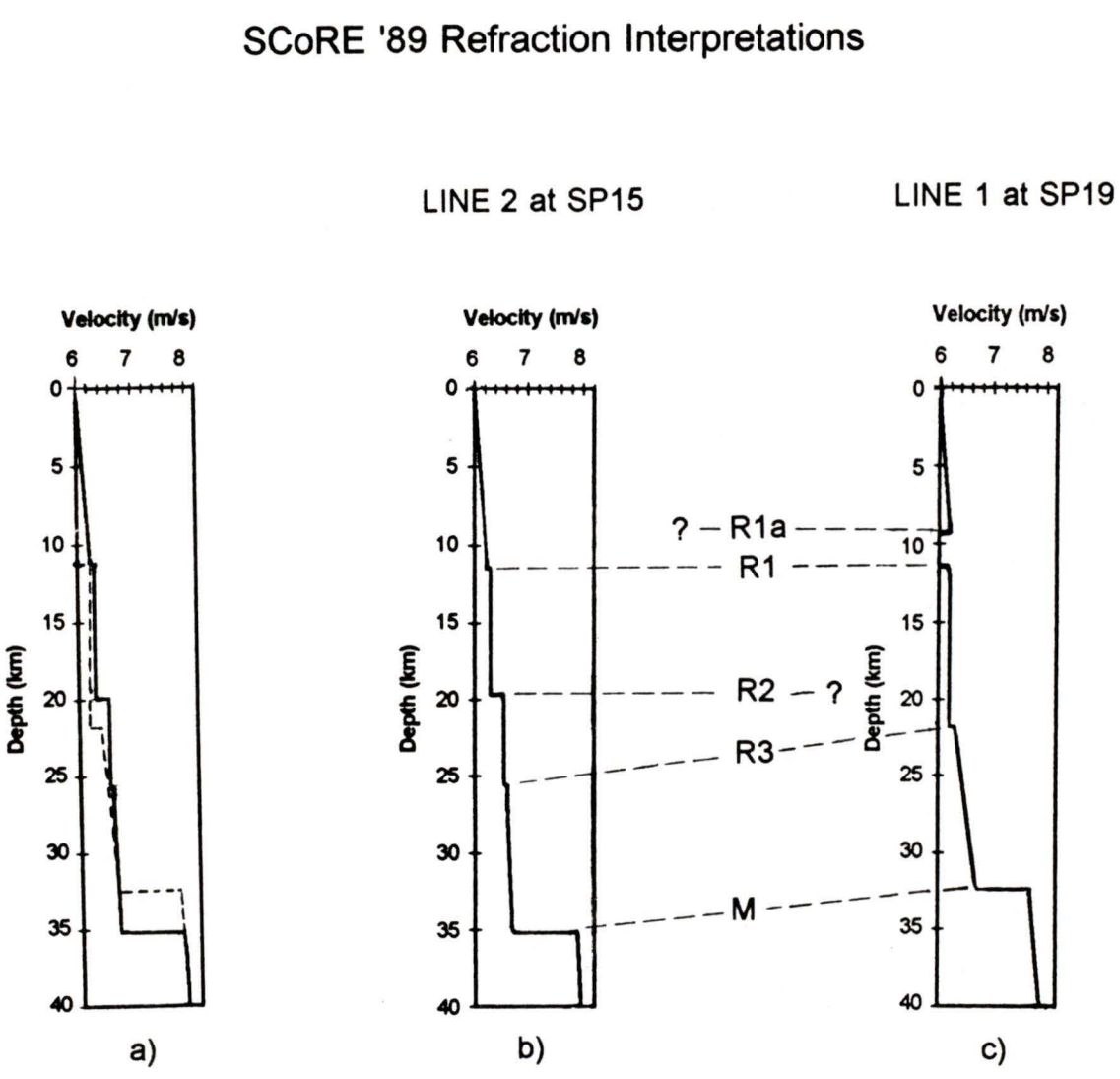

FIGURE 17. (a) Shows the comparison of the 1-D velocity versus depth profiles for the refraction interpretations of Line 2 at SP15 and Line 1 at SP19 (Zelt et al., 1992). The solid line represents the profile from Line 2 and the dotted line represents the profile from Line 1. Figures (b) and (c) indicate correlation of velocity discontinuities observed on Lines 1 and 2. Labels R1, R2, and R3 refer to the upper, middle, and lower crustal reflectors observed by Line 2 data, R1a is an upper crustal reflector imaged on Line 1 but not on Line 2. M indicates the Mohorovic discontinuity. The label '?' indicates an apparent discrepancy in the velocity structure.

Although this discrepancy is within the limits of the estimated uncertainties of the model parameters, it may also be attributed to the difference in orientation of the two refraction lines.

4.3.1b Comparison of Line 2 with Line 3:

Line 2 is coincident with Line 3 (Zelt et al., 1993) from SP8 to SP10, beyond which Line 2 deviates northwest into Coast Belt while Line 3 continues directly east. The maximum depth of penetration of rays west of SP10 is ~ 15 km. Discrepancies in the velocity structure above this depth should not be present between SP8 and SP10 if each of the velocity structural models are accurately resolved. Below this depth, the traveltime rays are no longer being traced to common receiver locations (refer to Figure 1) so velocity structural differences may become apparent. For instance, at the location of the next shot point along each profile, the offset between Line 2 and Line 3 is 100 km and increasing. Clearly, each line is imaging a different section of the Earth's crust.

Figure 18a displays the comparison of the velocity depth structure of Lines 2 and 3 just east of SP9. As rays do not constrain the entire model beneath either SP8 or SP9, a comparison of models was made midway between SP8 and SP10 beneath the Strait of Georgia. To a depth of 15-20 km, the velocity models show no discrepancies outside of the range of those allowed by absolute uncertainty estimates of the model parameters (up to 0.3 km/s and 1.0 km). As well, the velocities in the upper and middle crust along Line 2 exhibit the same general trend as observed by the Line 3 data, with velocities in the west higher than those in the east. The contrast in velocity structure is associated the Harrison Fault along Line 2, which is consistent with the location of the velocity contrast observed on Line 3 (Zelt et al., 1993).

Below a depth of 15-20 km, the models tend to differ. Beneath Vancouver Island, velocities in lower crust are lower on Line 2 (6.65 -6.8 km/s) than those observed on Line 3

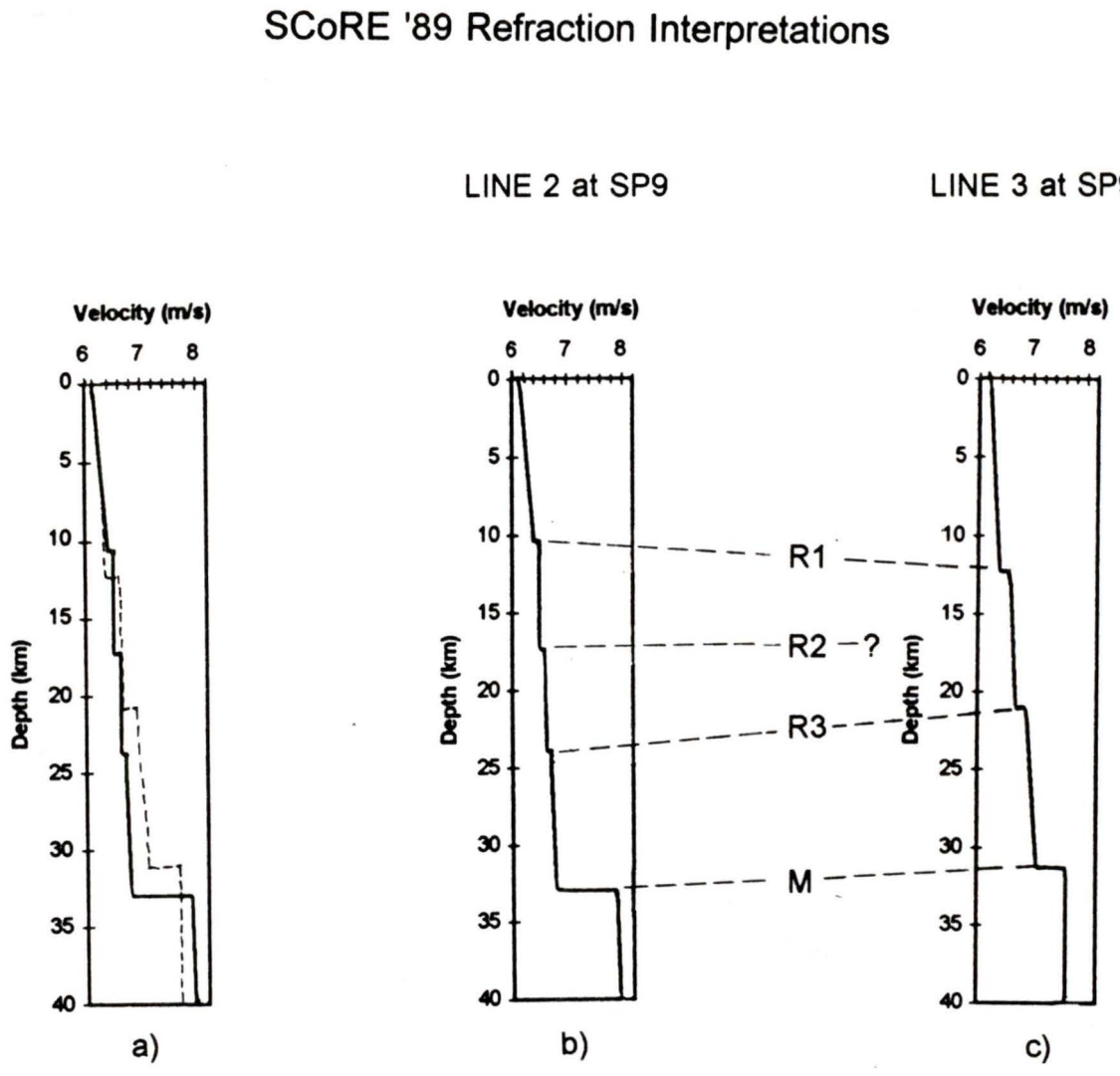

FIGURE 18. (a) Shows the comparison of the 1-D velocity versus depth profiles for the refraction interpretations of Lines 2 and 3 (Zelt et al., 1993) east of SP9. The solid line represents the profile from Line 2 and the dotted line represents the profile from Line 3. Figures (b) and (c) indicate the correlation of the velocity discontinuities observed on Lines 2 and 3. Labels R1, R2, and R3 refer to the upper, middle, and lower crustal reflectors as imaged by the Line 2 data set. M indicates the Mohorovic discontinuity. The label '?' indicates an apparent discrepancy in the velocity structure.

(6.9 - 7.1 km/s) and velocities in the upper mantle are higher on Line 2 (7.9 km/s) than those observed on Line 3 (7.65 km/s). The interpretations of reflecting horizons for the middle and lower crustal structure are also different. The Line 2 data imaged a mid-crustal discontinuity (R2) at ~ 17 km depth beneath the Strait of Georgia. There is no direct counterpart in the Line 3 velocity model. It is undetermined whether this horizon merges with the base of the upper crust (R1) or dips westward beneath Vancouver Island. The discrepancy between the two velocity models may be attributed to lack of resolving power by both data sets with the corresponding phase being obscured by other arrivals.

On Line 2, the arrivals identified as the R3 reflector were observed between offsets of 100 km and 190 km on SP8 and SP9 (Figures 4a and 5a). The R3 reflector was not interpreted as the Moho because its shallow depth (25 km) was not consistent with the Moho depth (34 km) determined from the SP6 record section (see Figures 8a and 16). On Line 3, a similar set of arrivals for SP8 and SP9 extended to offsets of 250 km and were identified as arrivals from the crust-mantle discontinuity. Using somewhat larger traveltime picks and a higher velocity in the lower crust, Zelt et al. (1993) determined the Moho to be at 31 km depth. This is deeper than the R3 reflecting horizon defined by Line 2 but shallower than the Moho determined from the SP6 record section.

It is emphasized that although a similar set of arrivals were observed by both surveys, the receiver locations were not common at offsets greater than 100 km. Because of the difference in character of the observed phase as the lines deviate, it is likely that the structure at this depth in the Western Coast Belt is not the same to the south. On Line 2, the absence of Moho arrivals for SP8 and SP9 and the termination of R3 arrivals at 190 km offset indicates the presence of a geological structure beneath Line 2 which is scattering lower crust and mantle energy, consistent with Berry and Forsyth (1975). This structure is not present to the south along Line 3 since lower crust or mantle arrivals extend to offsets of 250 km.

4.3.1c Comparison of Line 2 with Line 10:

The refraction Line 10 of SCoRE '90 (O'Leary et al., 1993) intersects Line 2 at SP6. The velocity values in the upper, middle, and lower crust are almost identical between the two models (Figure 19). Typical values are 6.3 km/s and 6.4 km/s in the upper and middle portions of the crust, and ~ 6.65 km/s in the lower crust. Upper mantle velocities were much lower on Line 2 (7.95 km/s) compared to Line 10 (8.15 km/s). However, O'Leary et al. (1993) asserted that these values may be dubious because of the limited number of Pn arrivals observed by the data set. At the intersection of Line 2 and Line 10, the Harrison Fault is virtually coincident with Line 10. The velocity values observed on Line 10 are comparable to values observed along the eastern portion of Line 2 which are indicative of velocities observed in the Intermontane Belt. This indicates that the Insular superterrane, dominated by Wrangellia terrane, extends in the subsurface no farther east than the Harrison Fault, consistent with the Line 3 survey to the south (Zelt et al., 1993).

The Line 2 data exhibit the same distinct features as the Line 10 data (Figure 19). The velocity structure of the crust is divided into three layers separated by wide-angle reflections. Clearly, the crustal and upper mantle velocity structure of the two models closely agree, with the exception of the structure in the lower crust. The interpreted depth to the base of the mid-crustal unit (R2) along Line 10 is ~ 20 km, 4 km shallower than the base of the mid-crust (R3) determined by the Line 2 survey. The 20 km depth is consistent with the depth to a mid-crustal discontinuity (R2) imaged by the Line 2 data but it is an entirely different horizon. The difference in the mid-crustal structure between the two models may indicate the difference in resolving power of the two data sets. The Line 2 data set was able to distinguish a difference between two very close reflecting horizons whereas the Line 10 data set was only able to distinguish one horizon. The corresponding phase for the second horizon may have been obscured by other arrivals. Also, the Line 2 data did not image the wide-angle reflector in the lower crust of the Line 10 model. The difference in orientation of the two refraction lines may account for the discrepancies in the velocity structural models. Line 10 was oriented N-S within the Coast Belt and Line 2 was oriented NE-SW cross-strike the Fraser Fault system;

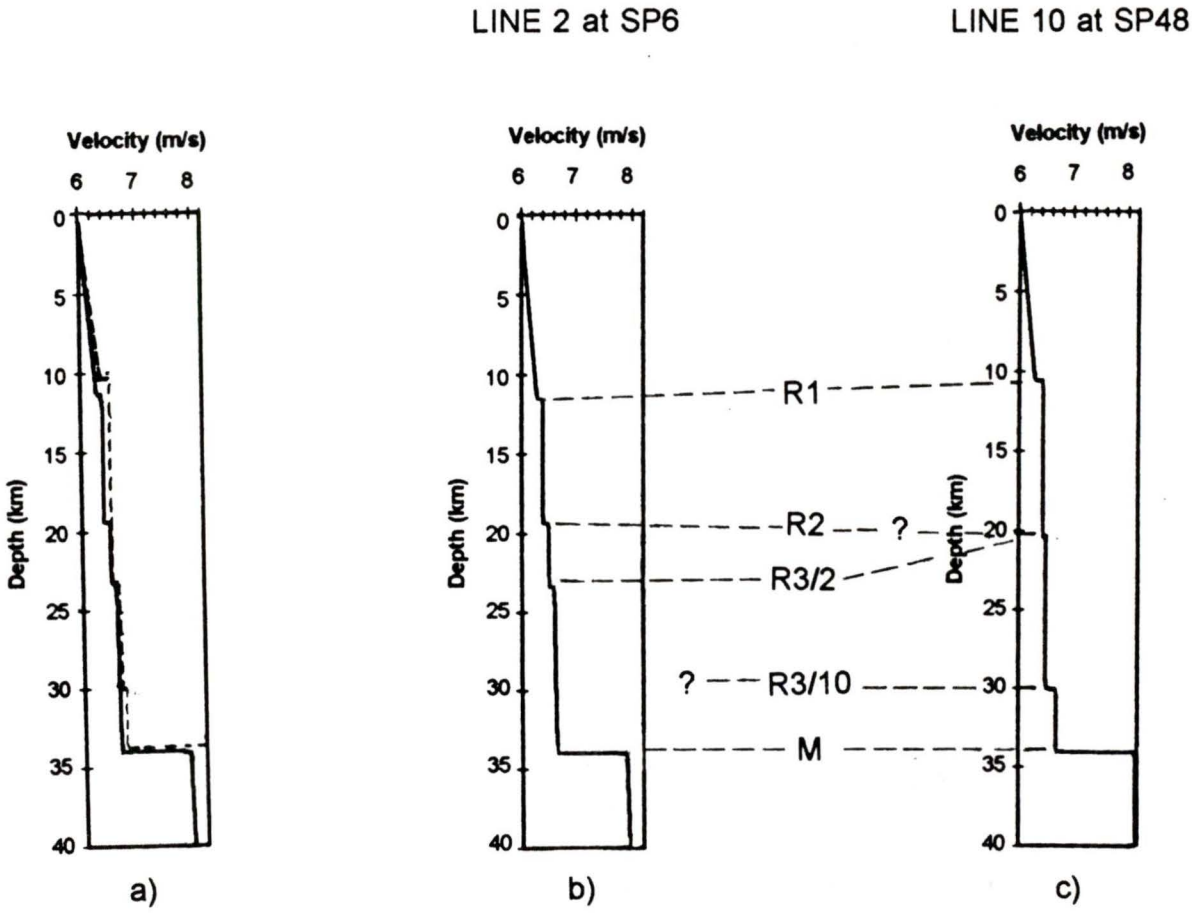

FIGURE 19. (a) Shows the comparison of the 1-D velocity versus depth profiles for the refraction interpretations of Line 2 at SP6 and Line 10 at SP48 (O'Leary et al., 1993). The solid line represents the profile from Line 2 and the dotted line represents the profile from Line 10. Figures (b) and (c) indicate the correlation of the velocity discontinuities observed on Line 2 and Line 10. Labels R1 and R2 refer to the upper and middle crustal reflectors. Labels 'R3/2' and 'R3/10' refer to the R3 reflector defined by Line 2 and Line 10, respectively. M indicates the Mohorovic discontinuity. The label '?' indicates a possible discrepancy in the velocity structure.

structures may be elongated along the length of a line and have only limited lateral extent in the perpendicular direction.

4.3.2 Comparison with LITHOPROBE Reflection Data

The comparison of reflection and refraction data provides insight into the interrelationships of the component terranes comprising the crustal section of the refraction survey. The LITHOPROBE reflection profile 88-13 is virtually coincident with Line 2. Two other reflection profiles near the region of Line 2 are profiles 88-16 and 88-18 (Figure 1). Profile 88-16 is located in the Western Coast Belt approximately 50 km north of Line 2 and profile 88-18 runs cross-strike to the Fraser Fault system 60 km to the south of Line 2. Interpretation of the reflection profiles was completed initially by Monger and Journeay (1992), then in more detail by Varsek et al. (1993) with additional analysis on profile 88-18 provided by Perz (1992). An earlier LITHOPROBE profile, profile 84-01, ran east-west across Vancouver Island; the eastern end of this profile is near SP9 (Figure 1). These data were interpreted by Green et al. (1986) and by Clowes et al. (1987). The reflection profiles, 88-13, 88-16, 88-18 and 84-01, are shown in Figures 20 to 22 on which the interpretational boundaries of Varsek et al. (1993) are indicated.

The interpretations of the LITHOPROBE reflection data by Monger and Journeay (1992) and by Varsek et al. (1993) indicated very similar models for the upper crust, but the models deviated in the interpretations of the lower crustal features. Many of the upper crustal structures visible in the reflection sections undoubtedly arose from the Mesozoic crustal shortening adjustments that accommodated terrane accretion (Monger and Journeay, 1992). Both interpretations indicated the juxtaposition of Insular and Intermontane materials and concluded that the collision site of the Insular and Intermontane superterranes is confined to a region east of the Harrison Fault. This is consistent with the contrast in crustal velocity structure observed along Line 2. Varsek et al. (1993) proposed a collision model based upon crustal imbrication in which fingers of Wrangellia terrane have wedged into the Intermontane superterrane. Monger and Journeay (1992) proposed a crustal delamination model which

suggested that the Wrangellia terrane has been pushed up over the Intermontane superterrane.

4.3.2a Comparison of Line 2 with Profile 88-13:

Profile 88-13 (Figure 20a) displays a cross-cutting relationship in the upper and middle crust. East-dipping reflectors in the upper crust are truncated by west-dipping reflectors in the middle and lower crust. The east-dipping lower crustal reflectors imaged in the Western Coast Belt are correlated with the Insular ramp. In the lower crust, a pronounced package of Moho reflections start at ~ 10.9 s. Figure 20b shows the corresponding simplified schematic of the 88-13 reflection interpretation of Varsek et al. (1993). Horizons representing velocity discontinuities in the velocity structural model of Line 2 are superimposed on the reflection interpretation. The conversion of the refraction velocity model from depth to two-way traveltime was accomplished by the averaging of reciprocal velocities from the surface downward, thus allowing for refraction imaged reflections to be compared to the reflection data. Although reflection profile 88-13 was coincident with Line 2 over ~ 60 km, an exact correspondence is not expected for a number of reasons: (i) the possibility of lateral averaging in the refraction velocity model; (ii) 3-D effect introduced by the non-linearity of Line 2 and (iii) crustal anisotropy;

The R1 reflector is not well-constrained in the region west of SP12 (Figures 14 and 16) which is consistent with the lack of a definite reflection in this region (Figure 20a) at ~3.5 s. However, the R1 reflector imaged by the Line 2 data is coincident with the base of the Shuksan terrane in the Central Coast Belt (Figure 20b). In the Western and Eastern Coast Belts, this horizon coincides with west-dipping reflectors which define the base of the upper crust. The R2 reflector was modelled at ~ 6.6 s and is consistent with a horizontal band of reflectors in the Central and Eastern Coast Belts (Figure 20b). This reflector may correspond to the top of a segment of Wrangellia terrane in the Western Coast Belt (Figure 20b). The bottom of this wedge of material is consistent with the R3 reflector. In the Eastern Coast Belt, the R3 reflecting horizon dips to the east; however, there is no corresponding band of reflectors imaged by the refraction data (Figure 20a). The lower crustal east-dipping reflector

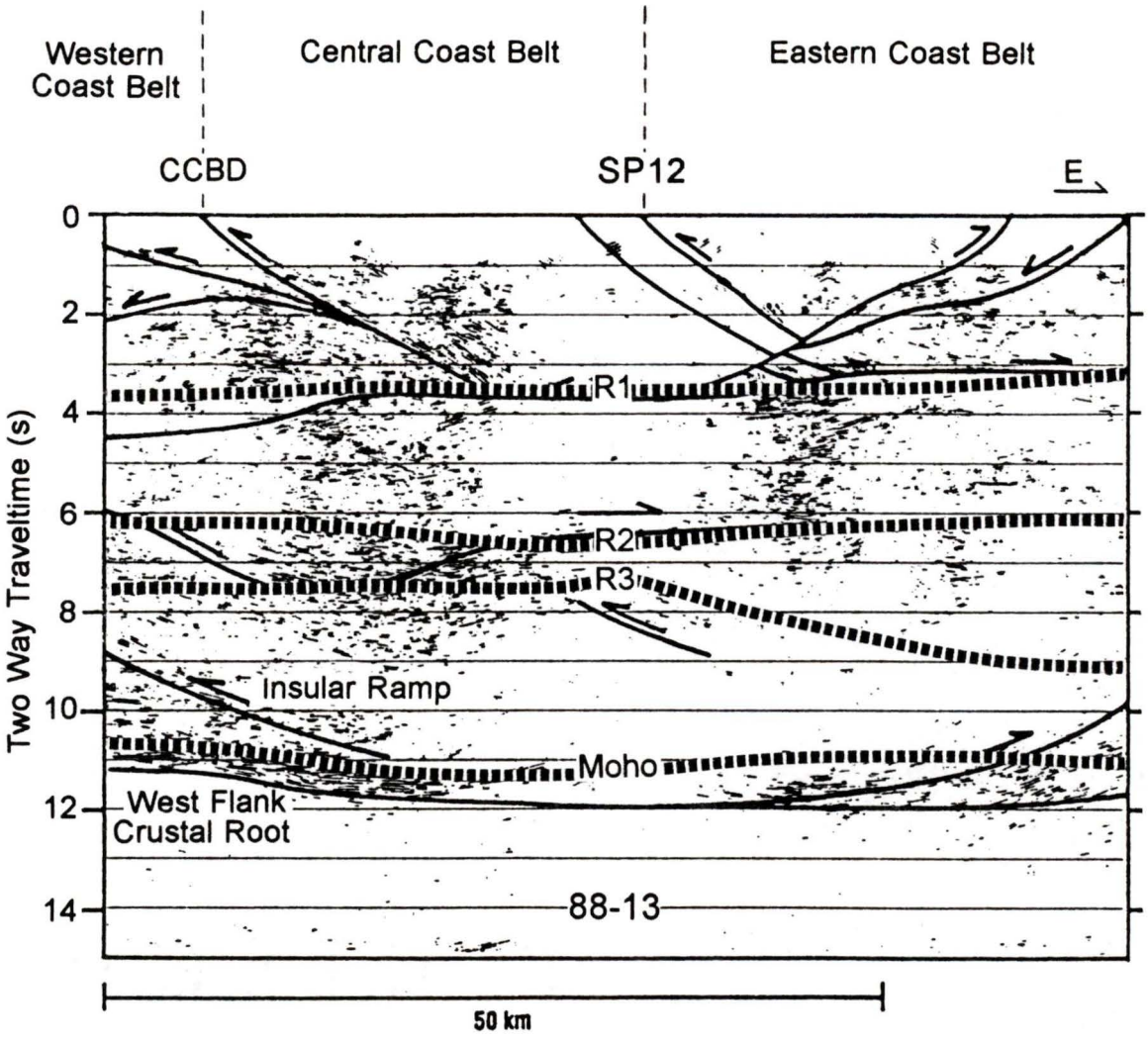

FIGURE 20: (a) LITHOPROBE reflection profile 88-13 migrated and coherency filtered, adapted from Varsek et at. (1993). The solid lines indicate the interpretational boundaries of Varsek at al. (1993). The dotted lines indicate the velocity structure of Line 2. CCBD indicates the Central Coast Belt Detachment.

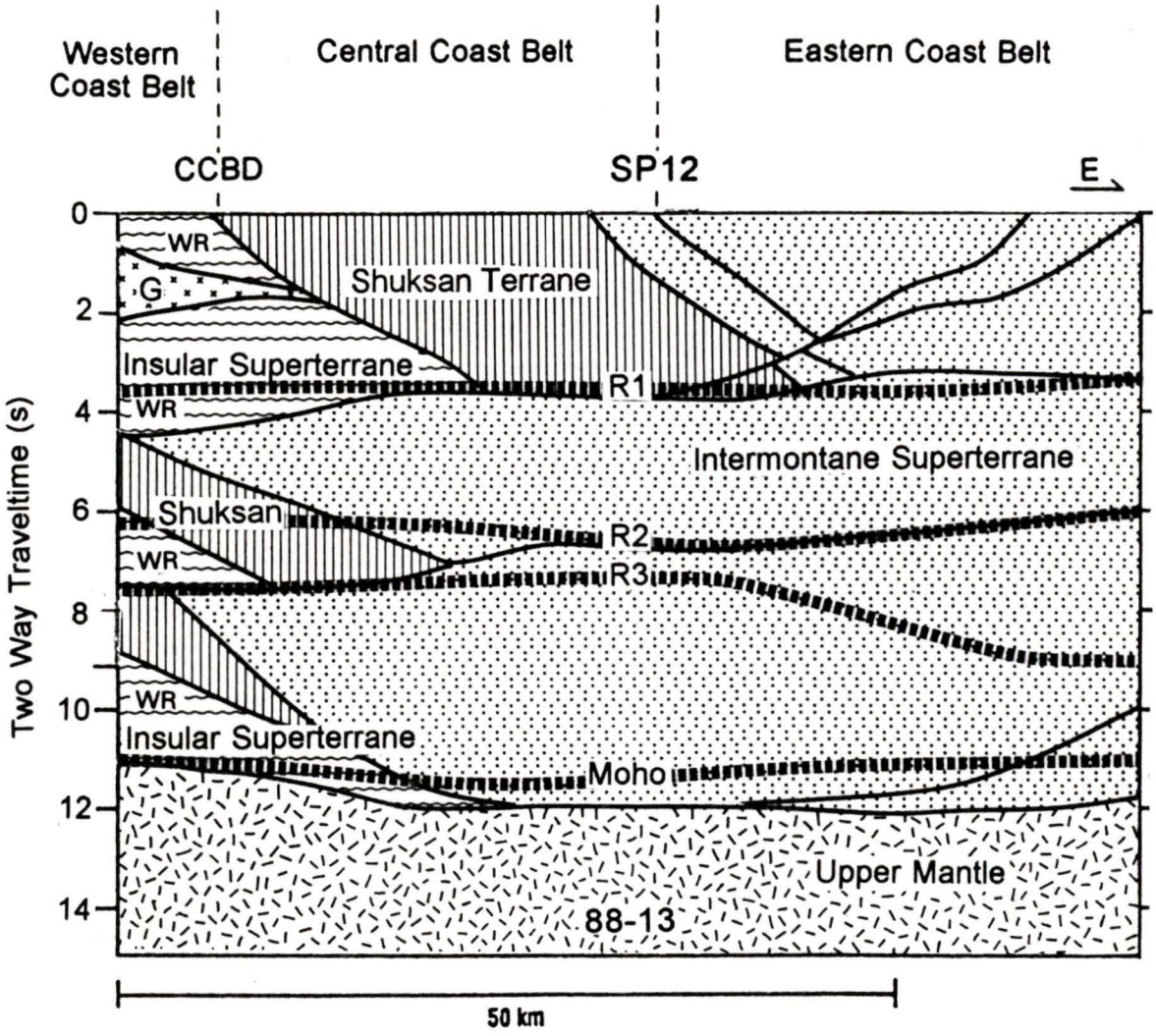

FIGURE 20: (b) Shows a simplified schematic of the 88-13 reflection interpretation of Varsek et al. (1993). Overlain is the velocity structure of Line 2 of SCoRE '89. CCBD denotes the Central Coast Belt Detachment, G denotes the Gambier Overlap Assemblage. WR indicates the interfingering of the Insular and Intermontane superterranes as proposed by the crustal imbrication model of Varsek et al. (1993).

interpreted as the Insular Ramp (Varsek et al., 1993) was not resolved by the Line 2 refraction data. The position of the refraction Moho (10.9 s) coincides with the top of a pronounced package of Moho reflections observed on profile 88-13. Clearly, the velocity structure model developed from the analysis of the Line 2 refraction data is consistent with the interpretation of the 88-13 reflection profile.

4.3.2b Comparison of Line 2 with Profile 88-18:

Reflection profile 88-18, which is 60 km south Line 2 at SP13, crosses the Fraser-Straight Creek Fault. The record section (Figure 21) displays a pronounced difference in structural styles on either side of the fault. In the Eastern Coast Belt, strong west-dipping reflectors are imaged in the upper crust while the lower crust images strong east-dipping reflectors. In the Intermontane Belt the reverse pattern is observed: east-dipping reflectors in the upper crust and west-dipping reflectors in the lower crust. In the Eastern Coast Belt, Varsek et al. (1993) proposed that the strong east-dipping reflectors in the lower crust may contain counterparts to exposed east-dipping thrust faults in the Coast Belt, perhaps the Central Coast Belt Detachment, and that the strong lower crustal ramp may have been carried eastward since it is truncated by west-dipping reflectors.

A prominent feature of the data section is a band of horizontal reflectivity in the middle crust observed on either side of the fault at ~ 6.0 s (Figure 21). This feature plays a vital role in the interpretation of the possible geometry of the Fraser-Straight Creek Fault. Three possible interpretations for the geometry of the Fraser-Straight Creek Fault are shown in Figure 21, labelled FFA, FFB, and FFC. Trajectory FFA flattens into the middle crust, trajectory FFB indicates that the fault begins to flatten into the lower crust but does not offset the Moho and trajectory FFC indicates that the fault penetrates the crust (Varsek et al., 1993). Varsek et al. (1993) indicated that trajectory FFA or FFB would be possible geometries of the Fraser-Straight Creek Fault but trajectory FFB was not preferred because of the apparent continuity of reflectors at 6.0 s across the fault zone. Perz (1992) reprocessed the seismic section and proposed deep crustal extent (trajectory FFB or FFC) of the Fraser-

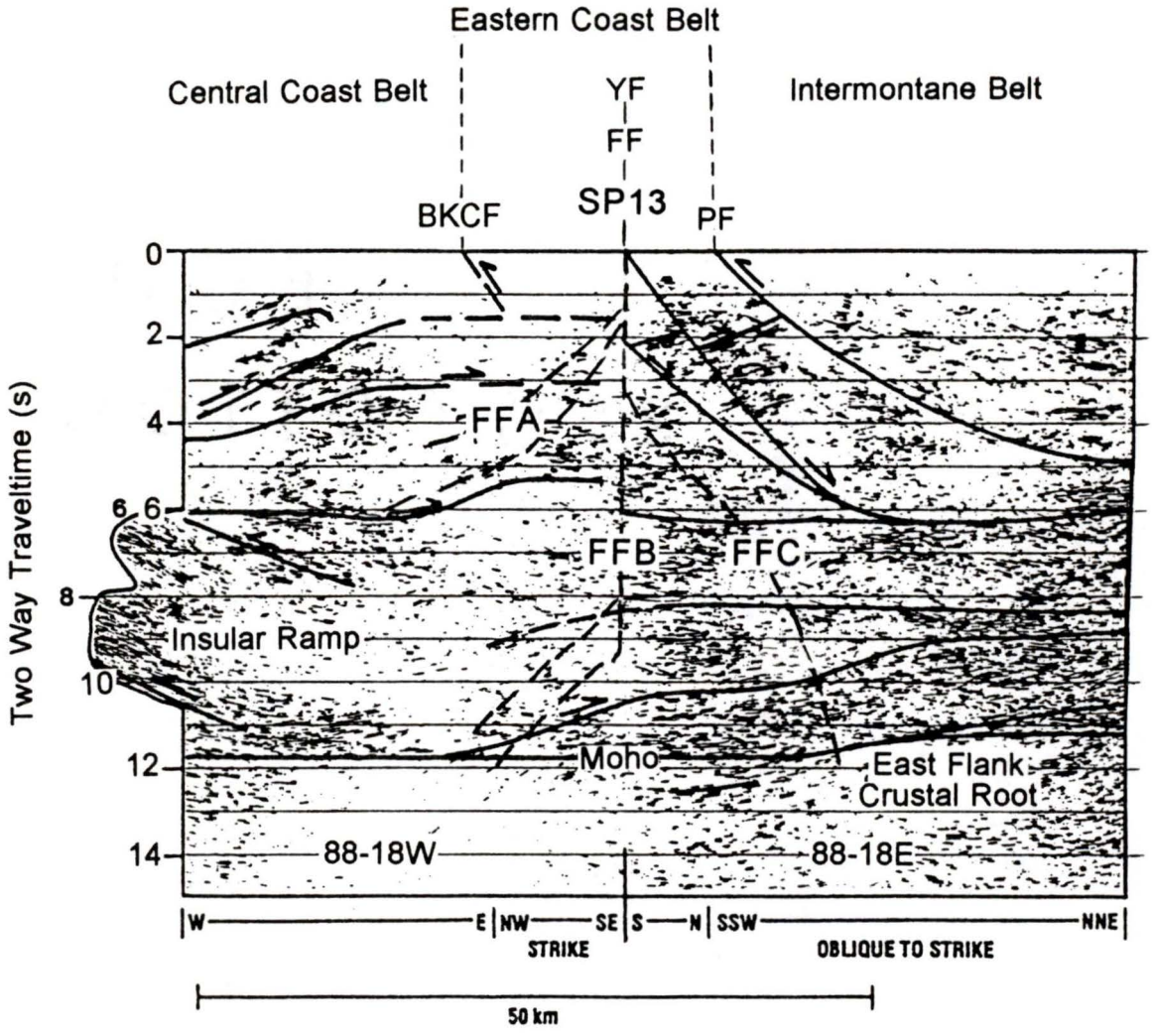

FIGURE 21: LITHOPROBE reflection profile 88-18, migrated and coherency filtered adapted from Varsek et at. (1993). The solid lines indicate the interpretational boundaries of Varsek at al. (1993). FFA, FFB, and FFC indicate the possible geometries of the Fraser-Straight Creek Fault (FF). YF is the Yalakom Fault, BKCF is the Bralorne-Kwoiek Creek Fault and PF is the Pasayten Fault. Shot Point 13 is offset to the north by ~ 60 km.

Straight Creek Fault based on the lack of evidence for continuity of the reflectors at 6.0 s across the fault zone. Also, the juxtaposition of different structural styles appears to extend to a great depth which implies that the fault has a sub-vertical geometry (Perz, 1992). Undoubtedly, there is a major contradiction of the possible subsurface position of the Fraser-Straight Creek Fault between the originally processed data and the re-processed data.

Because of the 60 km offset of the reflection profile from Line 2 it is not reasonable to compare a velocity versus two-way traveltime interpretation of Line 2 with the interpretation of the 88-18 reflection profile. However, features of the final velocity model of Line 2 seem to be consistent with the Perz (1992) interpretation of profile 88-18. A definite difference in structural styles across the fault zone is inherent in the Line 2 velocity model to near the base of the crust; sub-vertical geometry is indicated, and deep crustal penetration of the fault is implied as there appears to be a structural offset in the R2 and R3 reflectors on either side of the fault zone (Figure 14). Each of these reflectors, particularly the R3 reflector, have large undulations beneath the surface location of the fault, so the continuity of these reflectors across the fault zone must be questioned. Considering the resolving power of the refraction data, it is likely that the R2 and R3 reflectors are not continuous across the fault.

There does not appear to be evidence for vertical displacement within the upper mantle indicating that the Fraser-Straight Creek Fault may penetrate the crust but does not penetrate the upper mantle. The interpretation of Varsek et al. (1993) suggested a west-side down Moho from 11 s to 11.7 s (~ 34 to 37 km). A similar result was interpreted by Zelt et al. (1993) for the Line 3 refraction data and for the 3-D interpretation south of profile 88-18 (Zelt et al., 1995), although the variations observed in this data were associated with large uncertainties. Perz (1992) indicated a flat Moho across the region at 11.2 s (35 km) and explained the discrepancy between interpretations as resulting from processing techniques. The Line 2 model images the Moho at 34.9 km at the Fraser-Straight Creek Fault and does not indicate crustal thickening to the west; in contrast the Moho depth decreases slightly to the west. Taking into account the estimated uncertainties associated with the Moho depth

(up to 2.0 km), the refraction data can be considered consistent with the reflection data but does not imply a west-side down Moho. The crust-mantle discontinuity imaged by the refraction data is best correlated with the top of the reflective package near 11 s. If a thicker crust is the preferred analysis for the Eastern Coast Belt near the reflection profile 88-18, the Line 2 refraction implies crustal thinning to the north.

4.3.2c Comparison of Line 2 with Profiles 84-01 and 88-16:

Figure 22 displays LITHOPROBE reflection profiles 84-01 and 88-16. Profile 84-01 displays two prominent bands of east-dipping reflectors (C and E) in the middle and lower crust. Clowes et al. (1987) interpreted these reflectors as the upper and lower boundaries of a high density and high velocity slab composed of mafic rocks derived by the continuous accretion and underplating of materials from the top of the subducting oceanic crust. Analysis of profile 84-01 tentatively places the crust-mantle boundary at ~ 10.5 s (~ 34 km depth) at the west end of the profile (Figure 22a), although Clowes et al. (1987) indicated that the Moho may become as deep at 38 km at the east end of the profile near SP9 of Line 2.

The upper portion of profile 88-16 (Figure 22) is characterized by weak crustal reflectivity while the lower western half of the survey imaged a number of reflectors in the middle crust and upper mantle (UM16A, UM16E). The upper structure of the Western Coast Belt is generally undeformed and so little reflectivity is expected. The eastern half of the profile is oddly lacking in reflectivity. This feature possibly correlates with the 'lack' of PmP arrivals on the four record sections of Line 2 in the Insular and Western Coast Belts (SP8 - SP11). Varsek et al. (1993) indicated that reflectivity in the lower crust decreased with proximity to the Garibaldi volcanic belt, perhaps due to disruption of older structures by rising magmas or homogenization of the crust due to higher temperatures.

Analysis of the reflection data revealed two possible positions of the crust-mantle boundary and possible continuations of the 'C' and 'E' reflectors beneath the mainland. In the first scenario (Figure 22a), the 'C' reflector bounds the top of the lower crustal wedge and

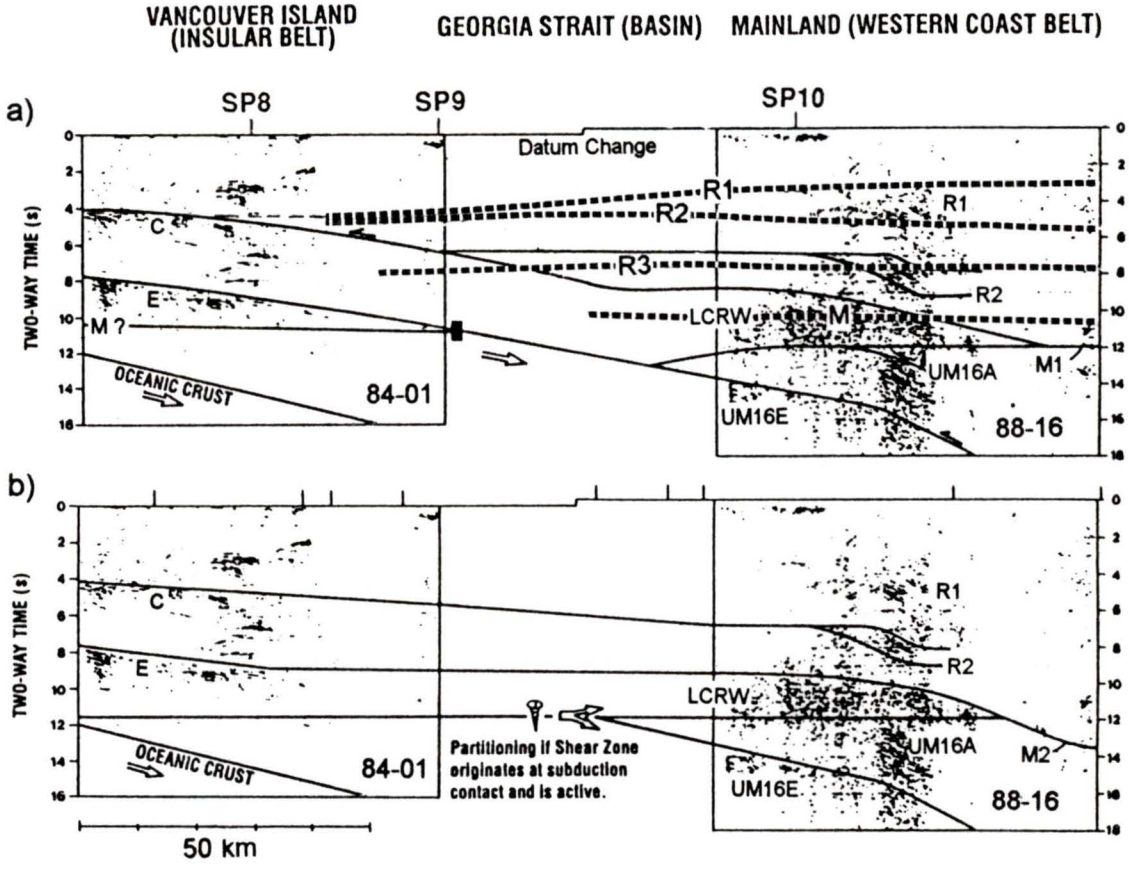

FIGURE 22: LITHOPROBE reflection profiles 84-01 and 88-16, migrated and coherency filtered, adapted from Varsek et at. (1993). Figures (a) and (b) display the possible continuation of the seismic data from Vancouver Island to the mainland. The solid lines indicate the interpretational boundaries of Clowes et al. (1987) for profile 84-01 and Varsek at al. (1993) for profile 88-16. The dotted lines indicate the preferred interpretation of the reflection data based on the Line 2 analysis. C and E indicate the reflective 'C' and 'E' zones beneath Vancouver Island, LCRW denotes a lower crustal wedge, M, M1, and M2 indicate the possible positions of the Moho, UM16A and UM16E are strong east-dipping upper mantle reflectors.

flattens into the Moho at about 12 s in which case the 'E' reflector is continuous with an upper mantle reflector (Varsek et al., 1993). This is the preferred interpretation of the reflection data. Clowes et al. (1995), who synthesized analyses from many refraction lines in the Cordillera, also preferred this interpretation. In the second case (Figure 22b), the 'C' reflector is correlated with the mid-crustal R2 reflector; the 'E' reflector defines the top boundary of the lower crustal wedge and then flattens into the Moho at about 13.5 s, in which case the upper mantle reflectors have no counterparts beneath Vancouver Island (Varsek et al., 1993).

The two possible depths to the crust-mantle boundary, 12 s and 13.5 s, are inconsistent with the Line 2 interpretation. Using the velocity structure of Line 2, these two-way traveltimes correspond to depths of 39 km and 43.5 km indicating a significant increase in crustal thickness to the north of Line 2. Nevertheless, it appears that both the reflection and the refraction data predict the presence of Wrangellia terrane throughout the Insular Belt and into the Western Coast Belt. In the preferred interpretation of the reflection data, Wrangellia is found above the 'C' reflector and above the reflective wedge in the lower crust (Clowes et al., 1987; Varsek et al., 1993). The higher velocities observed by the Line 2 data are correlated with Wrangellia terrane and are maintained from beneath Vancouver Island as far east as the Harrison Fault.

Alternatively, it is suggested in this thesis that the crust-mantle boundary beneath profile 88-16 occurs at ~ 10.0 s (Figure 22), near the top of the package of reflectors interpreted by Varsek et al. (1993) as a lower crustal wedge. Thus, all the strong reflectivity below 10.0 s is mantle reflectivity corresponding to previously subducted lithosphere which could also cause scattering of lower crustal and upper mantle energy indicated by the Line 2 data. Assuming no significant changes occur in the upper and middle crustal structure to the north, the depth of the Moho would be ~ 32 km which can be considered consistent with the Line 2 analysis. In this interpretation, the R1 and R2 reflectors on Line 2 are correlated with a package of upper crustal reflections (R1) on profile 88-16. No corresponding package of reflectivity was observed at the eastern edge of profile 84-01; however, the depth to the R1

reflector is consistent with the depth of the 'C' reflector at the western edge of profile 84-01. The R3 reflector on Line 2 coincides with a package of lower crustal reflectors (R2) on profile 88-16. Since there is no corresponding reflection on profile 84-01, the R3 reflector may represent imbricated structures within the Wrangellia basement.

4.4 Comparison with Other Geophysical Studies

4.4.1 Heat Flow Studies

The heat flow values for the Intermontane Belt are uniform and moderately high, averaging 73 mW/m^2, with slightly higher values in the Coast Belt, averaging 75-95 mW/m^2 (Lewis et al., 1992). High heat flow in the interior is consistent with a thin crust as determined by this study and other seismic surveys in the area. Further west, heat flow values decrease significantly to extremely low values (< 50 mW/m^2) in the Insular Belt. The observed low in the Insular Belt, and inland high, can be attributed solely to the 'heat sink' effect of the subducting Juan de Fuca plate (Hyndman et al., 1976). A thick crust is not necessary to explain the lower temperatures.

A widely-accepted hypothesis to explain reflectivity in the lower crust is aqueous porosity layering in which the pressure in the crust is sufficient to maintain thin open pores where fluid is trapped and high reflectivity coefficients are generated. This model also provides an explanation for regions with high electrical conductivity (Hyndman and Shearer, 1989). Support for this type of model is provided by the theory that a correlation exists between the depths to the top of characteristic reflective bands often observed in the lower crust and regional heat flow (Klemperer, 1987), such that reflectors are shallower where crustal temperatures are high.

Two of the more important temperature changes in the lower crust are the transition points of the brittle-ductile zone, the 450°C isotherm, and the transition from a wet to dry mineralogy, the 730°C isotherm. Typically, the 450°C isotherm has corresponded to the top

of the characteristic, sub-horizontal reflection bands in the lower crust and the 730°C isotherm has corresponded to the bottom of these characteristic bands (Lewis et al., 1992). Correlations between the isotherms and the top and bottom of the seismically reflective band in the lower crust have been made on many of the LITHOPROBE reflection profiles across the Cordillera. In the region of the Fraser Fault system, profiles 88-13 (Figure 20) and 88-18 (Figure 21) display strong reflectivity throughout the crust making it difficult to distinguish such bands of reflectivity. A tentative comparison was made by Perz (1992) for profile 88-18, by which the reflectivity observed between 4 s and 7 s (13 and 20 km depth) corresponded to the 450°C and 730°C isotherms, respectively. On profiles 84-01 and 88-16 (Figure 22), the top of the reflective 'E' zone has been correlated to the 450°C isotherm (Cook et al., 1988). It has already been concluded that the high density and high velocity slab of mafic material above the subducting Juan de Fuca plate is not imaged by the Line 2 data, thus a correspondence between the 450°C isotherm (top of the reflective 'E' zone) and reflectors in the lower crust is not validated.

In the Coast Belt, Lewis et al. (1992) have shown that the crustal temperatures suggested a depth to the 450°C isotherm ranging from 10 - 13.9 km and ~ 20 km to the 730°C isotherm, depending on the amount of surficial heat generation. In the Intermontane Belt, where heat flow values are more uniform, the depth to the 450°C isotherm is ~ 13.9 km and the depth to the 730°C isotherm is ~ 21 km. These depths coincide well with the depths to the R1 and R2 reflectors imaged by the refraction data.

Although the depth to the R1 reflector correlates with that of the 450°C isotherm, it lacks the qualities of a continuous reflector as it is only imaged in the Intermontane Belt and at the edge of the Western Coast Belt. In the Intermontane Belt, the R1 reflector is well-defined with moderate amplitudes. This reflector could possibly be generated by a shear zone originating from the inter-layering of smaller terranes in the region. At the western edge of the Coast Belt, the R1 reflector may be generated by a lithological contrast or trapped fluids caused by tectonic underplating due to the subduction of the oceanic plate.

In the case of the R2 reflector, it is virtually continuous across all three morphogeological belts except for the highly faulted region surrounding the Fraser-Straight Creek Fault. To correlate this reflector with the 730°C isotherm would ideally require an abrupt decrease in reflectivity below this depth (Lewis et al., 1992); however, this is not the case as the lower crust also images a strong, continuous reflector at ~ 25 km depth. A correlation between the 730°C isotherm and the R2 reflector would be possible only if heat flow values were below 75 mW/m^2. While this may be the case throughout many regions of the Intermontane and Coast Belts, it is not true for the entire area, hence any correlation between the two is debatable. The general synthesis of SCoRE refraction data (Clowes et al., 1995) also concludes that, over widespread regions in the Canadian Cordillera, there is no consistent correlation between the 3-D seismic structure and variations in heat flow or crustal isotherms.

4.4.2 Gravity Studies

The gravity anomaly data across the continental margin display a characteristic pattern (Keen and Hyndman, 1979). In the Insular Belt, gravity values are high with an associated low in the Coast and Intermontane Belts. The observed changes in Bouguer values across the region are attributed to either; (i) variations in the density of the crust or, (ii) variations in the density of the mantle (Stacey, 1973).

The observed inland low is considered to be a result of low upper mantle densities (Stacey, 1973), consistent with the moderately thin crust (34 km) observed by the Line 2 data and higher heat flow values. Analysis of gravity anomaly data in the Insular Belt favoured variations in the crustal density as being responsible for the gravity high as opposed to anomalous variations in upper mantle densities (Stacey, 1973; Riddihough, 1979). More specifically, it was concluded that beneath the Insular Belt a wedge of high-density material overlies the subducting Juan de Fuca plate (Dehler and Clowes, 1992; 1995), consistent with the seismic analyses of Spence et al. (1985) and Drew and Clowes (1990).

Although the depth of the crust-mantle boundary was not accurately resolved beneath Vancouver Island by the analysis of the Line 2 data, it appears to be at ~ 34 km. Analysis of Line 3 of SCoRE '89 placed the crust-mantle boundary at 29 km beneath the Insular Belt. Both of the values indicate a thinner crust beneath Vancouver Island than the 37 km thick crust estimated by Spence et al. (1985). The region of high-density material beneath Vancouver Island was not imaged by the Line 2 data, but the possible continuation of the upper boundary of this wedge, the 'C' reflector, beneath the Western Coast Belt is near the depth of the R3 reflector (Figure 22). The material below the R3 reflector may then be high-density material. Stacey (1973) indicated an alternative model which would satisfactorily image the Bouguer values across the Cordillera based on a thin crust (< 45 km) beneath Vancouver Island. In this model, the crust had a standard density throughout the region with variations occurring in the mantle density. Since the gravity decreases from the Insular Belt to the Coast Belt, it is possible that; i) the mantle density is significantly lower beneath the Western Coast Belt than beneath the Insular Belt, or ii) the density of the upper crust is lower in the Coast Belt, consistent with lower densities of plutonic rocks (Dehler and Clowes, 1992; 1995).

4.4.3 Electromagnetic Studies

In Phanerozoic regions such as the southern Cordillera, the lower crust is commonly reflective and electrically conductive while the upper and middle crust are more transparent and resistive (Hyndman and Shearer, 1989). This result is a surprising phenomena since it was generally believed that at lower crustal depths minerals would be dry and therefore very electrically resistive, due to dehydration processes caused by the high temperatures (Caner, 1970). It is argued that the conductive and reflective nature of the lower crust in the Cordillera is generally due to the presence of fluids at depth derived from the ongoing subduction of the Juan de Fuca plate (Gough, 1986; Gough and Majorowicz, 1992).

Recent magnetotelluric studies in the Cordillera indicate that conductivity in the middle and lower crust varies laterally in a predominantly east-to-west direction with little north-

south change (Jones et al., 1991a). Relative to the Coast Belt, the Intermontane Belt is more conductive in the upper crust and less conductive in the lower crust, consistent with slightly lower temperatures in the Intermontane Belt (Lewis et al., 1992). The change in conductivity occurs abruptly at the Fraser-Straight Creek Fault. The lower crust in the Insular Belt is generally resistive in nature.

A recent compilation of seismic refraction data within the Cordillera (Clowes et al., 1995) has indicated that seismic data in some regions of the Cordillera may not be sensitive to the same physical parameters as magnetotelluric data. This conclusion is supported by the Line 2 data. The seismic refraction data indicate higher velocities throughout the crust beneath the Coast Belt relative to the Intermontane Belt. Higher velocities are normally expected to be associated with higher resistivities. This relation appears to be observed in the upper crust, where both velocities and resistivities are higher in the Coast Belt than in the Intermontane Belt; however, high seismic velocities in the lower crust of the Coast Belt are associated with low resistivities, in contrast to the expected relation. Jones et al. (1992a) indicated that a more conductive lower crust in the Coast Belt could be associated with an increase in porosity or partial melt, but this does not appear to be supported by the seismic data.

Variations in conductivity or resistivity in the upper crust are attributed to the geological properties of the rocks. In the Coast Belt, the resistive upper crust is correlated with the presence of massive granitoid plutons with low fracture densities which extend to depths of ~ 14 km beneath Line 2, consistent with the base of the upper crust which is defined by the R1 reflector. Conductive zones in the upper crust of the Intermontane Belt are correlated with highly fractured basalts.

Jones et al. (1992b) indicated that there were four possible geometries for the Fraser-Straight Creek Fault but concluded that the best possible trajectory to explain the differences in conductivity in the lower crust would be a sub-vertical geometry. This would imply deep

crustal penetration of the Fraser-Straight Creek Fault which contradicted the interpretation of the pre-processed reflection data across the fault (Varsek et al., 1993). Additional analysis of the reflection data (Perz, 1992) indicates that deep crustal penetration of the Fraser-Straight Creek Fault could be a possible geometry for the fault consistent with the conductivity results. The Line 2 model implies a structural offset in the R2 and R3 reflectors on either side of the Fraser Fault system which may signify a sub-vertical trajectory, consistent with the magnetotelluric data.

V: DISCUSSION AND CONCLUSIONS

5.1 Discussion of Results

A geophysical interpretation of the Line 2 velocity structural model (Figure 14) is presented. The velocities of the near-surface layer correlate well with the surface geology. Higher velocities (> 4.7 km/s) are associated with the plutonic rocks of the Coast Belt and the volcanics of the Quesnellia terrane (Figure 2). Lower velocities (< 4.7 km/s) are associated with sedimentary cover in the Georgia Basin and in the Intermontane Belt, including the Cache Creek terrane. The most significant velocity low (2.6 - 2.8 km/s) can be linked to the Upper Cretaceous Nanaimo and overlying Tertiary sediments of the Georgia Basin (Mustard, 1994). A similar low was observed along Line 3 (Zelt et al., 1993). The thickness of the near-surface layer is variable across the line. Note that the near-surface velocities apply only to the immediate vicinity of the shot point (i.e., 3-4 km) and it is difficult to extrapolate the shallow velocity model over the entire extent of a terrane.

The upper crustal velocity structure is well-resolved by the Line 2 data set. There are no apparent discrepancies in the velocity structures of near-coincident seismic interpretations which cannot be accounted for. Over the upper 10 km of crust a transition from higher velocities in the west (6.4 km/s) to lower velocities in the east (6.1 km/s) is consistent with the analyses of the Line 3 data (Zelt et al., 1993) and the Line 10 data (O'Leary et al., 1993). Along Line 2, the transition is associated with the Harrison Fault. However, over the upper 5 km of crust, the transition to lower velocities occurs beneath SP12; this is located at the Bralorne-Kwoiek Creek Fault, a strike-slip fault which separates the Central and Eastern Coast Belts. The contrast in velocities, which continues into the mid-crustal unit, could indicate a significant crustal extent for the Harrison Fault, perhaps to depths of 10 km.

The upper crustal velocities are slightly higher (6.47 km/s) in the Insular Belt than in the Coast Belt (6.35 km/s) and are correlated with upper crustal rocks of the Wrangellia terrane. The difference in velocities may be due to a contrast in lithology between the two regions or

perhaps due to the lower temperature gradients in the Insular Belt. Slightly lower velocities are observed in the Western Coast Belt, as displayed by the 6.0 km/s velocity contour (Figure 14). In this region, the upper crustal layer may be correlated to the plutonic assemblages of the Western Coast Belt. The Line 2 data indicates that the plutonic suite extends to ~ 12 km depth beneath Line 2 which correlates well with the low conductivity observed in the upper crust of the Western Coast Belt (Jones et al., 1992a). Dehler and Clowes (1992; 1995) conclude that low density plutonic rocks must overlie the higher density Wrangellia rocks to interpret the observed low Bouguer gravity values. Laterally, these velocities are maintained as far east as the Harrison Fault which is consistent with the extent of plutonic rock in the Western Coast Belt. The reflection profile 88-16 (Varsek et al., 1993) did not resolve the geometry of the intrusive mass.

East of the Harrison Fault, Line 2 traverses several tectonostratigraphic terranes: the Cadwallader, Bridge River and Methow terranes of the Central and Eastern Coast Belts, and the Cache Creek and Quesnellia terranes and Tertiary sediments of the Intermontane Belt. On Figure 14, the 6.0 km/s and 6.2 km/s velocity contours show significant variations which may be related to the different terranes. The depth extent of the terranes is not resolved by the refraction data but is assumed thin (< 10 km) based on the interpretation of seismic reflection data in the region (Varsek et al., 1993). The lowest velocities are associated with the oceanic Bridge River and Cache Creek terranes, as illustrated by two prominent valleys in the 6.0 km/s velocity contour. This is not a surprising feature since the Bridge River terrane has no direct affinity to either the Coast or Intermontane Belt and may have once been continuous with the Cache Creek terrane (Gabrielse and Yorath, 1989). Higher velocity regions, indicated by peaks in the 6.2 km/s velocity contour, are associated with the Tertiary sediments of the Intermontane Belt and the Methow and Quesnellia terranes. The lower average crustal velocities in this region define the upper crustal structure east of the Harrison Fault, most prominently the Intermontane composite terrane.

The depth to the base of the upper crust is defined by the R1 reflector. This reflector is

well-constrained at the Insular-Coast Belt boundary and in the Intermontane Belt. In the Coast Belt, the depth to this discontinuity is not well constrained by the data but is consistent with the estimated depth extent of the plutonic assemblages. A lack of crustal reflectivity in this region was also observed on reflection profiles 88-13 and 88-16 (Figures 20 and 22, Varsek et al., 1993). There are no distinct geological features at either end of the refraction model which could account for the discontinuity which separates the upper and middle crust. At the Insular-Coast Belt boundary, the depth to this reflector is consistent with the 'C' reflector observed on profile 84-01 beneath western Vancouver Island, but there is no corresponding reflector imaged by the reflection data at the eastern edge of the survey (profiles 84-01 and 88-16, Figure 22). A possible source of the R1 reflector is trapped fluids caused by tectonic underplating due to the subduction of the Juan de Fuca plate. However, magnetotelluric studies indicate that the upper crust of the Insular Belt is resistive in nature and the presence of fluids would normally be associated with increased conductivity. In the Intermontane Belt, the R1 reflector most likely originates from a shear zone caused by the inter-layering of smaller terranes in the region. The depth to this horizon is consistent with the depth estimate to the 450°C isotherm but any correlation between the two is tenuous due to the intermittent nature of the reflector.

Below the R1 reflecting horizon, the mid-crustal structure is characterized by the same velocity trend as the upper crust. Average mid-crustal velocities in the Insular and Western Coast Belt are high with respect to velocities at the same depth east of the Harrison Fault. The interpreted mid-crustal velocities along Line 2 are consistent with those interpreted for the Wrangellia terrane of the Insular Belt (McMechan and Spence, 1983; Spence et al., 1985; Drew and Clowes, 1990) and north of Line 2 (reflection profile 88-16, Varsek et al., 1993). The high mid-crustal velocities in the Insular Belt correspond to a region of high Bouguer values (Dehler and Clowes, 1992; 1995).

Previous interpretations of the subsurface nature of the Western Coast Belt concluded that Wrangellia extended at least 40 km into the Coast Belt (Monger et al., 1990). This study

infers that the upper unit of Wrangellia extends from beneath Vancouver Island to as far east as the Harrison Fault, implying that the Harrison Fault is the location of the suture between the Insular and Intermontane superterranes. This is consistent with the analyses of refraction Line 3 (Zelt et al., 1993) and Line 10 (O'Leary et al., 1993) and reflection profile 88-13 (Varsek et al., 1993). However, higher mid-crustal velocities are inconsistent with the observed high in conductivity (Jones et al., 1992a) and high crustal temperatures (Lewis et al., 1992).

The mid-crustal velocity structure east of the Harrison Fault is more uniform than the upper crustal structure for the same region. This implies that the smaller terranes of the Intermontane Belt do not extend to large depths as inferred in the analysis of seismic reflection data (Varsek et al., 1993). Lower average values, compared to those in the west, indicate the character of the deep Intermontane superterrane, possibly the middle crust of the Quesnellia terrane. Lower average velocities are inconsistent with low conductivities (Jones et al., 1992a) but are consistent with high crustal temperatures. The mid-crustal velocity structure of the Intermontane Belt determined from the Line 2 data set is consistent with the analysis of Line 1 data (Zelt et al., 1992).

The mid-crustal unit is divided into an upper and lower portion by an interface (R2) across which velocities decrease discontinuously. Below this interface, the velocity structure tends to be more uniform. The transition from higher average velocities in the west to lower average velocities in the east is still apparent, although not as prominent. (Figure 14). As in the upper crustal structure, the lowest velocities occur beneath SP12 which is located at the geological boundary that separates the Central and Eastern Coast Belts.

The R2 reflector is generally well-defined across the survey except for the highly faulted region surrounding the Fraser Fault system. The trajectory at the western edge of Line 2 is uncertain; it could merge into the base of the upper crust or dip westward beneath Vancouver Island. This is the only discontinuity imaged by the Line 2 data which is continuous across

the survey. The depth to this discontinuity is consistent with the estimated depth to the 730°C isotherm but to correlate this reflector with the isotherm would not satisfy other constraints. Specifically, an abrupt decrease in reflectivity below this depth is not observed.

Across the Coast Belt, the velocity contrast across the R2 reflector is not large (refer to Figures 4, 5, 8 and 9) and could originate from the inter-layering of Wrangellia and granitic rocks. Within the Insular Belt, the R2 reflector is characterised by a larger velocity contrast as displayed on SP10 and SP11 (Figures 6 and 7). The origin of the reflecting boundary is most likely trapped fluids in the mid-crustal unit due to dewatering of the subducting oceanic plate. A similar velocity contrast is observed in the Intermontane Belt (refer to SP14, SP15 and SP1, Figures 11-13). A shear zone, perhaps separating lower crustal units of the Quesnellia terrane, could be responsible for this discontinuity.

The depth to the base of the mid-crustal unit is defined by the R3 reflector. This reflector is characterised by a large velocity contrast but it is intermittent across the line. Any correlation with a geothermal isotherm is not appropriate. The velocity structure of the lower crust is generally uniform across the region except beneath SP12 where a trend to lower velocities is still apparent.

Beneath Vancouver Island two prominent reflectors ('C' and 'E' reflectors) are imaged (Clowes et al., 1987). A tentative continuation of the 'C' reflector beneath the mainland was provided in the analysis of profile 88-16 (Varsek et al., 1993). The region between the two reflectors is interpreted as high velocity underplated material from the subducting oceanic plate (Clowes et al., 1987). Gravity interpretations (Dehler and Clowes, 1992; 1995) have extended the high density and high velocity material below the 'C' reflector to the region beneath the mainland; however, the refraction data did not image the reflective 'C' zone nor is there a corresponding region of high velocity material (> 7.4 km/s) in the lower crust. In the Insular Belt, the R3 reflector was too deep to be constrained by the refraction data (Figure 14). In the Western Coast Belt, the depth to this reflector is near the top of a reflective

package imaged on profile 88-16 (Figure 22), interpreted as a possible continuation of the 'C' reflector (Varsek et al., 1993). This would imply that the lower crust must be high velocity oceanic material which is not consistent with the interpretation of the refraction data. Since there is no discontinuity in the middle crust which is significant enough in amplitude to define the base of Wrangellia, the structure below the R3 reflector is interpreted as lower crustal rocks of Wrangellia.

Beneath the surface location of the Fraser-Straight Creek Fault both the R2 and R3 reflectors experience large, abrupt undulations which can be interpreted as a structural discontinuity across the fault zone. East of this region, the lower crustal structure is interpreted as the lower rocks of the Intermontane superterrane. A similar interpretation was made for reflection profile 88-18 (Perz, 1994). South of Line 2, reflection profile 88-18 indicated a change in structural styles across the fault zone in the upper and middle crust. In the lower crust, there are contradictory interpretations between the initially-processed and re-processed data. Interpretation of the initial data (Varsek et al., 1993) indicated a flattening of the Fraser-Straight Creek Fault into the middle crust, while interpretation of the re-processed data (Perz, 1992) indicates deep crustal penetration of the fault. This is consistent with the analysis of magnetotelluric data (Jones et al., 1992b) which imaged an abrupt change in lower crustal conductivity across the fault and consistent with the analysis of the refraction data.

A comparison of refraction data recorded along Line 2 and Line 3 (Zelt et al., 1993) indicate a pronounced difference in structural styles in the lower crust within a small region of the Western Coast Belt. A similar conclusion has been observed between refraction data recorded in the Coast Belt and in the Pacific Northwest (Clowes et al., 1995). In these studies, the apparent change in structural styles results from differences in the tectonic development of the two regions (Monger, 1991). The discrepancies between the velocity structural models of Line 2 and Line 3 remain unresolved, although in both models the lower crust is interpreted as Wrangellia. The Line 2 data seems to indicate a disruption of refraction

energy, not observed by the Line 3 data or the PACNW data (Clowes et al., 1995). A similar phenomena was observed in a previous refraction study across the Insular-Coast Belt boundary completed by Berry and Forsyth (1975).

Moho depth throughout the region is uniform, ~ 34.5 km depth. The Line 2 data did not image an increase in crustal thickness of 2-3 km below the Coast Belt or the sudden decrease in crustal thickness below the Insular Belt as observed on Line 3 (Zelt et al., 1993) and the 3-D interpretation (Clowes et al., 1995). Conversely, Varsek et al. (1993) indicate a Moho depth of ~ 12 s (39 km depth) on profile 88-16 indicating a significant increase in crustal thickness in the Western Coast Belt. This is also inconsistent with the Line 2 interpretation. An alternative interpretation of profile 88-16 places the Moho at ~ 10 s, consistent with the Line 2 analysis. In this interpretation, the strong package of reflectivity below 10 s could be interpreted as previous subducted lithosphere which may be the cause of the scattering of lower crustal and upper mantle energy indicated by the Line 2 data. In the Western Coast Belt, heat flow values are extremely high at the Garibaldi volcanic belt which is ~ 20 km inland. It is inferred that high crustal temperatures may also correspond to the unusual nature of the lower crust and upper mantle in this region.

An upper mantle reflector was modeled at ~ 46 km depth. The data were unable to resolve the nature of the polarity across the discontinuity. Although the velocity structural model indicates an increase in velocity across the horizon, tests reveal that the data is also consistent with a velocity decrease. The material below this reflector could then be correlated with the top of the asthenosphere.

5.2 Conclusions

Insight into the structure of the Earth's crust comes from the interpretations of geophysical data. Although some of the interpretations may be more qualitative than quantitative, each plays a prominent role in understanding the complexity of the tectonic

processes which have occurred to develop the present day configuration of the Cordillera.

In this thesis, analysis of seismic refraction data has been carried out by the application of traveltime inversion and amplitude forward modelling yielding a 2-D velocity structural model across three morphogeological belts. The model features a thin (< 2.0 km) near-surface layer with large lateral and vertical variations in velocity gradients representing the near-surface geology. Below the near-surface layer, the crust is divided into three major units. Each crustal unit is bounded below by a discontinuity in velocity. The upper crust has an average velocity of 6.4 km/s in the west and 6.1 km/s in the east, and it extends to an average depth of 11.5 km. The middle crust, which extends to ~ 24.7 km, has an average velocity of 6.5 km/s in the west and 6.3 km/s in the east. This crustal unit is divided into upper and lower portions by a wide-angle reflector at 18.5 km depth. The lower crust extends to the crust-mantle boundary at ~ 34.5 km and has a more uniform velocity structure, 6.7 km/s in the west to 6.6 km/s in the east. Upper mantle velocities are uniform across the survey at 7.9 km/s. An upper mantle reflector at ~ 46 km depth is consistent with a velocity decrease representing the top of the asthenosphere.

A striking feature of the model is the large lateral variation in velocities in the crustal unit, with a change to lower velocities occurring near the Harrison Fault. This is interpreted as the suture zone of Insular to Intermontane superterrane. The location of the transition is also consistent with the analysis of refraction Line 3 (Zelt et al., 1993) and Line 10 (O'Leary et al., 1993) and the interpretation of reflection profile 88-13 (Varsek et al., 1993) which displays the interfingering of the Insular crust and Intermontane crust near the Central Coast Belt Detachment zone.

The upper crustal velocity structure is well-resolved. High velocities in the Insular Belt correlate with upper crustal rocks of Wrangellia. The intrusive mass of the Western Coast Belt is outlined by a region of slightly lower velocities with respect to those in the Insular Belt. The base of the upper crust (R1) defines the vertical extent of the plutonic suite. The

lateral and vertical extent of the plutonic assemblage is consistent with high resistivities determined from magnetotelluric studies (Jones et al., 1992a). East of the Harrison Fault, velocities in the upper crust are highly variable and the average value is lower than to the west. There is a gross correlation between seismic velocities and lateral extent of the smaller terranes within the Central and Eastern Coast Belts and the Intermontane Belt. The vertical extent of these units is not clearly resolved by the refraction data, although reflection data (Varsek et al., 1993) indicate they are thin (< 10 km).

The middle and lower crust of the Insular and Western Coast Belts is interpreted as the lower crust of Wrangellia. The 'C' reflective zone beneath Vancouver Island and its corresponding continuation beneath the mainland, as inferred by Varsek et al. (1993), was not resolved by the Line 2 data. Although the depth to the base of the mid-crustal unit (R3) was consistent with the interpretation of profile 88-16 (Varsek et al., 1993), it is intermittent in nature and a significant increase to higher velocities is not apparent. The lack of a reflector prominent enough to define the base of the Wrangellia unit provides the basis for concluding that Wrangellia rocks extend into the lower crust in the Insular and Western Coast Belts. The middle and lower crustal velocity structure east of the Harrison Fault predominantly represents rocks of the Intermontane superterrane, most likely the lower crust of the Quesnellia terrane which may be associated with a lower average velocity and lower conductivity than rocks to the west of the Harrison Fault.

The depth to the Mohorovic discontinuity and upper mantle velocity structure in the Insular and Western Coast Belts are poorly constrained. The Moho was interpreted at ~ 34.5 km depth, consistent with the rest of the model. Conversely, the analysis of the Line 3 data (Zelt et al., 1993) and the 3-D interpretation (Clowes et al., 1995) indicated a sudden increase in crustal thickness to 37 km west of the Fraser Fault system and a further decrease to 31 km in the southern Insular Belt. The discrepancy between the interpreted velocity structures cannot be accurately resolved and could be attributed to an abrupt change in structural styles in the Western Coast Belt. A similar contrast was observed south of Line 3 by the PACNW

data (Clowes et al., 1995), and so it is reasonable to infer a similar scenario to the north. A re-interpretation of reflection profile 88-16, to the north of Line 2, indicates a Moho at ~ 32 km depth (~ 10 s), consistent with the Line 2 refraction data. Interestingly, mantle arrivals are not seen propagating eastward from within Insular Belt by the Line 2 data, in contrast to Line 3 (Zelt et al., 1993). Refraction energy is somehow disrupted; Berry and Forsyth (1975) indicated a similar phenomena. This region of "unusual" Moho corresponds to region of strong upper mantle reflectivity on profile 88-16 (Varsek et al., 1992) which may be obscuring refraction arrivals. Heat flow values are also extremely high in the Western Coast Belt.

The Line 2 data indicate a vertical displacement in reflecting horizons beneath the surface location of the Fraser-Straight Creek Fault. This may be interpreted as implying deep crustal penetration of the fault, consistent with magnetotelluric studies (Jones et al., 1992b) and the analysis of reflection profile 88-18 (Perz, 1992). It is inferred that the Harrison Fault must penetrate the crust to depths of 10 km based on the abrupt contrast in crustal velocity values below the surface location. However, it may not penetrate into the mid-crustal unit and certainly does not penetrate the lower crust since a reflector at ~ 18 km depth is well-defined and laterally continuous beneath the fault.

BIBLIOGRAPHY

BERRY, M. J. and FORSYTH, D. A., 1975. Structure of the Canadian Cordillera from seismic refraction and other data. Canadian Journal of Earth Sciences, **12**, p. 182-208.

CANER, B., 1970. Electrical conductivity structure in western Canada and petrological interpretations. Journal of Geomagnetism and Geoelectricity, **22**, p. 113-129.

ČERVENY, V., MOLOTKOV, I. and PŠENČÍK, I., 1977. Ray method in seismology. Charles University Press, Prague.

CONEY, P. J., JONES, D. L., and MONGER, J. W. H., 1980. Cordilleran suspect terranes. Nature, **288**, p. 329-333.

CLOWES, R. M., BRANDON, M. T., GREEN, A. G., YORATH, C. J., SUTHERLAND-BROWN, A., KANASEWICH, E. R., SPENCER, C., 1987. LITHOPROBE - Southern Vancouver Island: Cenozoic subduction complex imaged by deep seismic reflections. Canadian Journal of Earth Sciences, **24**, p. 31-51.

CLOWES, R. M., ZELT, C. A., AMOR, J. R., ELLIS, R. M., 1995. Lithospheric structure in the southern Canadian Cordillera from a network of seismic refraction lines. Canadian Journal of Earth Sciences (in press).

COOK, F. A., GREEN, A. G., SIMONY, P. S., PRICE, R. A., PARRISH, R. R., MILIKEREIT, B., GORDY, P. L., BROWN, R. L., COFLIN, K. C., and PATENAUDE, C., 1988. LITHOPROBE seismic reflection structure of the southeastern Canadian Cordillera: initial results. Tectonics, **7**, p. 157-180.

DREW, J. J. and CLOWES, R. M., 1990. A re-interpretation of the seismic structure across the active subduction zone of western Canada. *In* Studies of laterally heterogeneous structures using seismic refraction and reflection data. Edited by A. G. Green. Geological Survey of Canada, Paper **89-13**, p. 115-132.

DEHLER, S. A. and CLOWES, R. M., 1992. Integrated geophysical modelling of terranes and other structural features along the western Canadian margin. Canadian Journal of Earth Sciences, **29**, p. 1492-1508.

DEHLER, S. A. and CLOWES, R. M., 1995. Structure of the northern Cascadia subduction zone derived from integrated geophysical modelling. Canadian Journal of Earth Sciences, in revision following review.

GABRIELSE, H. and YORATH, C. J., 1989. Decade of North American Geology #4; The Cordilleran orogen in Canada. Geoscience Canada, **16**, p. 67-83.

GOUGH, D. I., 1986. Mantle upflow tectonics in the Canadian Cordillera. Journal of Geophysical Research, **91**, p. 1909-1919.

GOUGH, D. I. and MAJOROWICZ, J. A., 1992. Magnetotelluric soundings, structure, and fluids in the southern Canadian Cordillera. Canadian Journal of Earth Sciences, **29**, p. 609-620.

GREEN, A. G., CLOWES, R. M., YORATH, C. J., et al., 1986. Seismic reflection imaging of the subducting Juan de Fuca plate. Nature, **319**, p.210-213.

HYNDMAN,R. D., 1976. Heat flow measurements in the inlets of southwestern British Columbia. Journal of Geophysical Research, **81**, p. 337-349.

HYNDMAN, R. D. and SHEARER, P. M., 1989. Water in the lower continental crust: modelling magnetotelluric and seismic reflection results. Geophysical Journal International, **98**, p. 343-365.

IRVING, E. and WYNNE, P. J., 1990. Paleomagnetic evidence bearing on the evolution of the Canadian Cordillera. Philosophical Transactions of the Royal Society of London, Serial A, **331**, p. 487-509.

ISACHSEN, C., 1984. Geology, geochemistry and geochronology of the Westcoast Crystalline Complex and related rocks, Vancouver Island. M. Sc. Thesis, University of British Columbia, British Columbia.

JONES, A. G., GOUGH, D. I., KURTZ, R. D., DeLAURIER, J. M., BOERNER, D. E., CRAVEN, J. A., ELLIS, R. G., and McNIECE, G. W., 1992a. Electromagnetic images of regional structure in the southern Canadian Cordillera. Geophysical Research Letters, **12**, p. 2373-2376

JONES, A. G., GOUGH, D. I., KURTZ, R. D., DeLAURIER, J. M., BOERNER, D. E., CRAVEN, J. A., ELLIS, R. G., and McNIECE, G. W., 1992b. Electromagnetic constraints on strike-slip fault geometry - the Fraser River fault system. Geology, **20**, p. 561-564.

JOURNEAY, J. M., 1990. Structural and tectonic framework of the southern Coast Belt, British Columbia. *In* Current Research, Part E., Geological Survey of Canada, Paper **90-1E**, p. 183-197.

JOURNEAY, J. M. and FRIEDMAN, R. M., 1993. The Coast Belt thrust system: evidence of Late Cretaceous shortening in southwest British Columbia. Tectonics, **12**, p. 756-775.

KANASEWICH, E. R. and CHUI, S. K. L., 1985. Least-squares inversion of spatial seismic refraction data. Bulletin of the Seismological Society of America, **75**, p. 865-880.

KEEN, C. E. and HYNDMAN, R. D., 1979. Geophysical reviews of the continental margins of eastern and western Canada. Canadian Journal of Earth Sciences, **16**, p. 712-749.

KLEMPERER, S. L., 1987. A relation between continental heat flow and the seismic reflectivity of the lower crust. Journal of Geophysics, **61**, p. 1-11.

KURTZ, R. D., DELAURIER, J. M. and GUPTA, J. C., 1986. Magnetotelluric survey across Vancouver Island: a search for subducting lithosphere. Nature, **321**, p. 596-599.

LEWIS, T. J., BENTOWSKI, W. H., DAVIS, E. E., HYNDMAN, R. D., SOUTHER, J. G., and WRIGHT, J. A., 1988. Subduction of the Juan de Fuca Plate: thermal consequences. Journal of Geophysical Research, **93**, p. 15207-15225.

LEWIS, T. J., BENTOWSKI, W. H. and HYNDMAN, R. D., 1992. Crustal temperatures near the LITHOPROBE Southern Cordillera Transect. Canadian Journal of Earth Sciences, **29**, p. 1197-1214.

LEWIS, T. J., JESSOP, A. M., and JUDGE, A. S., 1985. Heat flux in southwestern British Columbia: the thermal consequences of plate tectonics. Canadian Journal of Earth Sciences, **22**, p. 1262-1273.

McMECHAN, G. A. and SPENCE, G. D., 1983. P-wave velocity structure of the Earth's crust beneath Vancouver Island. Canadian Journal of Earth Sciences, 12, p. 742-752.

MONGER, J. W. H., 1991. Correlation of Settler Schist with Darrington Phyllite and Shuksan Greenschist and its tectonic implications, Coast and Cascada mountains, British Columbia and Washington. Canadian Journal of Earth Sciences, **28**, p. 447-458

MONGER, J. W. H., 1993. Canadian Cordilleran Tectonics: from Geosynclines to Crustal Collage. Canadian Journal of Earth Sciences, **30**, p. 209-231.

MONGER, J. W. H. and JOURNEAY, J. M., 1992. A field guide to accompany the Penrose conference on the Tectonic evolution of the Coast Mountains orogen, May, 1992, 97 pages.

MONGER, J. W. H. and JOURNEAY, J. M., 1994. Basement geology and tectonic evolution of the Vancouver region. *In* Geology and Geological Hazards of the Vancouver region, Southwestern British Columbia. Edited by J. W. H. Monger. Geological Survey of Canada, Bulletin **481**, p. 3-25.

MONGER, J. W. H. and JOURNEAY, J. M., GREIG, C. J. and RUBLEE, J., 1990. Structure, tectonics and evolution of the Coast, Cascade and Intermontane Belts, southwestern British Columbia. Field trip B6, Geological Association of Canada - Mineralogical Association of Canada, 91 pages.

MONGER, J. W. H. and PRICE, R. A., 1979. Geodynamic Evolution of the Canadian Cordillera - progress and problems. Canadian Journal of Earth Sciences, **16**, p. 770-791.

MONGER, J. W. H., PRICE, R. A., and TEMPLE-KLUIT, D. J., 1982. Tectonic accretion and the origin of the two major metamorphic and plutonic welts in the Canadian Cordillera. Geology, **10**, p. 70-75.

MUSTARD, P. S., 1994. The Upper Cretaceous Nanaimo Group, Georgia Basin. *In* Geology and Geological Hazards of the Vancouver region, Southwestern British Columbia. Edited by J. W. H. Monger. Geological Survey of Canada, Bulletin **481**, p. 27-95.

O'LEARY, D. M., CLOWES, R. M. and ELLIS, R. M., 1993. Crustal velocity structure in the Southern Coast Belt, British Columbia. Canadian Journal of Earth Sciences, **30**, p. 2389-2403.

PERZ, M. J., 1992. Characterization of the Fraser Fault, southwestern British Columbia, and surrounding Geology through reprocessing of seismic reflection data. M. Sc. thesis, University of British Columbia, British Columbia.

RIDDIHOUGH, R. P., 1979. Gravity and structure of an active margin - British Columbia and Washington. Canadian Journal of Earth Sciences, **16**, p. 350-363.

RODDICK, J. A., 1983. Geophysical reviews and composition of the Coast Plutonic Complex, south of latitude 55°N. *In* Circum-Pacific Plutonic Terranes. Edited by J. A. Roddick. Geological Society of America, Memoir **159**, p. 195-211.

SHERIFF, R. E. and GELDART, L. P., 1982. Exploration seismology, volume 2: Data-processing and interpretation. Cambridge University Press.

SINGH, S. and HERRMANN, R. B., 1983. Regionalization of crustal coda Q in the continental United States. Journal of Geophysical Research, **88**, p. 527-538.

SPENCE, G. D., CLOWES, R. M., and ELLIS, R. M., 1985. Seismic structure across the active subduction zone of western Canada. Journal of Geophysical Research, **90**, p. 6754-6772.

SPENCER, C., ASUDEH, I., and CÔTÈ, T., 1989. SEGY-LDS Version 2.0 Format Reference Document, Manual Version 1.00. Geological Survey of Canada, Ottawa, 17 pages.

STACEY, R. A., 1973. Gravity anomalies, crustal structure, and plate tectonics in the Canadian Cordillera. Canadian Journal of Earth Sciences, **10**, p. 615-628.

WHEELER, J. O. and McFEELY, P., (comp.) 1991. Tectonic Assemblage Map of the Canadian Cordillera and adjacent parts of the United States of America. Geological Survey of Canada, Map 1712A, scale 1:2,000,000.

WHEELER, J. O., BROOKFIELD, A. J., GABRIELSE, H., MONGER, J. W. H., TIPPER, H. W., and WOODWORTH, G. J., (comp.), 1991. Terrane Map of the Canadian Cordillera. Geological Survey of Canada, Map 1713A, scale 1:2,000,000.

WHITE, W. R. H., BONE, M. N., and MILNE, W. G., 1968. Seismic refraction surveys in British Columbia, 1941-1966; a preliminary interpretation. American Geophysical Union, Geophysical Monograph, **12**, p. 81-93.

VAN DER HEYDEN, P., 1992. A middle Jurassic to early Tertiary Andean-Sierran arc model for the Coast Belt of British Columbia. Tectonics, **11**, p. 82-97.

VARSEK, J. L., COOK, F. A., CLOWES, R. M., JOURNEAY, J. M., MONGER, J. W. H., PARRISH, R. R., KANASEWICH, E. R., and SPENCER, C. S., 1993. LITHOPROBE Crustal Reflection Structure of the Southern Canadian Cordillera 2: Coast Mountains Transect. Tectonics, **12**, p. 334-360.

ZELT, C. A. and ELLIS, R. M., 1988. Practical and efficient ray tracing in two dimensional media for rapid traveltime and amplitude forward modelling. Canadian Journal of Exploration Geophysics, **24**, p. 16-31.

ZELT, B. C., ELLIS, R. M., and CLOWES, R. M., 1990. SCoRE '89: The Southern Cordillera Refraction Experiment Description of Data set. University of British Columbia, LITHOPROBE secretariat, LITHOPROBE Report No. **20**, 38 pages.

ZELT, B. C., ELLIS, R. M., and CLOWES, R. M., 1993. Crustal velocity structure in the eastern Insular and southernmost Coast Belts, Canadian Cordillera. Canadian Journal of Earth Sciences, **30**, p. 1014-1027.

ZELT, B. C., ELLIS, R. M., and CLOWES, R. M., 1995. Three-dimensional velocity structure of the southwestern Canadian Cordillera. Journal of Geophysical Research, in revision following review.

ZELT, B. C., ELLIS, R. M., CLOWES, R. M., KANASEWICH, E. R., ASUDEH, I., LUETGERT, J. H., HANAL, Z., IKAMI, A., SPENCE, G. D., and HYNDMAN, R. D., 1992. Crust and upper mantle velocity structure of the Intermontane Belt, Southern Canadian Cordillera. Canadian Journal of Earth Sciences, **29**, p. 1530-1548.

ZELT, C. A. and SMITH, R. B., 1992. Seismic traveltime inversion for 2-D crustal velocity structure. Geophysical Journal International, **108**, p. 16-34.

VITA

Surname: McLean Given Names: Nancy Ann

Place of Birth: Winnipeg, Manitoba, Canada

Educational Institutions Attended:

University of Victoria	1985 to 1995

Degrees Awarded:

B. Sc.	University of Victoria	1990

PARTIAL COPYRIGHT LICENSE

I hereby grant the right to lend my thesis (or dissertation) to users of the University of Victoria Library, and to make single copies only for such users or in response to a request from the Library of any other university, or similar institution, on its behalf or for one of its users. I further agree that permission for extensive copying of this thesis for scholarly purposes may be granted by me or a member of the University designated by me. It is understood that copying or publication of this thesis for financial gain shall not be allowed without my written permission.

Title of Thesis/Dissertation:

Crustal Seismic Velocity Structure of the Intermontane and Coast Belts, Southwestern Canadian Cordillera

Author [redacted]

Nancy Ann McLean
December, 1995
December 23, 1995